Universidade de Aveiro Departamento de Electrónica, Telecomunicações e Informática,
2017

Michael Rodrigues Duarte

Antena na banda dos 17 GHz para aplicações Wi-fi indoor/outdoor
Antennas for indoor/outdoor Wi-Fi applications at the 17 GHz band

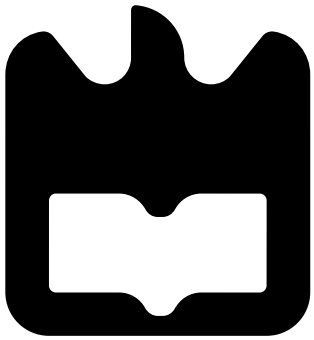

Michael Rodrigues Duarte

Antennas for indoor/outdoor Wi-Fi applications at the 17 GHz band

Dissertação apresentada à Universidade de Aveiro para cumprimento dos requesitos necessários à obtenção do grau de Mestre em Engenharia Eletrónica e de Telecomunicações, realizada sob a orientação científica do Professor Doutor João Nuno Pimentel da Silva Matos do Departamento de Eletrónica Telecomunicações e Informática da Universidade de Aveiro e o Professor Doutor Pedro Renato Tavares de Pinho do Departamento de Engenharia Electrónica Telecomunicações e Computadores do Instituto Superior de Engenharia de Lisboa.

o júri / the jury

presidente / president

Professor Doutor Atílio Manuel da Silva Gameiro
Professor Associado, Universidade de Aveiro

vogais / examiners committee

Professor Doutor João Nuno Pimentel da Silva Matos
Professor Associado, Universidade de Aveiro (orientador)

Doutor Ricardo Miguel Romão Gonçalves
Investigador Científico, Evoleo Technologies (arguente)

agradecimentos / acknowledgements

Gostaria de agradecer em primeiro lugar aos meus pais, irmão e restante família por todo o incentivo e apoio prestado ao longo de todo o meu percurso académico, pois sem eles era impensável chegar até aqui.

Aos meus orientadores, professor João Nuno Matos e professor Pedro Pinho, por toda a orientação, apoio e disponibilidade concedida ao longo da realização desta dissertação. Um agradecimento especial ao colaborador Tiago Varum pela sua disponibilidade e pelos conselhos prestados na elaboração desta dissertação.

Aos meus amigos, com uma atenção especial ao B&C e namorada, que sempre mostraram grande apoio e me proporcionaram momentos de descontração e diversão durante o meu percurso académico. Aos meus colegas do Laboratório de Rádio frequência que tornaram os longos dias de trabalho cheios de frustração em recordações divertidas.

Por fim, mas não menos importante à equipa técnica Instituto de Telecomunicações pelo suporte à realização desta dissertação.

Um grande obrigado a todos!

Palavras-chave Aplicações Wi-fi; Antena microstrip; Banda ISM; Alimentação por fenda

Resumo

O Wi-Fi permite estabelecer ligações sem fios de equipamentos à internet, sendo muito utilizado em casas, hotéis e espaços públicos. Opera nas bandas livres Industrial, Scientific, and Medical (ISM) nomeadamente nas faixas de 2.4 GHz e 5.8 GHz.

Nos dias de hoje, as interferências nas soluções que recorrem ao Wi-Fi têm vindo a aumentar devido à enorme utilização destas bandas de frequência reduzindo significativamente a qualidade do serviço fornecido aos utilizadores. Algumas altenativas têm vindo a ser testadas para minorar este problema, como por exemplo a utilização de frequências de operação, nomeadamente a banda ISM dos 24 GHz ou na banda dos 17 GHz.

Com esta dissertação pretendeu-se contribuir para esta solução através da construção de antenas que possam ser uma mais valia para o desenvolvimento das redes sem fios gama dos 17 GHz, visto que a banda dos 24 GHz é bastante afectada por atenuações que advêm das condições climatéricas (e.g. chuva).

Face às reduzidas dimensões das antenas, uma das dificuldades sentidas, durante o seu projecto, foi a sua alimentação, tendo sido realizado um estudo dos métodos de alimentação para antenas microstrip nesta frequência. O método de alimentação escolhido foi a alimentação por fenda que demonstrou conseguir um melhor desempenho a esta frequência de operação. De seguida, foi desenvolvida uma antena que cumpre os requisitos mínimos de operação para aplicações Wi-Fi em interiores, cujas as características, dependendo do cenário de instalação, deverão ter um ganho entre 0 e 6 dBi e ter uma grande rejeição da polarização inversa (é desejável que seja entre 30 e 40 dB). Por fim, foi realizada uma antena para comunicações que envolvam distâncias maiores, onde é desejável que as antenas possuam um ganho maior (desde 3dBi até 29 dBi dependendo da aplicação). Para obter ganhos desta ordem foi realizado um agregado planar(2x2) que apresentou um ganho por volta de 11 dBi.

Keywords Wi-fi applications (indoor/outdoor); Microstrip Antenna; ISM band; Aperture coupling feed

Abstract

Wi-Fi technology allows wireless connections of equipment to the Internet, being widely used in homes, hotels and public areas. It operates in the ISM band, also known as free bands , namely in the bands of 2.4 GHz and 5.8 GHz.

Nowadays, interference in solutions that use Wi-Fi technology has been increasing due to the considerable use of these frequency bands, significantly reducing the quality of service provided to users. Some alternatives to solve this problem have been tested, such as the use of operating frequencies, namely the 24 GHz ISM band or at the 17 GHz band.

With this dissertation it was intended to contribute to this solution through the construction of antennas that could be an asset for the development of wireless networks in the 17 GHz frequency range, since the 24 GHz band is greatly affected by attenuations due to the climatic conditions (e.g. rain).

Considering the small size of the antennas at 17 GHz, one of the difficulties during their design was their feeding. Thus, a study of the feeding methods for microstrip antennas was carried out. The feeding method chosen was the aperture coupling feed which shown a better performance at this operating frequency. Then, an antenna that meets the minimum operating requirements has been developed for indoor Wi-Fi applications, whose characteristics, depending on the installation scenario, should have a gain between 0 and 6 dBi as well as a high rejection level of the orthogonal polarization component (it is desirable to be between 30 and 40 dB). Finally, an antenna for communications involving great distances was developed, where it is desirable that the antennas present a higher gain (from 3 dBi up to 29 dBi depending on the application). In order to obtain higher gains, a planar array antenna (2x2) was produced, presenting a gain around 11 dBi.

Contents

List of Figures

List of Tables

Acronyms

ADS	Advanced Design System.
AF	Array Factor.
CST MWS	CST Microwave Studio.
HPBW	Half Power Beam Width.
IEEE	Institute of Electrical and Electronics Engineers.
ISM	Industrial, Scientific, and Medical.
LHCP	Left Hand Circular Polarization.
MIMO	Multiple-Input-Multiple-Output.
RHCP	Right Hand Circular Polarization.
SMA	Subminiature version A.
VNA	Vector Network Analyser.
WLANs	Wireless Local Area Network.

Chapter 1

Introduction

Wi-Fi is an technology that has grown rapidly, since it provides freedom and flexibility to the user to move around within a certain range and keep its connection [1]. Therefore, Wireless Local Area Network (WLANs) are very popular and widely used in offices, hotels, public places and homes to provide wireless access for portable computer and other mobile devices.

The Wi-Fi technology is known for being inexpensive to build/implement and free of fees, because it operates in the ISM (industrial, scientific, and medical) band, particularly in the bands of 2.4 GHz and 5.8 GHz. The Institute of Electrical and Electronics Engineers (IEEE) 802.11 (a,b,g,n,ac) standard defines rules for the WLANs. Since its creation, the IEEE 802.11 standards has been improved to meet the demand of higher throughput and distance coverage [2]. The speed of the data transfer has been increasing over the years, and this was achieved with the increase of bandwidth or by using complex data modulation. When it was not possible to further increase the bandwidth or to improve the modulation technique it was created the Multiple-Input-Multiple-Output (MIMO) standard, which uses multiple antennas to exchange communication between the transmitter and receiver taking advantages of the multipath phenomenon [2], [3].

Nowadays the wireless traffic in the mentioned ISM frequency bands has exponentially increased due to its extensive use for applications besides the Wi-Fi solutions, namely bluetooth, cordless phone, microwaves, etc, leading to interferences in the frequency spectrum. The increase of devices with Wi-Fi capabilities leads to the congestion of the Wi-Fi networks, significantly reducing the quality of service provided to the users, as can be seen in figure 1.1. One of the possible solution to these problems is add more Wi-Fi operation frequency band.

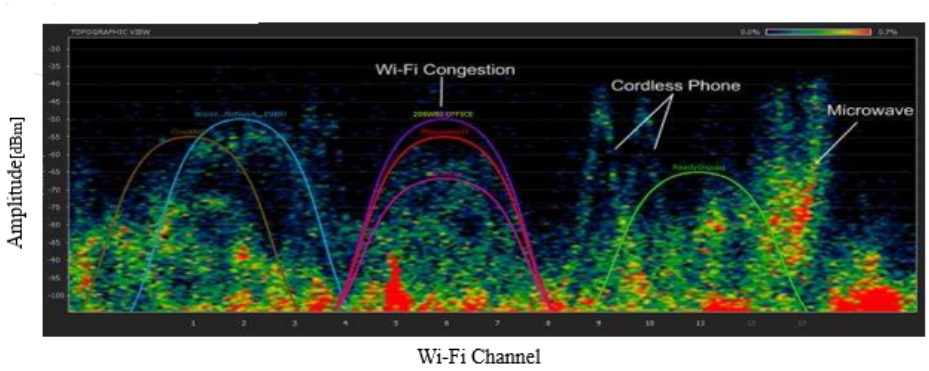

Figure 1.1: Example of the Wi-fi spectrum with interferences and congested [4]

There are some studies in the 17 GHz and 24 GHz band to overcome this problem, *"If wireless traffic grows and network becomes congested, either the cell size must be reduced or an overlay network at another frequency band has to be deployed so that the increased capacity demand can be met"* [5]. The change of the operating frequency of the Wi-Fi systems implies that all the components of it will change including the antennas.

The use of the 17 GHz band is suggested since, since the 24 GHz ISM band is greatly affected by attenuations due to the climatic conditions (e.g. rain, steam) [6]. Therefore, this work will be focused on antennas for Wi-Fi applications in the proposed 17 GHz band.

Antennas have been studied over the years, to improve the coverage area, increase the gain and bandwidth to meet the demands of modern communications applications [7], [8]. The microstrip antennas have been one of the most studied types of antennas, since they present important features that fit to modern wireless communication systems [9], such as the low profile, high versatility, compactness, low cost, and easiness to manufacture [10]. Therefore, they present attractive features for Wi-Fi applications and were used in this work.

Wi-Fi antennas can be divided into three categories, regarding its different applications and features, as described in [8]:

- Indoor Fixed Antennas: They should be small and compact, due to the space and aesthetical concerns, and provide an omnidirectional coverage to the intended direction, with a gain from 0 to 6 dBi [8].

- Outdoor Fixed Antennas: The outdoor antennas are usually mounted in fixed base-stations, towers or buildings for line-of-sight (LOS) communications. These are known for being directional antennas and can have three different features, namely point-to-point links, point-to-multipoint links and sectoral coverage. Regarding the point-to-point links, it is desired to have an antenna with a gain up to 29 dBi. For point-to-multipoint links the antennas should provide gains from 3 to 16 dBi. Finally, sectoral coverage antennas should present a radiation pattern with a Half Power Beam Width (HPBW) of 60°, 90°, or 120°, having a gain between 15 and 20 dBi [8].

- Antennas for Mobile Devices: They should be physically and electrically small and compact, to be embedded into mobile phones, laptops, etc. It is desired to have an antenna that provides omnidirectional coverage with a gain from -5 to 5 dBi in respect to the intended direction [8].

In all of these cases it is advantageous to use circular polarized antennas with high isolation between the orthogonal components, usually around 30-40 dB [8].

Increasing the operating frequency from [2.4;5] GHz to 17 GHz leads to a reduction of the coverage that can be achieved by the Wi-Fi system antennas and the increase of the propagation loss. On the other hand, with the frequency increase it is possible to use higher bandwidths that lead to higher bit rates.

Note that in this dissertation it was considered that the 17 GHz frequency band was used for WLANs as mentioned by Electronic Communications Committee in the ERC Report 25 [11]. However, in a more recent ERC Report 25 it was noticed that this frequency band was only used for Radiolocation as defence system [12]. If the suggested project of modifying the frequency operation of the Wi-Fi system was implemented, it would require the 17GHz frequency band to be an ISM band.

1.1 Objectives

As mentioned before, a possible solution to avoid the interferences in the Wi-Fi systems is to change the operating frequency. The 17 GHz band has been investigated and tested to be the next operating frequency of the Wi-Fi systems. The objective of this work is to study and develop microstrip antennas that can add value to the progress of the wireless networks in this new range of frequencies, at the 17 GHz band.

The goal is to develop a microstrip antenna for indoor that presents at least the same characteristics described before using only a single element. It was also developed an antenna for outdoor Wi-Fi applications. Antennas for outdoor applications are characterized for having a high gain, which will be accomplished in this work through an antenna array.

1.2 Thesis Structure

This dissertation is composed by a total of 5 chapters.

Chapter 2 presents some basic notions and the fundamental antenna parameters, focusing on the microstrip antennas. This chapter also includes information regarding the antenna polarization and an introduction to the antenna array theory.

In chapter 3 it is conducted a study on the feeding methods for microstrip antennas in order to select the one that presents the best performance at the intended operating frequency.

Chapter 4 is focused on the design and production of an antenna for indoor Wi-Fi applications, also exhibiting the crucial parameters of the antennas for this application, all the design steps, intermediate and final results.

Chapter 5 starts by presenting the types of antennas for outdoor Wi-Fi applications, then it describes all the design steps, production steps and results obtained from the antenna developed in this work for this application, ending with a discussion of the accomplished results.

This dissertation terminates with the chapter 6 that summarizes all the work performed and the main conclusions drawn. Suggestions of possible future work to further deepen and improve this topic are also presented in this final chapter.

1.3 Original Contributions

Two papers have been submitted:

- M. Duarte, T. Varum, J. Matos and P. Pinho, "In house development of 17GHz antennas: potentialities and difficulties", 11.º Congresso do Comité Português da URSI - Novas tecnologias para a mobilidade;
- T. Varum, M. Duarte, J. Matos and P. Pinho, "Microstrip Antenna for IoT/WLAN applications in Smart Homes at 17GHz", 12th European Conference on Antennas and Propagation (2018 edition of EuCAP).

Chapter 2

Microstrip Antennas

Antennas are a fundamental element of all wireless communication systems [9], [10]. The antenna is the interface from the guided electromagnetic waves, in the electric circuit, to the propagated electromagnetic waves, in the air. There are different types of antennas as wire antennas, aperture antennas, microstrip antennas, reflector antennas, horn antennas, amoung other deviations. From all these types of antennas the microstrip antenna has been one of the most studied. This fact is due to the constant decreasing in size of the communication systems because of a greater integration of electronics, so there is a need for more compact antennas. Microstrip antennas can answer these demand from technology since they are, as mentioned by [10], small, compact, low cost and easy to manufacture. Therefore, these were chosen for this dissertation, since they present the necessary characteristics to be inserted in Wi-Fi systems. However, this type of antennas presents some disadvantages as low efficiency, low gain, narrow bandwidth, low power handling capacity, poor polarization purity and spurious feed radiation [10]. It is possible to overcome some of these disadvantages, as for example, the low gain, by implementing an array configuration and the narrow bandwidth and spurious radiation, by selecting proper feeding methods that can improve the bandwidth and reduce the spurious radiation of the microstrip antennas.

As a first approach, it is presented the microstrip antenna structure, which is divided into four parts: patch, ground plane, substrate and feed line, as presented in figure 2.1.

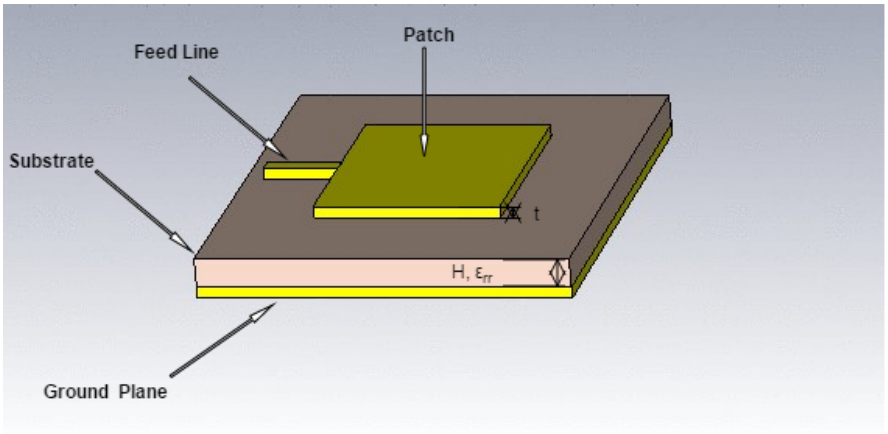

Figure 2.1: Patch antenna.

The patch can have different shapes, as shown in Figure 2.2. However, the most common are the rectangular and circular, since they are the easiest to fabricate and analyse [10]. In the following section it is described one of the existing methods of analysis.

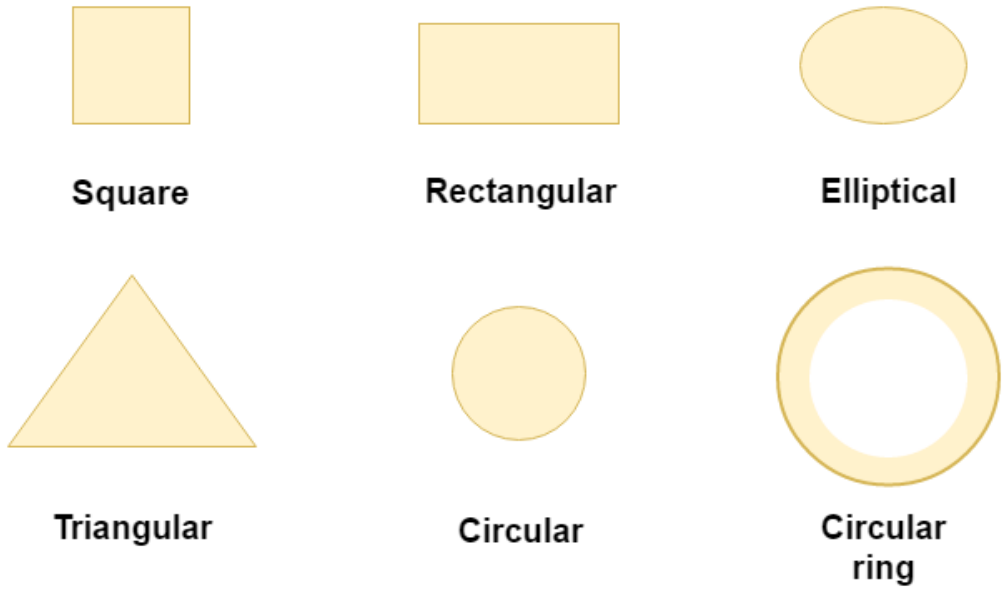

Figure 2.2: Examples of possible shapes for patch antennas.

2.1 Methods of Analysis for microstrip antennas

There are generalist numerical methods to analyse a microstrip patch antenna. These models were developed to achieve an estimation of the parameters of these antennas, such as input impedance, antenna dimensions, bandwidth and others [13].

The antenna models allows the understanding of the operating principles, being useful to recognize which are the modifications necessary on the antenna parameter to achieve a desired configuration and reducing the number of trial and error during the design process. It is helpful to obtain an estimation of the antenna performance [14].

The simplest and popular models are the *transmission-line* and *cavity* [10]. In this work it was applied the transmission line model to obtain an aproximation of the antennas dimentions. Therefore, a brief review of it will be conducted in the following section.

2.1.1 Transmission Line Model

A rectangular patch and a microstrip transmission line present a similar physical shape. Therefore, the transmission line model is one of the most simple and intuitive, but it can only be applied to rectangular and square shapes [14].

This model consider a rectangular microstrip patch antenna as two radiating slots with a width of W. Each radiating slot will be represented by a parallel equivalent admittance that is separated by a transmission line with a length equal to L and terminated in open circuit at

both ends. A schematic of the rectangular transmission line is presented in Figure 2.3. The input impedance and propagation constant of the transmission line are imposed by the patch size (W, L) and the substrate parameters [10], [14].

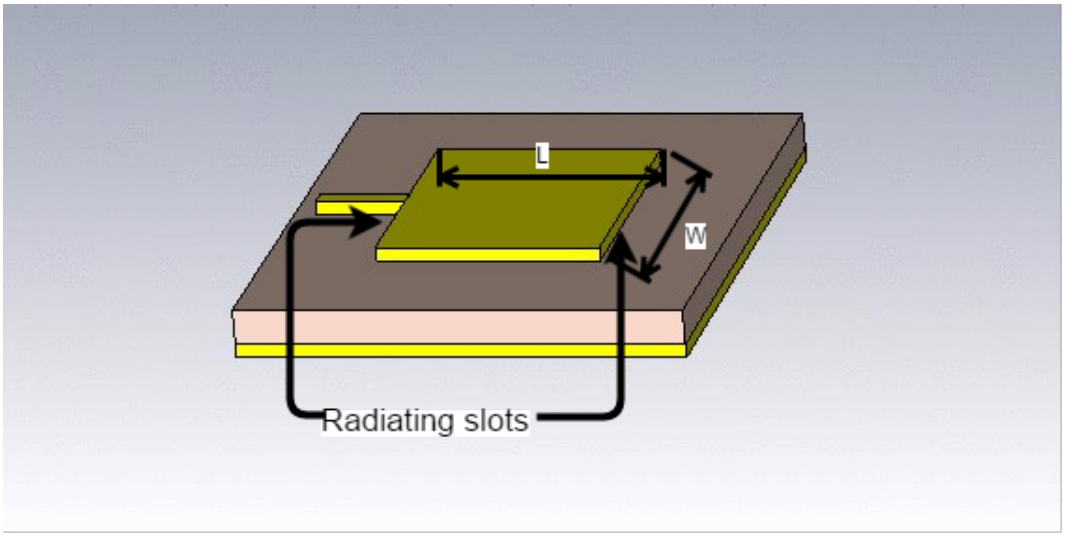

Figure 2.3: Radiating slots of a rectangular patch antenna

The transmission line model takes into account the impact of the fringing effects.

The microstrip antenna presents finite dimensions (L ,W). Therefore, the field that arises from the radiating edges of the patch undergoes fringing, as Figure 2.4 illustrates [10]. The fringing field depends on the antenna parameters (W,L,h, ε_r and f_r (frequency of operation)).

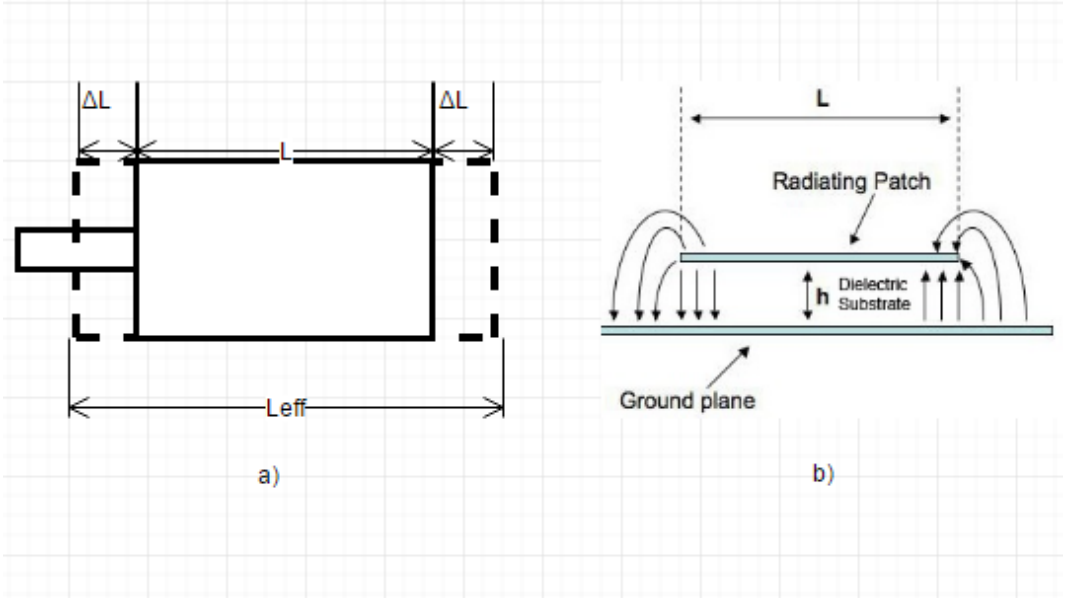

Figure 2.4: a) Schematic of the length expansion; b) Schematic of the fringing effect field [15]

As it can be observed in Figure 2.4, the electromagnetic field is not just enclosed in the

substrate, it also goes through the air. This implies the calculation of the effective dielectric constant(ϵ_{ff}), that considers the fringing effects on the wave propagation in the line. The ϵ_{ff} is the dielectric constant value such that the actual structure embedded in a non-homogeneous medium behaves identically to a structure embedded in a homogeneous dielectric constant medium [10],[16]. In other words, the ϵ_{ff} is obtained by combining the dielectric constants of the materials by which the electromagnetic waves created by the patch cross.

The value of the effective dielectric constant is closer to the dielectric constant of the substrate when $\varepsilon_r >> 1$, since most of the electric field is concentrated in the substrate [10].

According to Balanis [10], the effective dielectric constant is obtained by the flowing expression:

$$\varepsilon_{ff} = \frac{\varepsilon_r + 1}{2} + \frac{\varepsilon_r - 1}{2 * \sqrt{1 + \frac{12h}{W}}} \tag{2.1}$$

Due to the fringing effects, the electrical length of the patch is greater than the physical length, an schematic of it is presented in 2.4 a).The length expansion that occur due to this phenomenon can be obtained by the expression 2.2. The length extension(ΔL) depends mainly on the effective dielectric constant and the width-to-height ratio [10].

$$\Delta \mathrm{L} = 0.412\mathrm{h} * \frac{(\varepsilon_{ff} + 0.3) * (\frac{W}{h} + 0.264)}{(\varepsilon_{ff} - 0.258) * (\frac{W}{h} + 0.0.8)} \tag{2.2}$$

For the dominant mode TM_{010} the resonant frequency of the microstrip antenna is a function of its length, then the effective length of the patch is given by:

$$L_{eff} = \frac{c}{2 * f_r * \sqrt{\varepsilon_{ff}}} \tag{2.3}$$

Since the length extension occurs in each side of the patch, the physical length of the patch is given by:

$$L = L_{eff} - 2 * \Delta \mathrm{L} \tag{2.4}$$

In the dominant mode TM_{010} there are no fringing fields along the width of the patch, therefore for an efficient radiation the width is approximately [10],

$$W = \frac{C}{2 * f_r} * \sqrt{\frac{\varepsilon_r + 1}{2}} \tag{2.5}$$

where f_r is the resonant frequency and C the speed of light [14]. The transmission line model can determine the input impedance of the patch antenna along the central line. This is a crucial parameter, to obtain a good impedance matching between the feedline and the feed point.

As mentioned before, each radiating slot is represented by the transmission line model as parallel equivalent admittance. The model is presented in Figure 2.5.

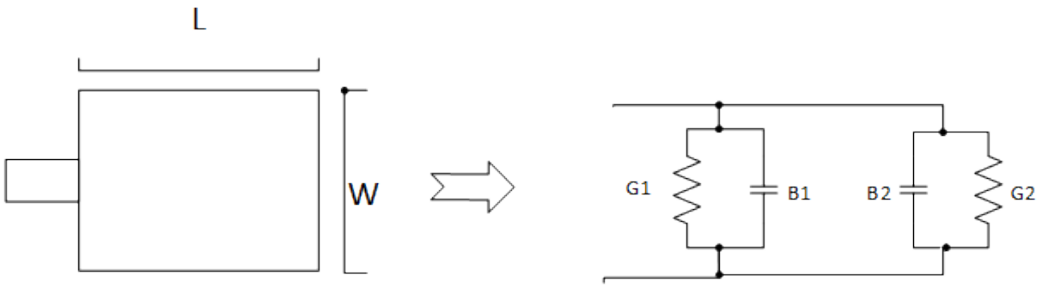

Figure 2.5: Transmission line representation of a rectangular patch antenna

It is known *a priori* that both slots are similar. The conductance of a single slot can be obtained by the field expression of the cavity model [10].

$$G_1 = \frac{1}{120\pi}\int_0^{\pi}\left(\frac{\sin(\frac{K_0*W}{2}\cos\theta\ )}{\cos\theta}\right)^2 \sin(\theta)^{\ 3}\ d\theta \tag{2.6}$$

In an ideal design, the slots would be separated by L=λ/2. However, due to the mentioned fringing effects, the separation between the slot is less than the ideal. If the length reduction is well selected (0.48λ<L<0.49λ), the equivalent admittance of the second slot is transformed in its conjugate. This phenomenon can be explained in terms of impedance representation on the smith chart, where a rotation of λ/2 will result in the conjugate impedance of the one observed in the starting point.

Then, it is easy to understand that the input impedance, considering the mutual effects between the slots, is given by the following expression [10].

$$Rin = \frac{1}{2(G_1 + G_{12})} \tag{2.7}$$

Mutual conductance:

$$G_{12} = \frac{1}{120\pi}\int_0^{\pi}\left(\frac{\sin(\frac{K_0*W}{2}\cos\theta\ )}{\cos\theta}\right)^2 * J_0(K_0 * L * \sin\theta\ )\sin(\theta)^{\ 3}\ d\theta \tag{2.8}$$

Where J_0 is the Bessel Function.

However, the expression 2.7 just expresses the input impedance in the edge of the patch antenna and, as mentioned before, it is possible to obtain the input impedance along the central line. It is known that the current is low at the edge and increases when moving towards the centre of the patch, the opposite occurs with the voltage. Therefore it is possible to conclude that the impedance at the edge is high and low at the centre [10],[17],[18].

Observing the Figure 2.6 it is possible to see that the variation of the impedance follows a square cosine, depending on the length of the patch and the distance from the edge to the centre (d) [18], [19].

$$Rin(d) = Rin(0) * \cos^2\left(\frac{\pi}{L} * d\right) \tag{2.9}$$

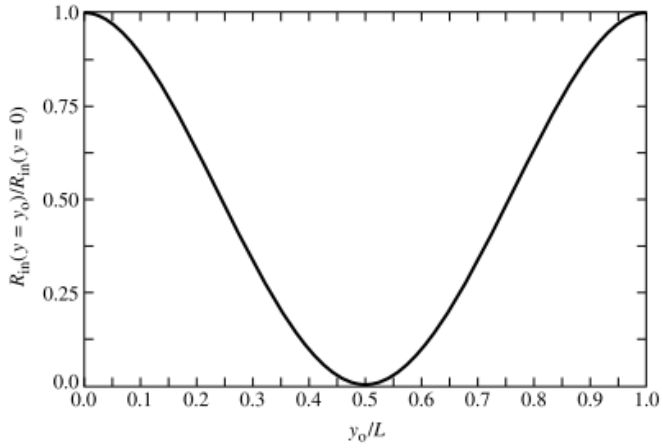

Figure 2.6: Variation of the normalized input impedance along the central line of the patch [10]

2.2 Feeding methods

Microstrip patch antennas can be fed in different ways, the most popular are the coaxial probe, microstrip line, aperture coupling and proximity coupling [10]. These methods can be divided into two categories, contact and non-contact feed. Contact feed methods have narrow bandwidth and are more sensitive to deviations from the etching process [13]. On the other hand, they are more simple to manufacture [13].

Each feeding method has its own characteristics, advantages and disadvantages.

2.2.1 Coaxial

The coaxial probe is widely used since it is easy and inexpensive to implement. As it can be observed in Figure 2.7, the inner conductor of the coax passes through the substrate and the ground plane, without any contact by making a hole on them, and is attached directly to the radiating element. The outer conductor is connected to the ground plane [10], [13].

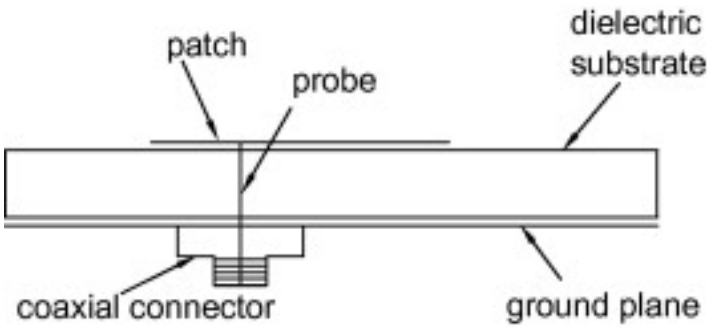

Figure 2.7: Schematic of a Coaxial feed [20]

This feeding method has an advantage of simplicity the impedance matching that is obtained by simply selecting the feed location that provides the desired impedance, and has low

spurious radiations, since the probe is directly attached to the radiating patch and isolated from the patch. On the other hand, it is difficult to perform adjustments in the structure, provides a narrow bandwidth (1-5%) and the probe is a radiating element causing cross-polarization [10], [13], [21].

2.2.2 Microstrip line feed

The microstrip line or edge feed is a simple and the mostly used feeding method, since the microstrip line is directly attached to the edge of the radiating patch. The radiating patch and the microstrip line are coplanar as it can be observed in Figure 2.8. Therefore, the fabrication process is easy, it is well suited for arrays and it is easy to apply a method of impedance matching as a quarter-wavelength transformer or by simply controlling the inset position [10], [13].

This method has some drawbacks, the feed line is also a radiating element which leads to undesired radiation that will increase the cross-polarization level since the radiating patch and the feed line are in the same plane. In summary, this method suffers from surface wave losses, spurious radiation feed and has low bandwidth (2-5 %); these disadvantages are more evident when is used a thicker substrate [10], [13], [16].

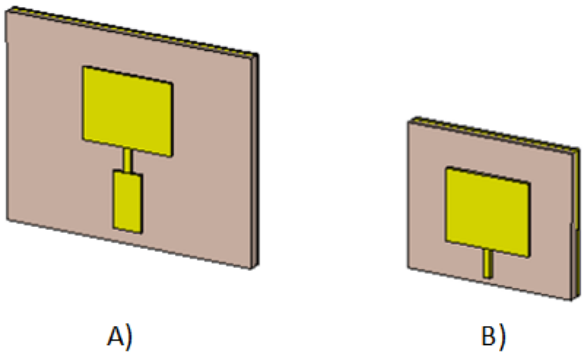

Figure 2.8: A) Microstrip line feed using a Quarter-Wavelength Transformer; B) Direct microstrip line feed

2.2.3 Aperture coupling feed

The aperture coupling feed is composed by two dielectric substrates, the patch substrate placed above the ground plane and the feed line substrate under it, Figure2.9 [10].The patch and the feed line are coupled through a slot/aperture created on the ground plane , the slot is centered with the patch to achieve maximum coupling and low cross polarization [22].

Typically, the patch substrate presents a low dielectric constant to improve the radiation of the patch and the feed line substrate with a high dielectric to improve the transmission in the feed line [23].

As advantages, the aperture coupling feed provides a large number of parameters that can be adjusted to achieve the intended performance (shape of the slot aperture, dielectric of the substrate, slot aperture can be resonant or not (a resonant aperture creates another resonance into the one from the patch increasing the bandwidth, on the other hand it increases the back

radiation [24])); the ground plane between the radiating patch and the feedline minimizes the spurious radiations and increases the polarization purity [10], [24], [25].

On the other hand, the aperture coupling feed is a multi-layer feeding method that implies difficulties on the fabrication process.

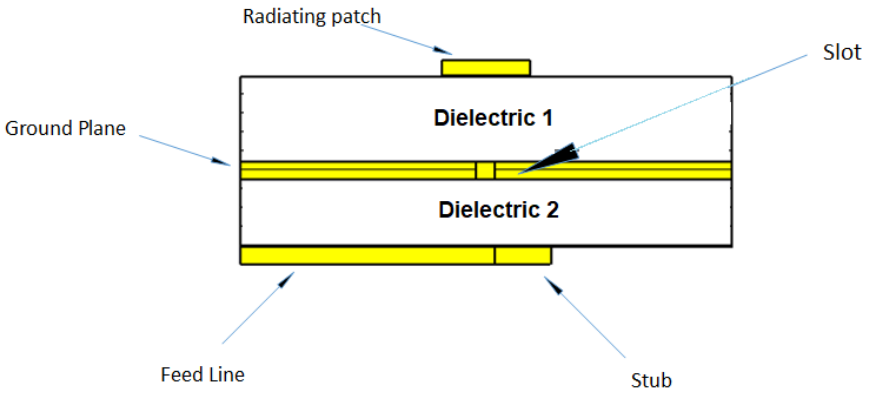

Figure 2.9: Aperture coupling feed

2.3 Polarization

An electromagnetic wave, as it can be observed in Figure 2.10, is composed by the electric and the magnetic fields that are perpendicular to each other and to the direction of propagation.

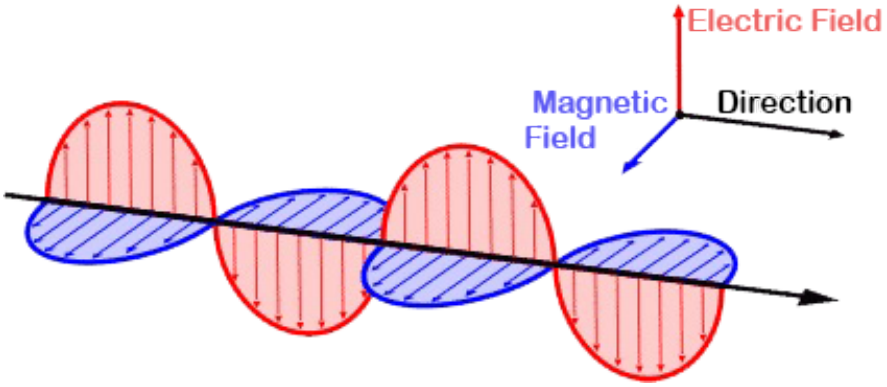

Figure 2.10: Electromagnetic wave [26]

Polarization is a property of electromagnetic waves that describes the relative magnitude and direction of the electric-field vector in function of the time. Polarization is a curve formed by the instantaneous electric-field vector [10].

Polarization of an antenna is the polarization of the electromagnetic wave radiated by the antenna in a given direction. When its direction is not stated the polarization is assumed to be in the direction of its maximum gain [10].

To achieve a better performance in the wireless communication link, maximum power transfer, the transmitting and receiving antennas should have the same polarization.

The geometric figure drawn by the instantaneous vector of the electric field defines the type of polarization, which can be elliptical, circular or linear. The circular and linear polarizations are special cases of the elliptical polarization [10], [13]. This work regards these two types of polarization, which are described in the sections 2.3.1 and 2.3.2.

2.3.1 Linear polarization

The linear polarization is simple to obtain since the electric field varies along the same straight line. This happens when the field vector presents just one component, or two orthogonal linear components that are in time phase or multiples of 180° out-of-phase [10].

The most common types of linear polarization are presented in Figure 2.11. Vertical polarization occurs when the electrical field is perpendicular to the surface of the earth, and horizontal polarization occurs when the electrical field is parallel to the surface of the earth [27].

Figure 2.11: A) Vertical linear polarization; B) Horizontal linear polarization [13]

2.3.2 Circular polarization

Circular polarization is commonly used in the wireless communication system since it presents some important advantages over the linear polarization. An antenna circularly polarized radiates power in all planes in the propagation direction, therefore the receiving and transmitting antenna does not have to present the same orientation, is more robust to signal degradation and is able to minimize the propagation anomalies [27].

In the circular polarization the electric-field vector draws a circle around the propagation axes in function of the time, as shown in figure 2.12. The rotation of the field defines if it is a Right Hand Circular Polarization (RHCP) or Left Hand Circular Polarization (LHCP) [10], [13]. This type of polarization is obtained when the electric field is composed by two orthogonal linear components with the same magnitude and present a time-phase difference of 90° between them [13].

Figure 2.12: A) Left-hand circular polarization; B) Right hand circular polarization [13]

In microstrip antennas is rather simple to achieve circular polarization by simply feeding the patch antenna at two different points to excite two orthogonal propagation methods. The time-phase difference can be obtained by using powers dividers, as the Hybrid. It also can be obtained by a single feed [13]. This will be studied further in this work.

2.3.3 Axial Ratio

The axial ratio is a parameter that quantifies the wave polarization quality of an antenna. Typically, an antenna radiates an electromagnetic wave that presents elliptical polarization. The axial ratio of the radiated wave is the ratio between the major axis and minor axis (the two orthogonal components of the field), as presented in figure 2.13 [10].

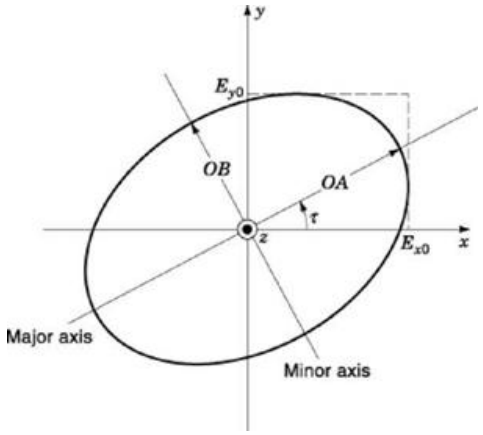

Figure 2.13: General polarization ellipse [28]

$$AR = \frac{(majoraxis(OA))}{(minoraxis(OB))} \tag{2.10}$$

Typically, the axial ratio is expressed in dB as

$$AR_{dB} = 10\log(AR) \tag{2.11}$$

For an elliptical polarized antenna, the axial ration is greater than one and less than infinity.

For a linear polarized antenna, the axial ratio is infinity since one of the components of the field is zero.

For a circular polarized antenna, the axial ratio is 1 (0 dB) since the field components have the same magnitude. In practice, for a acceptable circular polarization the axial ratio should be below 3 dB where 0 dB is the optimal case.

2.4 Antenna Array theory

As mentioned before, a single element presents low gain and directivity, a wide radiation diagram, specially microstrip antennas that are not capable to provide more than 10 dBi of gain [13]. However, in some applications it is necessary to have antennas with high gain, for example, long range wireless communications.

An antenna with high gain and directivity can be accomplished by enlarging the antenna's dimensions or by creating an array that is basically assembling typically identical single elements in an electrical and geometrical configuration [10].

An antenna array, besides increasing the gain and directivity, allows the control of the radiation pattern.

The field of an array is given by the addition of the fields created by each array element. Therefore, to achieve a directive pattern, the field of each element has to be added constructively in the desired and cancel each other in the undesired [10].

The radiation pattern can be controlled by the following parameters [10]:

- Geometrical configuration (e.g. linear, circular, rectangular);
- Distance between the elements;
- The excitation amplitude and phase of the elements;
- Pattern of each element.

2.4.1 Uniform Linear array

An array composed by identical elements placed along the same axis with identical magnitude between the elements is called a uniform linear array.

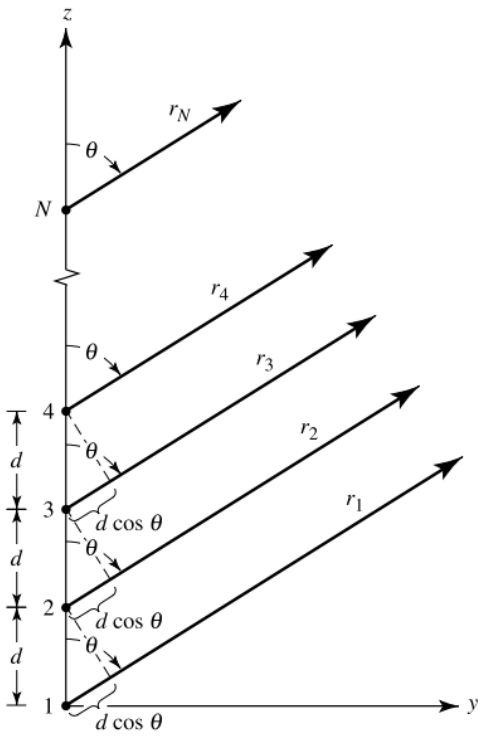

Figure 2.14: Uniform linear array of N elements spaced by a distance d and placed along the Z axis [10]

The array radiation pattern is obtained by multiplying the Array Factor (AF) by the field of one element, as can be observed in the equation 2.12.

$$Array\ Pattern = Element\ Pattern * AF \tag{2.12}$$

The AF depends on the number of elements of the array (N), spatial angular frequency ,the distance (d) and phase difference (α) between the elements and frequency (since $\beta = (\pi * 2)/\lambda$). It is mathematically described by the equation 2.13.

$$AF = \frac{\sin(N * \frac{\psi}{2})}{\sin(\frac{\psi}{2})};\ \psi = \beta * d * \cos\theta + \alpha \tag{2.13}$$

The increase of elements leads to a narrow main lobe, the number of lobes increases but the level of the secondary lobes decreases tending to a constant value (arround -13 dB) [10]. This phenomenon can be observed in Figure 2.15.

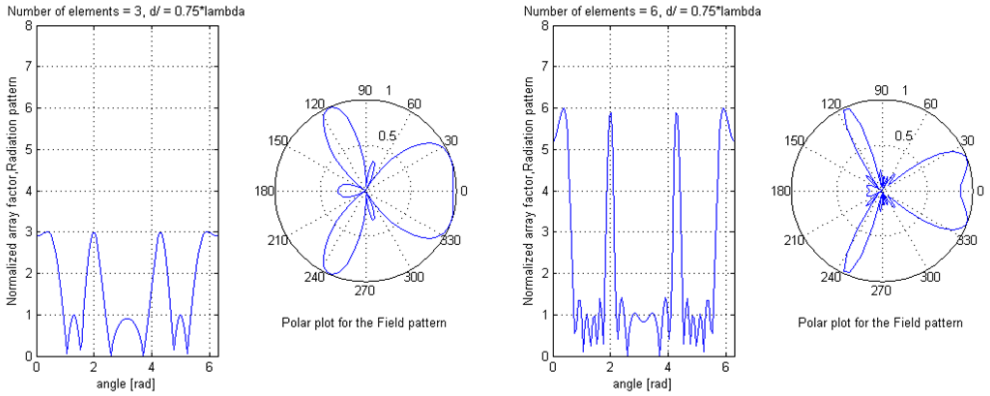

Figure 2.15: Array factor for different number of elements(N)

2.4.2 Uniform Planar array

In a planar array the identical elements are placed along a plane.

As in the previous case, if the elements are feed with the same magnitude the aggregate is called Uniform Planar array. The AF of this array considers the two components of the plane where the single elements are distributed.

Considering that the elements are distributed along a x-y plan, the total AF will be the multiplication between the AF of the x-axis and the AF of the y-axis, it can be verified observing the equation 2.14.

$$AF = \frac{\sin\frac{N_x * \psi_x}{2}}{\sin\frac{\psi_x}{2}} * \frac{\sin\frac{N_y * \psi_y}{2}}{\sin\frac{\psi_y}{2}} \tag{2.14}$$

where $\psi_x = \beta_x * d * \cos\theta_x + \alpha_x$ and $\psi_y = \beta_y * d * \cos\theta_y + \alpha_y$.

Planar arrays are more versatile. They provide more symmetrical patterns with lower side lobes, higher directivity and the main beam scanning can be done to any direction [13].

2.4.3 Microstrip array

A microstrip array besides being able to present the characteristics described before, offers the possibility to have the feed network and the radiating on the same layer, simplifying the construction process of the antenna.

Microstrip arrays can present the same geometry as any other array, linear or planar. In both cases there are two important important design parameters, the inter-element spacing and the feed network [13].

Typically, in arrays with fixed beams the spacing between the elements is set to be less than a λ, to avoid grating lobes, and greater than $\lambda/2$, to have enough space for the feed network.

According to [10], the most used and well known feeding networks are the following:

- Series-feed network

  As it can be observed in the following figure, the array is fed by a single element that simplifies the fabrication process. Therefore, it is a good feed network for arrays with fixed beam or for frequency shift beam scan. The main drawback of this feed technique

is the sensitivity to any change on the feedline or in a single element will affect the performance of the array.

Figure 2.16: Series-feed network

- Corporate-feed network

  This feed technique provides power splitters of 2^n through tapered line or quarter wavelength impedance transformers [10]. This is a more general and versatile solution, since it is possible to control the feed of each element. That is an advantage when the purpose is to create a scan phased array, multi-beam array or shaped-beam array [10].

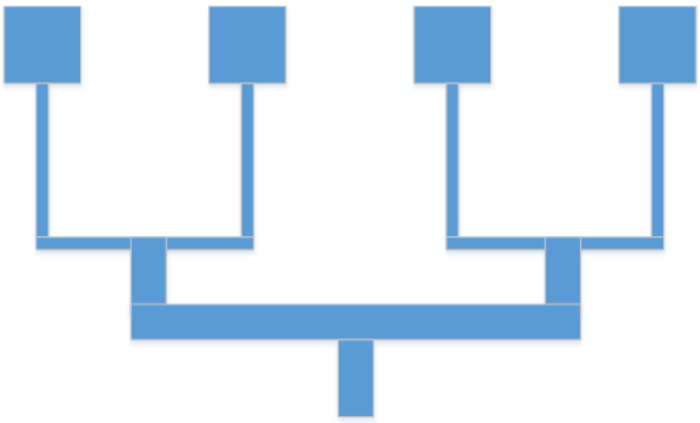

Figure 2.17: Corporate-feed network

Chapter 3

Selection of the feeding method

One of the main difficulties during the design of antennas at 17 GHz is their feeding due to their small size (patch dimensions around 6.62x5.05 mm). Thus, a study of different types of feeding methods to adapt the input impedance will be conducted to select the one that presents a better performance for the application at 17 GHz.

The feeding methods studied were:

- Microstrip line feed using a Quarter-Wavelength Transformer;
- Inset-fed;
- Aperture coupling feed.

The comparison will be performed using the simulations results. All the calculations and design steps are presented. The simulations were performed on CST MWS, the theoretical antenna dimensions were obtained using MATLAB.

3.1 Design of a microstrip line feed using a Quarter-Wavelength Transformer

The feed with a Quarter-Wavelength transformer is a direct/contact feed. Usually the impedance at the edge of the patch antenna is high, which implies the use of a quarter-wavelength to match the impedance between the 50Ω line and the edge impedance of the patch antenna.

The figure 3.1 presents the structure of this feeding method.

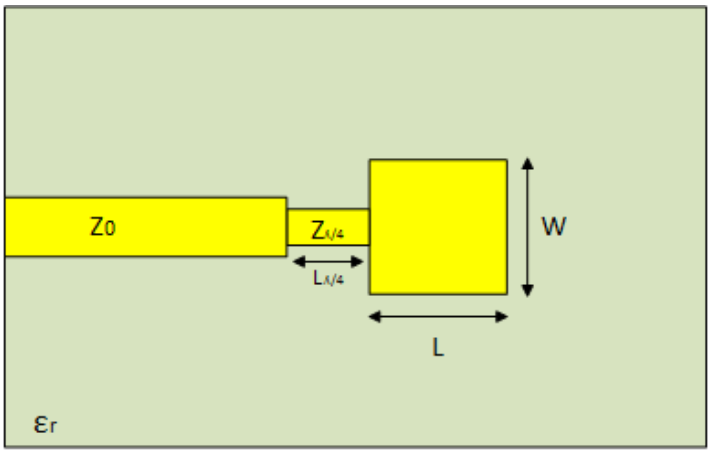

Figure 3.1: Patch antenna with a quarter-wavelength matching section

3.1.1 Design steps

The parameters of the patch antenna were obtained using the Transmission-Line model described in chapter 2. The procedure presented in Balanis [10] was followed. It needs some specified information *a priori* such as the operating frequency, the dielectric constant and the thickness of the substrate. *A posteriori* in the antenna simulation the loss tangent (tan δ) of the substrate is a crucial parameter to achieve results as close to reality as possible.

The substrate used was the Rogers RO4725JXR, it was the available substrate that present good characteristics either for radiation and for power transmission. This substrate presents a thickness of 0.78 mm (h), a dielectric constant of 2.55 (ϵ_r) and a tan δ of 0.0026@10GHz. The pretended operating frequency is 17 GHz. With this information it is possible to calculate the Width (W) and Length (L) of the patch using the expressions 2.1, 2.2, 2.3, 2.4 and 2.5 presented in section 2.1.1.

Once the antenna patch dimensions are known it is possible to calculate an approximation the resonant input impedance of the patch. The edge impedance of the patch is mainly affected by the ratio between the length and the width of the patch [10].

$$Zin = 90 * \frac{\varepsilon_r^2}{\varepsilon_r - 1} * \left(\frac{L}{W}\right)^2 \tag{3.1}$$

To match the input impedance of the patch to the pretended 50Ω (Z_0), it is necessary an impedance transformer. In this case, it is used a quarter-wavelength transformer. The impedance of the quarter-wavelength transformer to match the characteristic impedance with the edge impedance is obtained in the following way.

$$Z_{\frac{\lambda}{4}} = \sqrt{Z_0 * Zin} \tag{3.2}$$

Finally, in the microstrip patch antennas theory the ground plane is considered to be infinite. However, practically it is not possible. Therefore, it is necessary to guarantee that the ground plane dimensions are at least equal or bigger than the ones obtained by the equations 3.3 and 3.4 (this was ensured in all this dissertation) [10], [29].

$$L_g = 6 * h + L \tag{3.3}$$

$$W_g = 6 * h + W \tag{3.4}$$

All the antenna dimensions and impedances calculated in this section are presented in table 3.1.

Antenna Parameter	Value
W	6.62 mm
L	5.07 mm
Z_0	50Ω
Zin	221.97Ω
$Z_{\lambda/4}$	105.35Ω
W_{Z_0}	2.17 mm
$W_{\lambda/4}$	0.54 mm
$L_{\lambda/4}$	3.12 mm
Minimum ground size	(11.3 x 9.75) mm

Table 3.1: Design Parameters (calculated)

3.1.2 Simulation and optimization

At this point the antenna was simulated in CST MWS using the parameters presented in the Table 3.1. However, these parameters leaded to a non-satisfactory result at the pretended operating frequency, since it was not achieved a good impedance matching. Therefore, some of these parameters were adjusted to obtain a good impedance matching at the intended resonant frequency. The parameters optimized were the width and length of the quarter wavelength feed line.

The input impedance obtained in the simulations was different from the one calculated above. This difference has an impact on the width of the transformer, since the characteristic impedance of a microstrip line is defined by its width.

In theory, the edge impedance of the microstrip antenna is real, but it is not correct, since it is observed an imaginary part in the simulations results. Therefore, to compensate the existing imaginary part, the length of the quarter wave-length transformer was adjusted.

After the optimization, the following parameters and results were obtained.

Antenna Parameter	Value
W	6.62 mm
L	5.07 mm
Zin	(242.90-13.04i) Ω
W_{Z_0}	2.7 mm
$W_{\lambda/4}$	0.48 mm
$L_{\lambda/4}$	1.72 mm
Antenna size	(34.48 x 34.49) mm

Table 3.2: Design Parameters (optimized)

The designed antenna in CST MWS is presented in Figure 3.2.

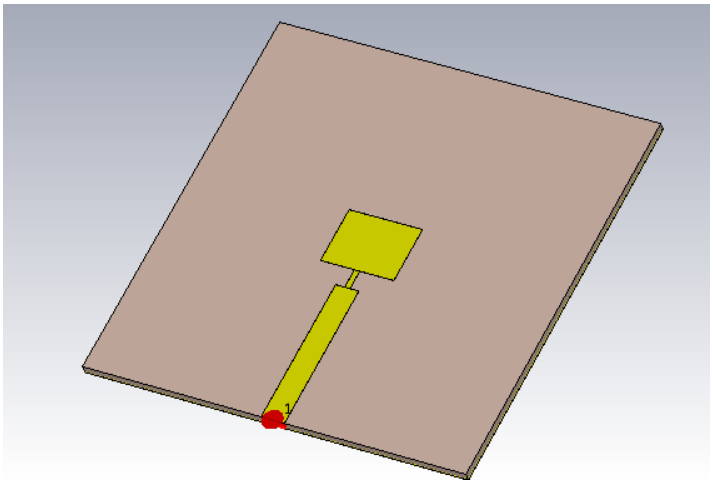

Figure 3.2: Microstrip feed patch structure implemented in CST MWS

Observing the Figure 3.3 is possible to conclude that a good impedance matching was achieved, since it presents a low return loss (-37.8 dB). In other words, the impedance seen at the port is close to 50Ω.

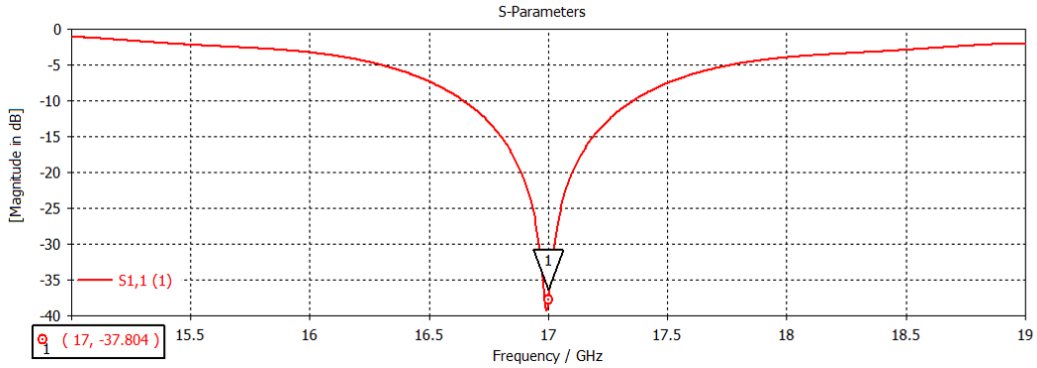

Figure 3.3: Return loss(S_{11}) of the patch antenna in dB referring to the frequency

It was considered a good performance of the antenna in terms of impedance matching, the range of frequencies that presented a return loss below -10 dB. Therefore, the antenna presents a bandwidth of 711MHz (4.2%).

Figure 3.4 and **??** presents the radiation pattern of the antenna in the two main planes.

Considering the radiation direction of θ=0°, which is the intended radiation direction in this dissertation, the antenna presents a gain of 4.9 dBi and a directivity of 5.3 dBi. At the operating frequency (17 GHz), the antenna has a radiation efficiency of 92%.

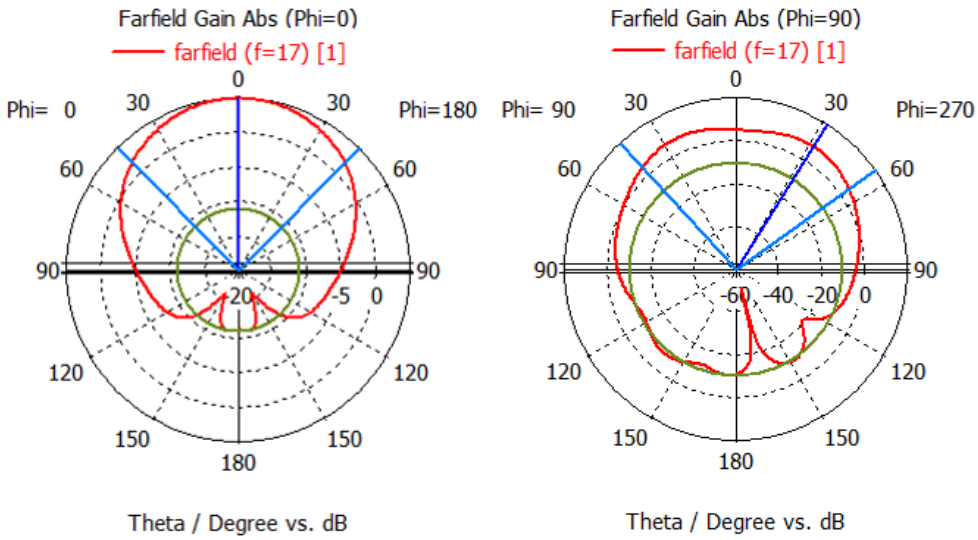

Figure 3.4: Vertical radiation pattern of the patch antenna at 17 GHz for $\phi = 0°$ and $\phi = 90°$, respectively

Observing the figure 3.4 it is possible to conclude that the antenna do not present its maximum gain to the desired direction (θ=0°). This occurs due to the radiating patch and the feed network being placed at the same plane. It is aggravated by the discontinuities inserted by the impedance transformer.

The antenna presents a HPBW of 89.5° and 97.3° in respect the cut plane of $\phi = 0°$ and $\phi = 90°$, respectively.

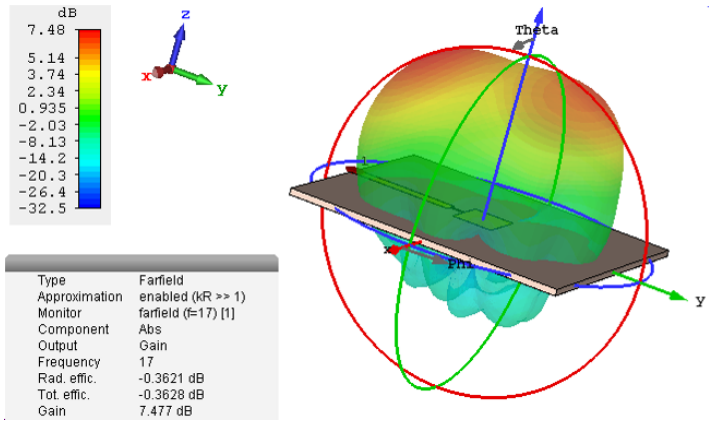

Figure 3.5: 3D radiation pattern of the patch antenna at 17 Ghz

3.2 Design of the inset-fed microstrip patch antenna

As observed in the previous feeding method, the edge impedance of the patch is high, which implies the use of an impedance transformer. The quarter wave-length transformer has the disadvantage of low bandwidth, since it will be a quarter wave-length just for a single frequency.

It is possible to feed the patch without the use of an impedance transformer, since the current is low at the edge of the patch and increases towards the centre. This leads to a lower impedance near to the centre of the patch [17]. Therefore, if the feeding point is near to the centre, the input impedance is lower, then it is not necessary to use an impedance transformer.

The Figure 3.6 presents a possibility to achieve a feed point near to the centre of the patch.

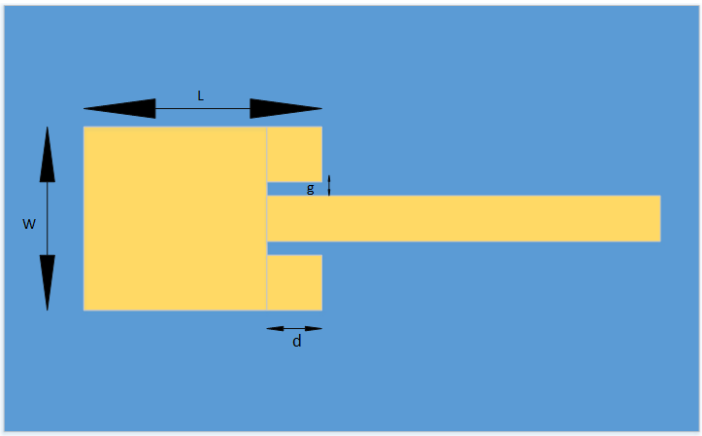

Figure 3.6: Schematic of inset-fed microstrip patch antenna

It is known *a priori* that *"For a fixed notch depth, the resonant input resistance decreases as the notch becomes wider"* [18]. Thus, the optimum impedance matching does not just depend of the feed point distance to the center of the patch it also determined on the notch parameters, the depth (d) and the gap width (g). Therefore, there are many possible solutions to obtain the desired 50Ω [18].

3.2.1 Design steps

The antenna parameters (W,L) are the ones calculated in the previous feeding method. The notch parameters were calculated following the steps and equations presented in [19].

Firstly, it was calculated the resistance seen at the edge of the patch antenna using the equations 2.6, 2.8 and 2.7 exhibited in section 2.1.1. The obtained input resistance was 221.97 Ω.

The observed input resistance depends on the notch depth. This dependence is define by a cosine-square function [18]. Therefore, by knowing the edge resonant resistance (Rin) of the patch and the pretended impedance to be seen at the feed port ($Z_0 = 50\Omega$) it is possible to obtained an approximation of the optimal notch depth, from equation 3.5.

$$Zo = Rin * \cos^2(\frac{\pi}{L} * d) \tag{3.5}$$

Finally, the notch width is calculated using the equation 3.6 [19].

$$g = \frac{c}{\sqrt{2 * \varepsilon_{ff}}} \frac{4 * 10^{-12}}{f} \tag{3.6}$$

The calculated parameters are listed in table 3.3.

Antenna Parameter	Value
W	6.62 mm
L	5.07 mm
Z_0	50Ω
W_{Z0}	2.17 mm
g	0.38 mm
d	1.77 mm
Minimum ground size	(11.3 x 9.75) mm

Table 3.3: Calculated antenna dimensions

3.2.2 Simulation and optimization

The antenna was simulated in CST MWS using as starting point the parameters presented in Table 3.3. The calculated parameters leaded to a non-satisfactory impedance matching of the antenna.

The physical notch introduced by the inset-fed have a big impact on the impedance matching of the antenna. Therefore, the notch parameters were adjusted to obtain the desired 50 Ω in the feed point. The length of the patch was also optimized to tune the operating frequency. The antenna dimensions achieved from this process are listed in table 3.4.

Antenna Parameter	Value
W	6.62 mm
L	5.24 mm
Z_0	50Ω
W_{Z0}	2.1 mm
g	0.32 mm
d	1.74 mm
Antenna size	(19.86 x 19.54) mm

Table 3.4: Design Parameters (optimized)

The antenna designed and simulated on CST MWS is presented in figure 3.7.

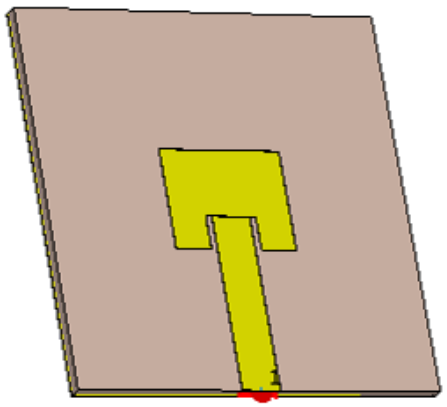

Figure 3.7: Microstrip patch with inset-fed implemented in CST MWS

Through the inset-fed method it was possible to achieve a good impedance matching, as it can be seen by the return loss of the antenna shown in figure 3.8.

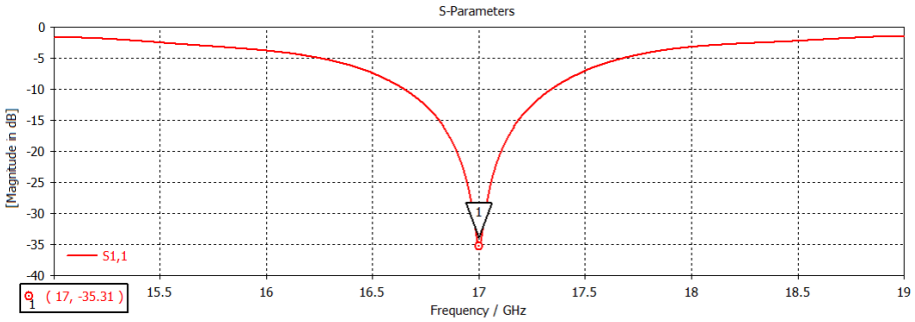

Figure 3.8: Return loss (S_{11}) of the patch antenna in dB with the frequency

The bandwidth achieved by this feed technique is 797 MHz (4.7 %). It is slightly bigger than the previous one, due to the absence of the quarter wave-length impedance transformer.

The radiation pattern of the antenna in the two main planes is presented in the figure 3.9. The antenna has a gain of 7.9 dBi, to the desired direction (θ=0°), and a radiation efficiency of 92.35%.

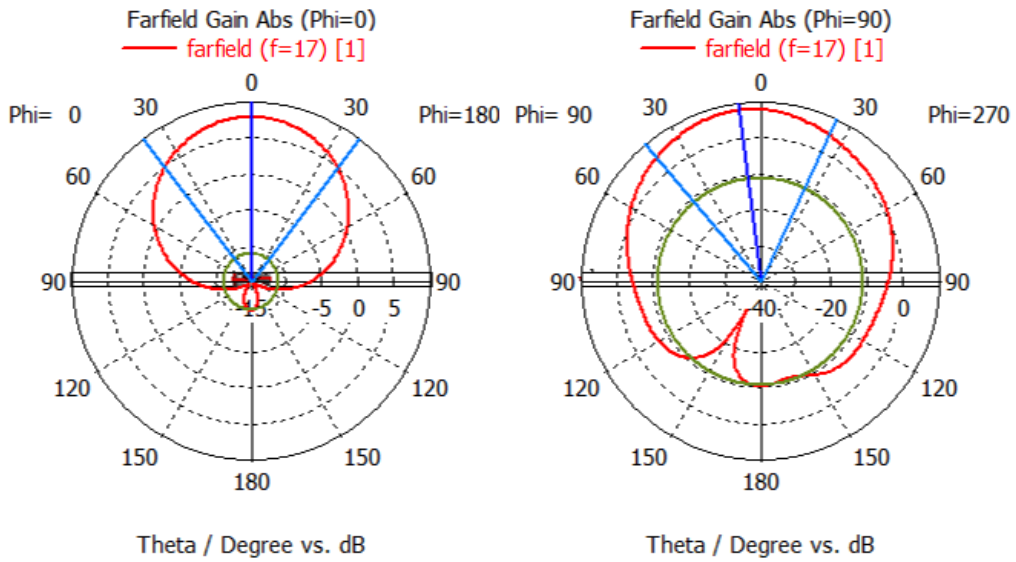

Figure 3.9: Vertical radiation pattern of the patch antenna at 17 GHz for $\phi = 0°$ and $\phi = 90°$, respectively

Once again it is possible to notice a deviation of the direction of maximum gain, in figure 3.9, that is created by the feedline.

The antenna presents a HPBW of 74.1° and 64.8° in cut plan of $\phi = 0°$ and $\phi = 90°$, respectively

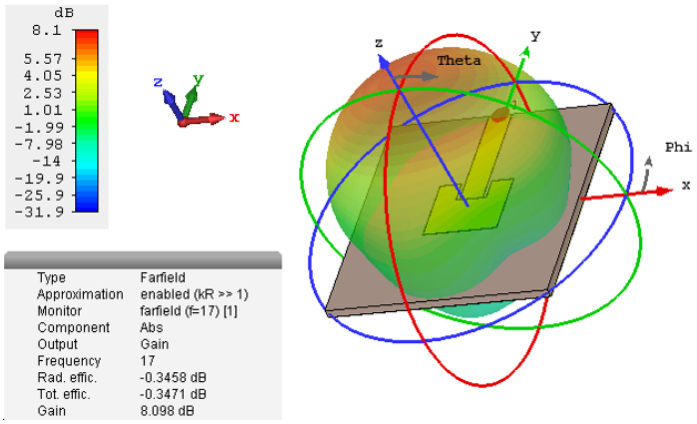

Figure 3.10: 3D radiation pattern of the patch antenna at 17 Ghz

3.3 Design of aperture coupling microstrip patch antenna

The last feed technique performed was a non-contact feed, named aperture coupling. As mentioned in Chapter 2, the antenna is composed by two layers, the patch substrate that is placed above the ground plane and the feedline substrate. The patch and the feedline are coupled through a slot created in the ground plane. This slot can have diverse shapes, for example circular, rectangular, H-shape or dog bone [23], [24]. Each shape conducts to a

distinct level of coupling.

In this work it was used the rectangular shape since it is simple to design and provides good levels of coupling [23].

The aperture coupling feed has a lot of dimension parameters that can be adjusted. They are listed as in [23] and can be seen in figure 3.11.

- Relative permittivity of the antenna substrate: Affects the antenna bandwidth and radiation efficiency. The work presented in [30] proved that the bandwidth and the permittivity are inversely proportional. Thus, a substrate with low permittivity provides a wider impedance bandwidth and improves the radiation efficiency.
- Thickness of the antenna substrate: With a thicker substrate, the coupling level is reduced but on the other hand it gives a better bandwidth. Increasing the thickness of the substrate the electromagnetic waves will be confined to the substrate leading to a decrease of the losses. Thus, increasing the bandwidth.
- Relative permittivity of the feed substrate: Should be high to achieve good proprieties for power transmission applications (5 to 10). With a high permittivity, the electromagnetic wave will be confined to the substrate since the difference between his permittivity and the air permittivity increases.
- Thickness of the feed substrate: It is recommended by Pozar [23] that it should be between 0.01λ and 0.02λ.
- Length of the patch: Controls the operating frequency of the antenna.
- Width of the patch: has a big impact on the impedance of the antenna, the directivity (wider patch increases directivity and presents lower resistance).
- Slot length: Has a big impact on the coupling level and the back-radiation level. Therefore, it should not be longer than the necessary.
- Slot width: Has some impact on the coupling level, usually its value is around 1/10 of the slot length.
- Position of the feed line and slot: For maximum coupling, the slot should be positioned in the centre of the patch and the feedline should be perpendicular to the slot.
- Length of the Stub: Eliminates the excess reactance of the antenna, usually the length of it is less than $\lambda_{eff}/4$.

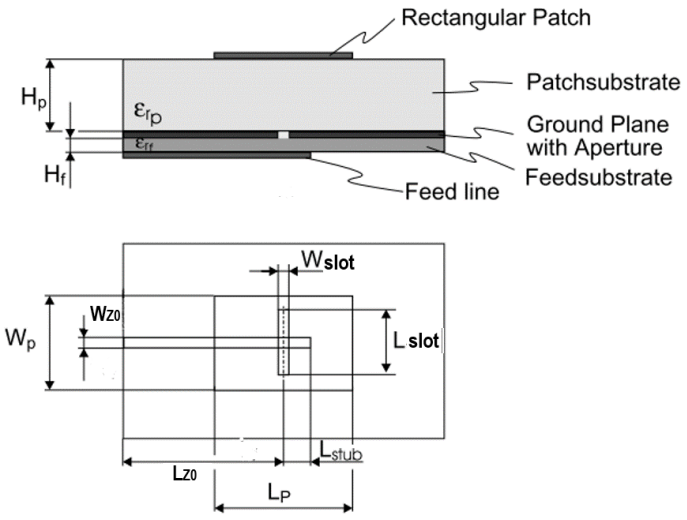

Figure 3.11: Top and side view of an aperture coupling feed microstrip antenna [31]

3.3.1 Design steps

In this work it was used the same substrate (Rogers RO4725JXR ϵ_r=2.55, h=0.78 mm), in the patch and feedline layers, to simplify the designed process. Therefore, the length and width of the patch are the same than in the previous feeding methods.

The feedline has an impedance of 50Ω. Its width was obtained using the TXline program.

As mentioned before, the Stub length should be shorter than a quarter effective wavelength. It was obtained by the following formula [24]:

$$Lstub = \frac{\lambda_{eff}}{4} - \Delta L \tag{3.7}$$

The slot calculation was performed in the following way [24]:

1. Assuming a slot width, in this work it was set to be 0.9 mm
2. The antenna parameters and the assumed width must obey to the following expressions:

$$0.006 \leq h/\lambda_0 \leq 0.06 \tag{3.8}$$

$$0.0015 \leq W_{slot}/\lambda_0 \leq 0.075 \tag{3.9}$$

$$2.22 \leq \varepsilon_r \leq 3.8 \tag{3.10}$$

3. Calculation of the slot wavelength:

$$\frac{\lambda_s}{\lambda_0} = 1.045 - 0.365\ln\varepsilon_r + \frac{6.3\left(\frac{W_{slot}}{h}\right) * \varepsilon_r^{0.945}}{238.64 + 100\left(\frac{W_{slot}}{h}\right)} - \left(0.148 - \frac{8.81\left(\varepsilon_r + 0.95\right)}{100 * \varepsilon_r}\right) * \ln(\frac{h}{\lambda_0}) \tag{3.11}$$

4. Slot length calculation:

$$L_{slot} = \frac{\lambda_s}{2} - 2 * \Delta \mathrm{L}slot \tag{3.12}$$

where $\Delta \mathrm{L}slot = 0.1 * \lambda_s$.

The antenna parameters obtained by these calculations are presented in the following table.

Antenna Parameter	Value
W	6.62 mm
L	5.07 mm
Wslot	0.9 mm
Lslot	3.99 mm
W_{z0}	2.17 mm
L_{z0}	12 mm
Lstub	2.54 mm

Table 3.5: Calculated antenna dimensions

3.3.2 Simulation and optimization

At this point the antenna was designed in CST MWS using the parameters presented in table 3.5. Once again, they leaded to non-satisfactory results, since the calculated parameters did not achieve a good impedance matching but they are a good starting point. The first approach to improve the performance of the antenna was studying the impact of each antenna parameter.

The first parameter studied were the patch dimensions (L,W) and it was possible to verify that the length of the patch controls the operating frequency of the antenna, as it can be confirmed in figure 3.12.

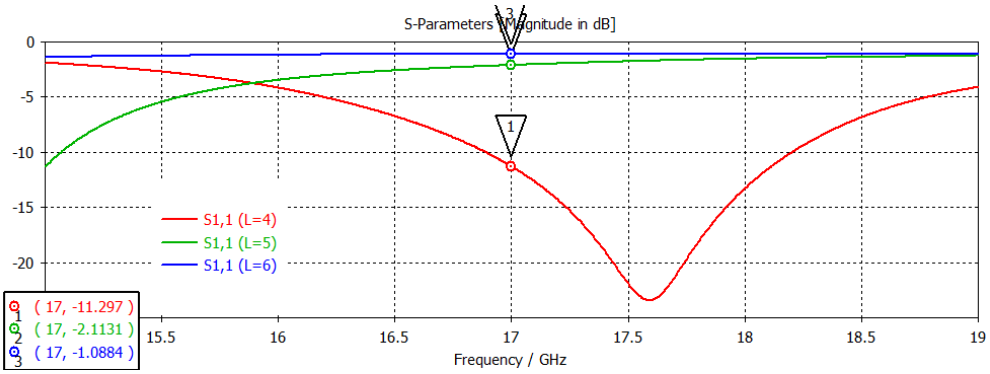

Figure 3.12: Return loss of the patch length sweep

The width of the patch has an impact on the impedance seen at the port as it can be seen in figure 3.13.

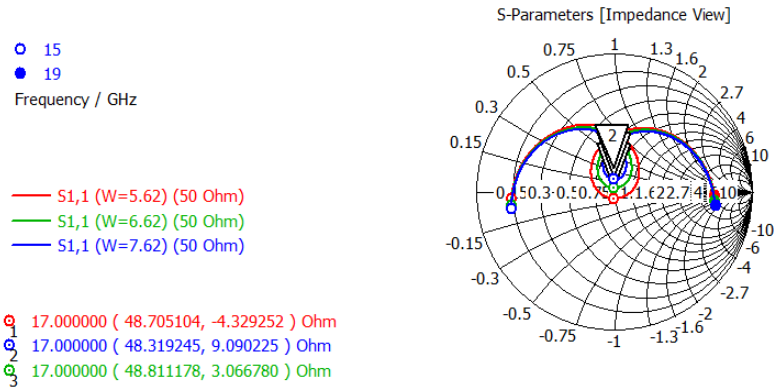

Figure 3.13: Smith chart of the patch width sweep

The next parameters studied were the slot dimensions. As it can be observed in figure 3.14, the slot width has a minor impact of the antenna in the antenna performance. However, it can be seen in figure 3.15 that has some impact on the coupling level. The coupling level is described by the radius of the slope presented on the smith chart, the bigger the radius, the bigger the coupling level [31].

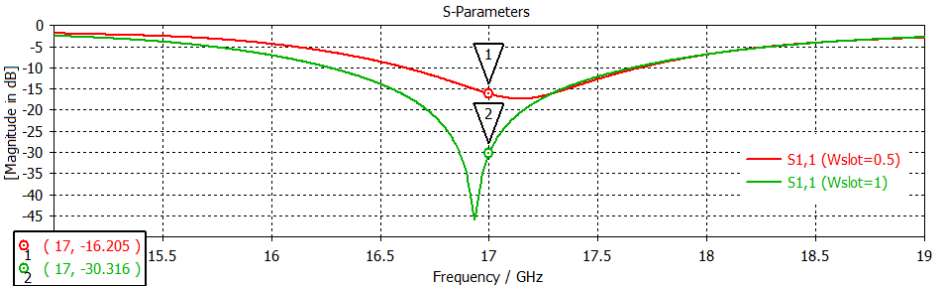

Figure 3.14: Return loss of the slot width sweep

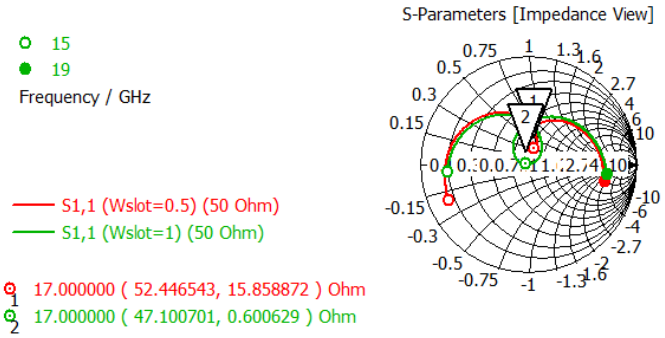

Figure 3.15: Smith chart of the slot width sweep

On the other hand, the length of the slot has a major impact in the impedance matching and operating frequency of the antenna. It controls the coupling level and it changes the impedance seen at the port. This can be confirmed observing the figures 3.16 and 3.17 .

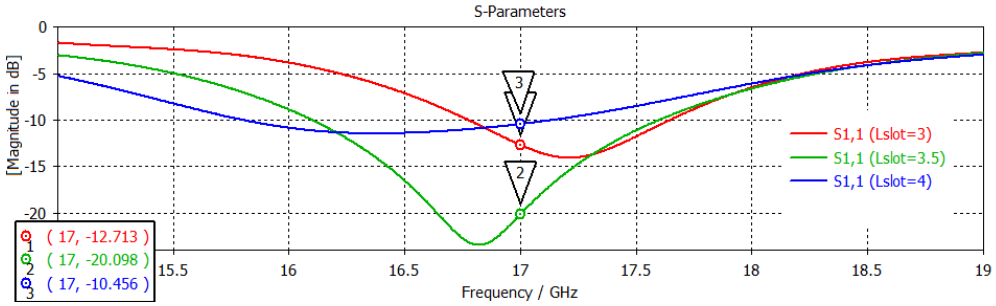

Figure 3.16: Return loss of the slot length sweep

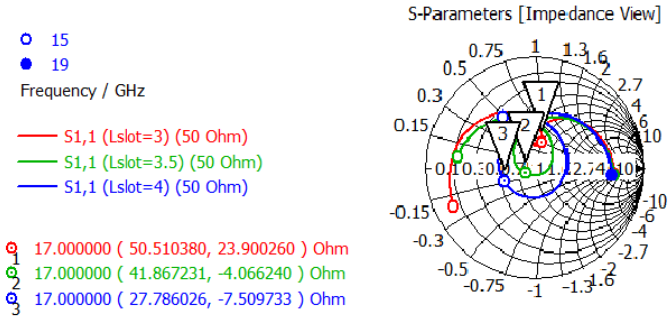

Figure 3.17: Smith chart of the slot length sweep

The last parameter analysed was the length of the stub, which has a major impact on the imaginary part of the impedance seen at the port.

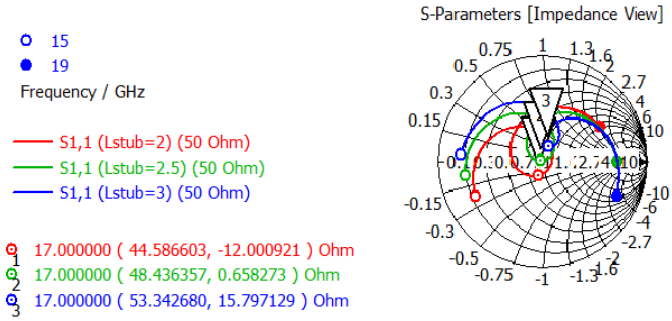

Figure 3.18: Smith chart of the stub length sweep

At this point the parameters of the antenna were optimized knowing that the more important parameters to achieve a good impedance matching are the slot and stub length. The optimized parameters that presented a good performance are presented in the following table.

Antenna Parameter	Value
W_p	6.62 mm
L_p	4.175 mm
Wslot	0.9 mm
Lslot	3.3 mm
W_{z0}	2.1 mm
L_{z0}	12 mm
Lstub	2.59 mm
Antenna size	(23.14 x 23.14) mm

Table 3.6: Design Parameters (optimized)

The figure 3.19 shows the antenna implemented in CST MWS. As it can be observed, the substrate of the patch was made shorter than the substrate of the feedline to be possible to solder the Subminiature version A (SMA) connector in the construction of the antenna. The four holes will be used to maintain both the layers together after the fabrication process trough screws.

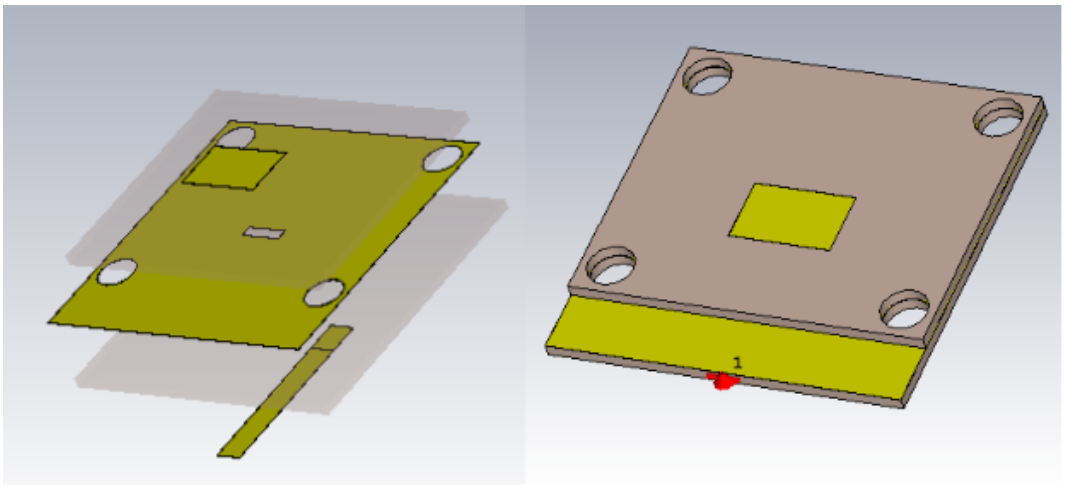

Figure 3.19: Microstrip patch with aperture coupling feed implemented in CST MWS (Layer and compact view)

The changes in the antenna structure did not have an impact on the impedance matching of the antenna, since the antenna presents a S_{11} of -46.2 dB at the 17 GHz, as it can be seen in figure 3.20. The simulated antenna presents a bandwidth of 1.38 GHz.

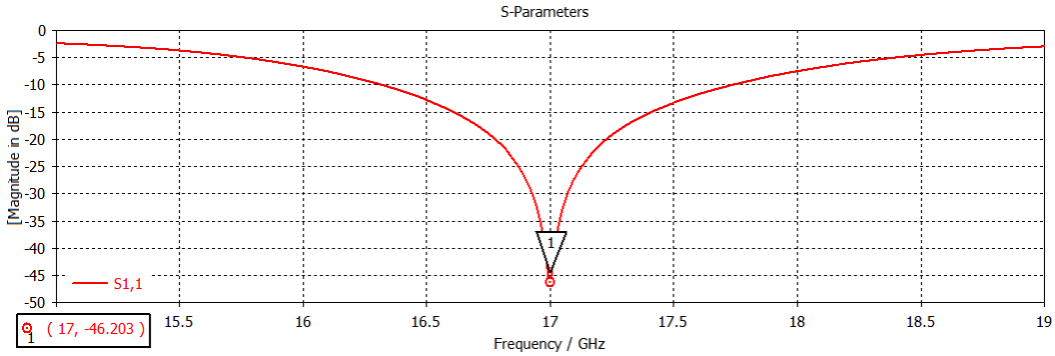

Figure 3.20: S_{11} of the patch antenna in dB referring to the frequency

This feeding method prevents the degradation of the radiation pattern by the feedline. However, the adjustment made in the antenna structure, such as shortening the patch substrate relative to that of the feed line, had some impact on the radiation pattern as it is possible to observe in Figures 3.21 and 3.22.

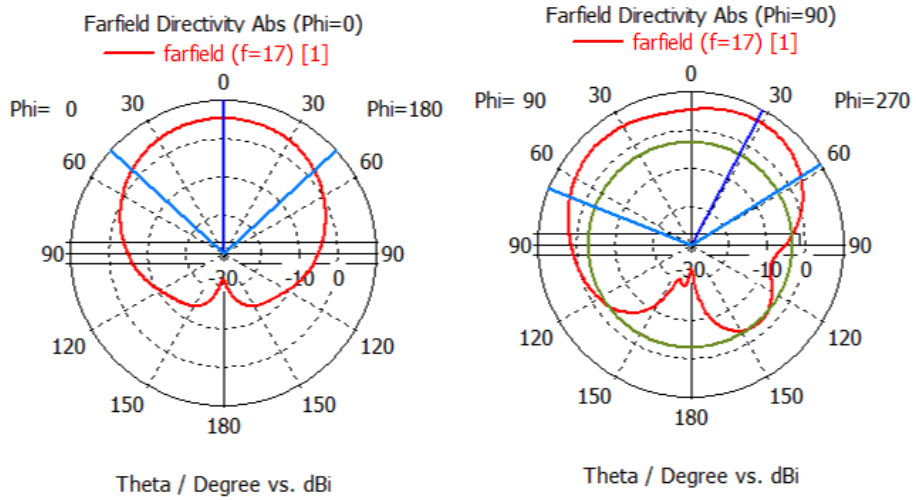

Figure 3.21: Vertical radiation pattern of the patch antenna at 17 GHz for $\phi = 0°$ and $\phi = 90°$, respectively

The antenna has a gain of 5 dBi at (θ=0°,$\phi = 0°$), having a radiation efficiency of 95 %.

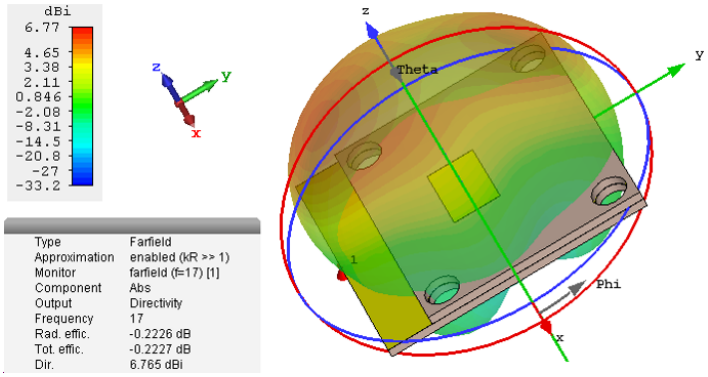

Figure 3.22: 3D radiation pattern of the antenna at 17 GHz

In terms of the HPBW, the antenna presented 94.50° and 126.40° for the cut angle of ϕ 0° and 90°, respectively.

3.4 Comparison of the feeding methods

To facilitate the comparison of the feeding methods the performance parameters are listed in the table 3.7.

All the feeding methods present a good impedance matching. By analysing the gain and bandwidth there are two feeding methods that stand out, the aperture coupling and the inset-fed. The aperture coupling presents the highest bandwidth, twice as high as the other feeding methods, the inset-fed presents the highest gain, around 3 dB above the other feeding methods.

As mentioned before, one of the advantages of using the 17 GHz band is the possibility of achieving higher bandwidths, which enables the increase of the bit rate and prevents the channel overlapping in in Wi-Fi solutions.

The aperture coupling feed is used to improve the bandwidth in circular polarized microstrip patch antennas [32]–[34]. To improve the reliability of the communications of Wi-Fi applications independently of the direction of the source, at these frequencies, there may be a requirement to use circular polarized antennas. The generation of circular polarization in patch antennas can be done easily through some modifications in the feeding structure. Therefore, the aperture coupling method was chosen to be used in the remaining work.

Parameter	Aperture coupling	Inset-fed	Transformer feed
Bandwidth(MHz)	1380	797	711
Directivity(dBi)	5.2	8.3	5.3
Gain(dBi)	5	7.9	4.9
Radiation efficiency	0.95	0.93	0.92
S_{11}(dB)	-46.20	-35.31	-37.80
Impedance seen at port(Ω)	49.92+0.48i	50.85+i1.51	50.80-i1.03

Table 3.7: Performance parameters of the simulated antennas

3.5 Practical test

To close this chapter and test the fabrication process the simulated antennas was produced.

For connectorization was used an SMA connector was used to inject the signal into the antenna.

Figure 3.23 shows the prototype of the microstrip patch antenna feed using a quarter wavelength transformer already with the SMA connector applied.

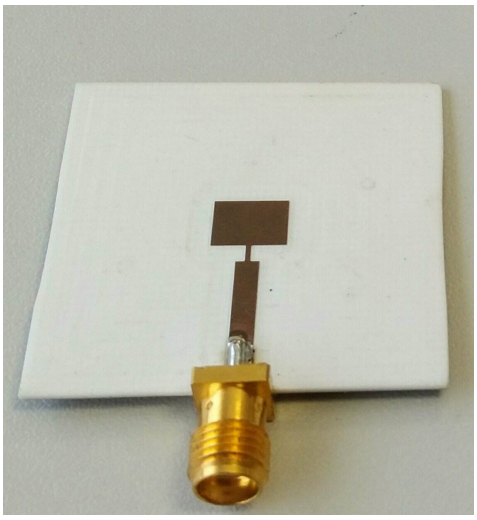

Figure 3.23: Prototype patch antenna with microstrip feedline using a $\lambda/4$ impedance transformer

The prototype of the inset-fed method with the SMA connector attached is presented in figure 3.24.

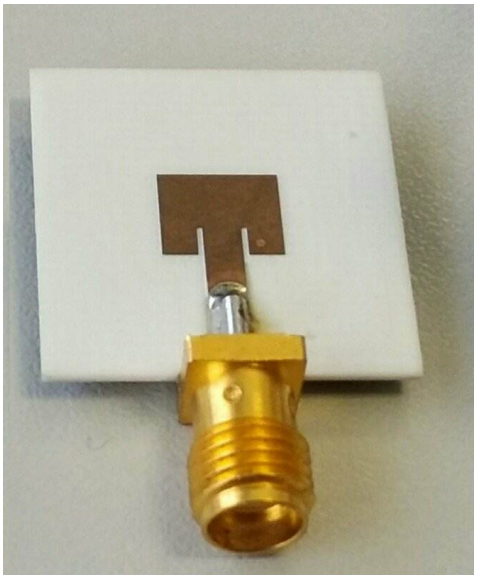

Figure 3.24: Developed patch with inset-fed

Finally, it is presented the aperture coupling feeding method prototype. It is shown a view of the final configuration, the ground plane where the slot is placed and a view of the feedline and stub.

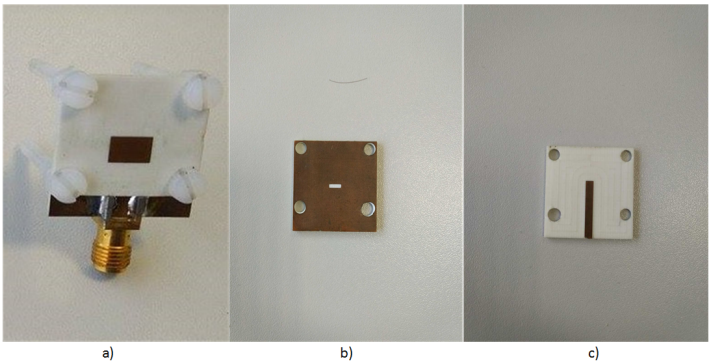

Figure 3.25: Prototype aperture coupling patch antenna

To analyse the performance of each antenna the return loss was measured using a Vector Network Analyser (VNA) .

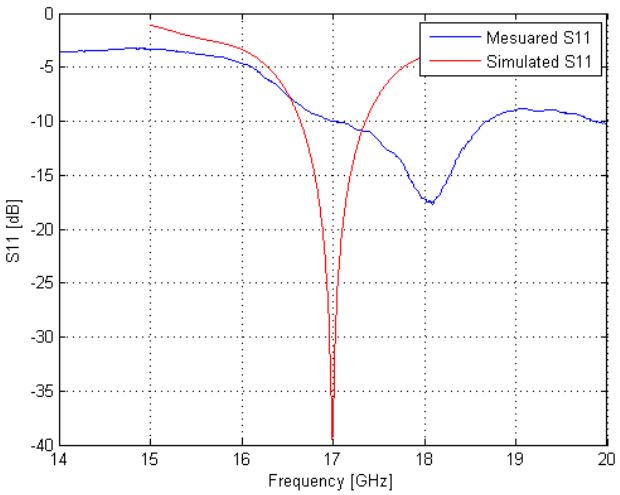

Figure 3.26: Measured S_{11} of the patch antenna with microstrip feedline using a $\lambda/4$ impedance transformer

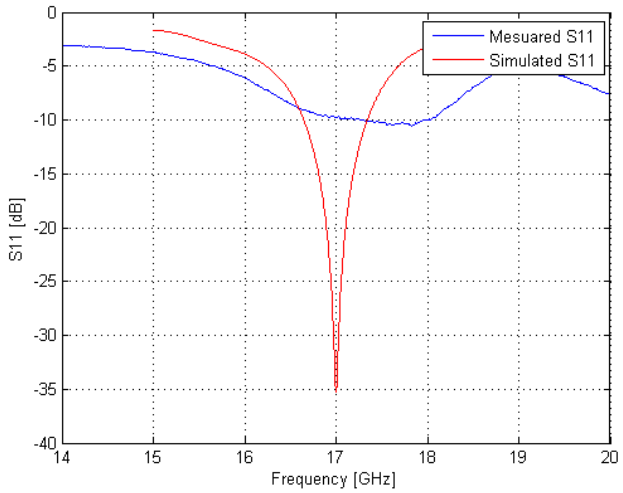

Figure 3.27: Measured S_{11} of the patch antenna with inset-fed

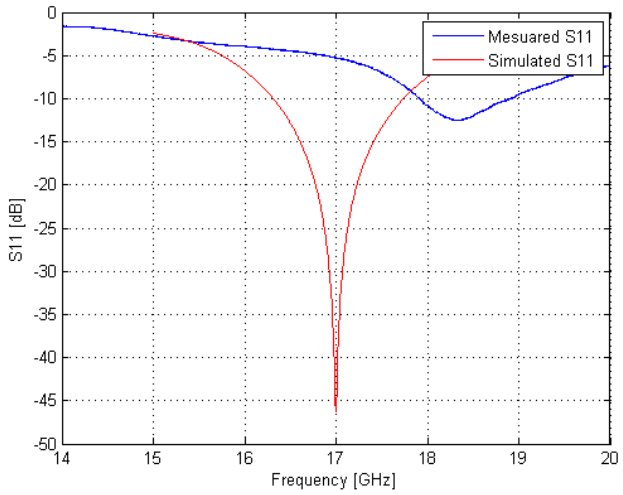

Figure 3.28: Measured S_{11} of the aperture coupling patch antenna

Observing the figures 3.26, 3.27 and 3.28 it can be seen a deviation of 1GHz in the operating frequency and all of them present a return loss far from the ones obtained in the simulation.

The poor practical results obtained may be due to:

- Antenna fabrication with low precision: the CNC uses a conical tool that decreases the precision of fabrication, modifying the dimensions of the antenna.
- The substrate can have different characteristics than those used in the simulation, since the loss tangent of the substrate is 0.0026@10GHz and the antennas are operating 7 GHz above.
- The SMA connector was not considered during the simulations.

Chapter 4

Antenna for indoor Wi-Fi applications

To improve the reliability of the communications of Wi-Fi applications independently of the direction of the source, at these frequencies, there may be a requirement to use circular polarized antennas. Circular polarized antennas are less propitious to depolarization, being an advantage for environments in which are present the multipath phenomenon and atmospheric attenuations (for outdoor application). They also does not require to have the transmitting antenna and receiving antenna in the same orientation (it prevents the misalignment) [34], [35].

It is desired that indoor Wi-Fi antennas provides a gain between 0 and 6 dBi, they also have to be small and low-profile due to the limited space and aesthetic concerns. Antennas that have circular polarization should present a high isolation level between the orthogonal components [8].

As mentioned in Chapter 2, the circular polarization is obtained by exciting two orthogonal modes simultaneously. In microstrip antennas there are several configurations to obtain it. The circular polarization in aperture coupling microstrip antennas can be obtained by a single feed using crossed slots or by using two orthogonal feeds [23].

It was demonstrated by [36] that it is possible to obtain circular polarization with two orthogonal non-overlapping slots in a square patch using a 90° hybrid coupler, also known as off-centered slot feed [23]. A problem of this approach is the structure asymmetry that deteriorates the axial ratio and limits the polarization purity [23].

Another approach is the crossed slot configuration, it is formed by a single microstrip feed placed diagonally to the cross [23], [27]. This approach leads to good polarization bandwidth, it does not create asymmetry on the patch antenna and it is more simple to design than the off-centered solution [23].

Figure 4.1 shows the most well-known configurations, that can be used to achieve circular polarization on microstrip patch antennas.

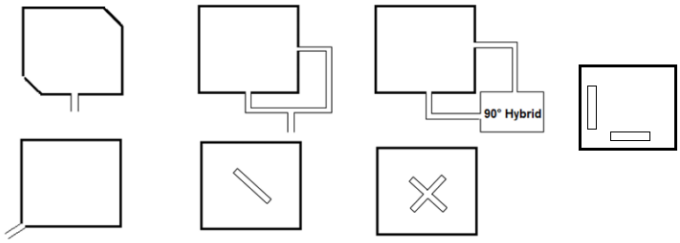

Figure 4.1: Possible configurations to achieve circular polarization in microstrip patch antennas [27]

4.1 Aperture coupling microstrip patch antenna with crossed slot

Before starting the design of the crossed slot configuration, some changes were done on the aperture coupling microstrip patch antenna, designed on chapter 3. The characteristic impedance was changed to 100 Ω to simplify the work in the antenna array design performed in chapter 5. Instead of using a rectangular patch it was used a square patch, because the cross-slot requires the use of nearly squares or circular patches [37]. The square patch was achieved by making the width of the patch equal to the length of the patch, since the length of the patch defines the operating frequency of a microstrip antenna. To achieve a good impedance matching the slot and stub were adjusted. The designed antenna and their dimensions parameters are presented in figure 4.2 and table 4.1, respectively.

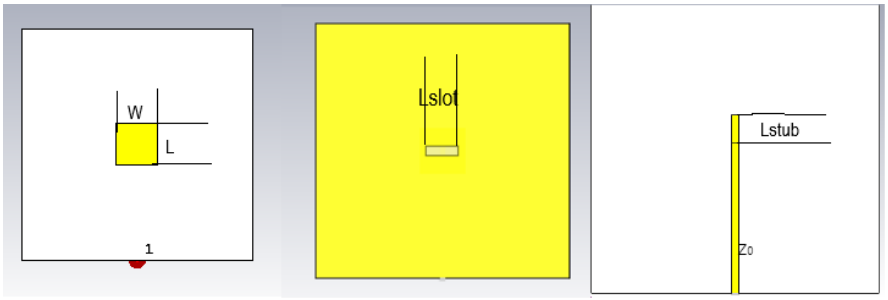

Figure 4.2: Aperture coupled microstrip square patch antenna

Antenna Parameter	Value
W	4.175 mm
L	4.175 mm
Wslot	0.80 mm
Lslot	3.00 mm
Z_0	100Ω
W_{z0}	0.55 mm
L_{z0}	12.00 mm
Lstub	2.30 mm

Table 4.1: Parameters of the aperture coupling square patch with a feed line of 100 Ω

Figure 4.3 shows the structure of a microstrip patch antenna with a cross-slot on the ground plane. The crossed slot is centered with the patch, and shifted 45° with respect to the microstrip feedline.

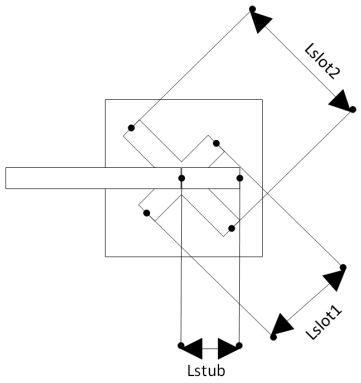

Figure 4.3: Geometry of a aperture-coupled microstrip square patch antenna with crossed slot

The structure of the antenna is shown in figure 4.4, where it is possible to observe that the antenna is divided into five layers: 3 metal layers (patch, ground plan and feed line) separated by 2 dielectric layers.

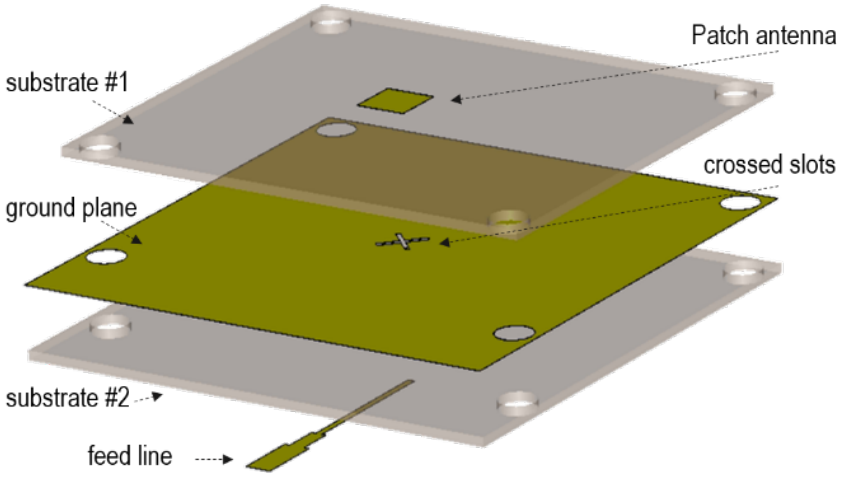

Figure 4.4: Antenna structure of a aperture-coupled microstrip square patch antenna with crossed slot

4.1.1 Parametric study and design steps of the cross slot patch antenna

As a primary test, the antenna was simulated in CST MWS using the same dimensions for the both slots. However, it resulted into a bad impedance matching and bad axial ratio (it is defined in chapter 2). Therefore, a study on the impact of each parameters on the antenna was performed. To simplify this study, the slot width was set to be 10 % of the respective slot length.

Then the impact of the cross-slot parameters was investigated starting by the shorter slot (Lslot1). It is possible to conclude, observing the figures 4.5 and 4.6, that the length of the short slot has a considerable impact on the return loss of the antenna and a major impact on the axial ratio.

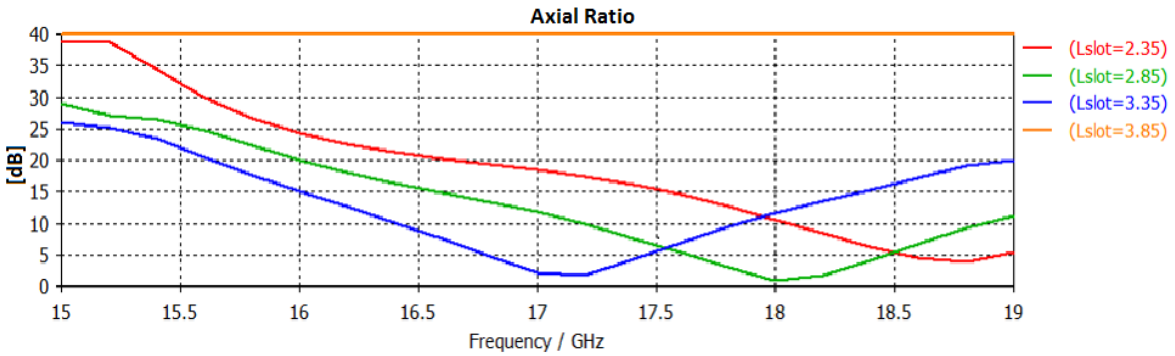

Figure 4.5: Sweep of the Lslot1 and its influence on the axial ratio

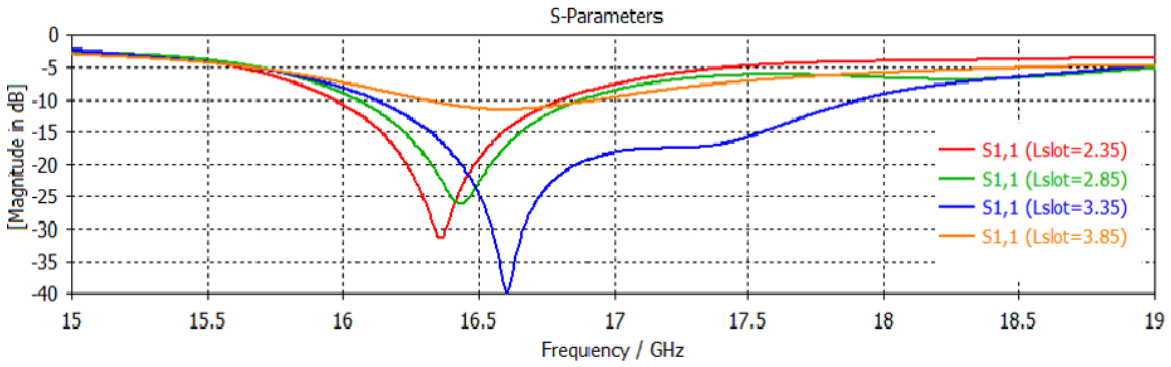

Figure 4.6: Sweep of the Lslot1 and its influence on the S_{11} level

The length of the longer slot has a impact on the return loss and the axial ratio of the antenna, as it can be seen in figures 4.7 and 4.8.

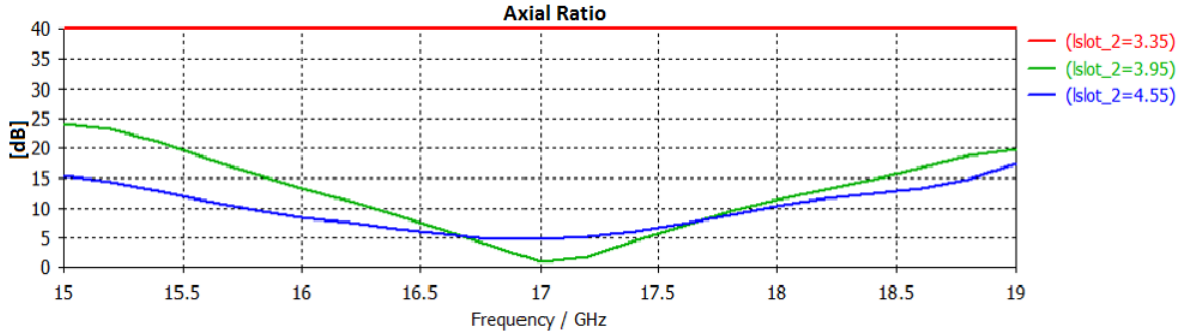

Figure 4.7: Sweep of the Lslot2 and its influence on the axial ratio

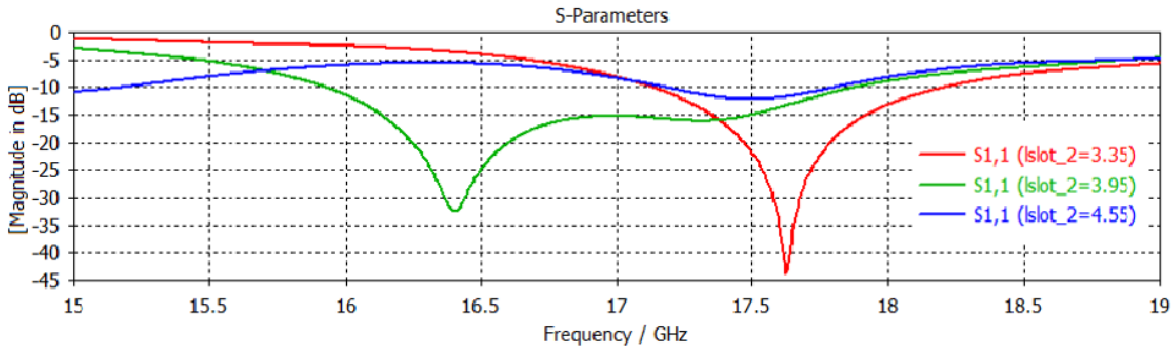

Figure 4.8: Sweep of the Lslot2 and its influence on the S_{11}

Observing the figures 4.5 to 4.8 it is possible to conclude that the bandwidth and the operating frequency depends on the slot length, since it defines the amount of coupling between the feedline and the patch. As it is mentioned in [37], *"the resonant frequency of the microstrip patch depends on the coupling slot?s length"*.

The axial ratio, in the patch antenna with crossed slots, is controlled not by the individual slot length, but by the ration between them, as mentioned by [27], [37], [38].

The length of the stub (*Lstub*) only affects the impedance matching of the antenna, as it can be concluded by looking at figures 4.9 and 4.10.

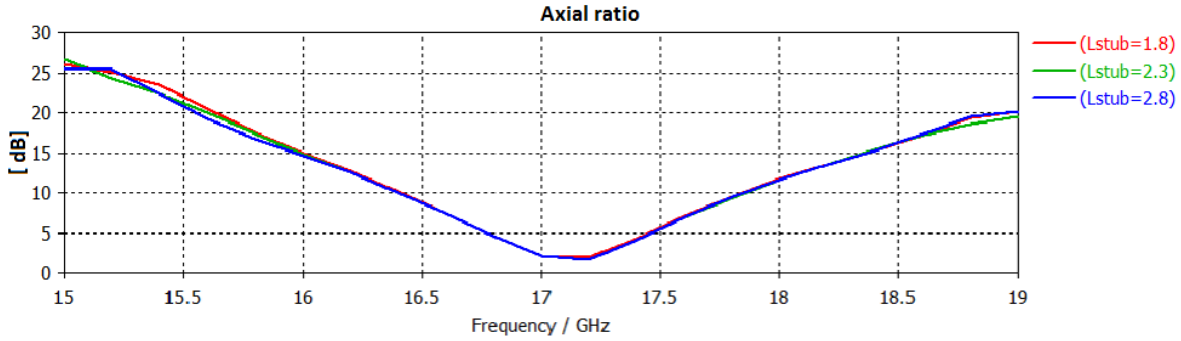

Figure 4.9: Sweep of the Lstub and its influence on the axial ratio

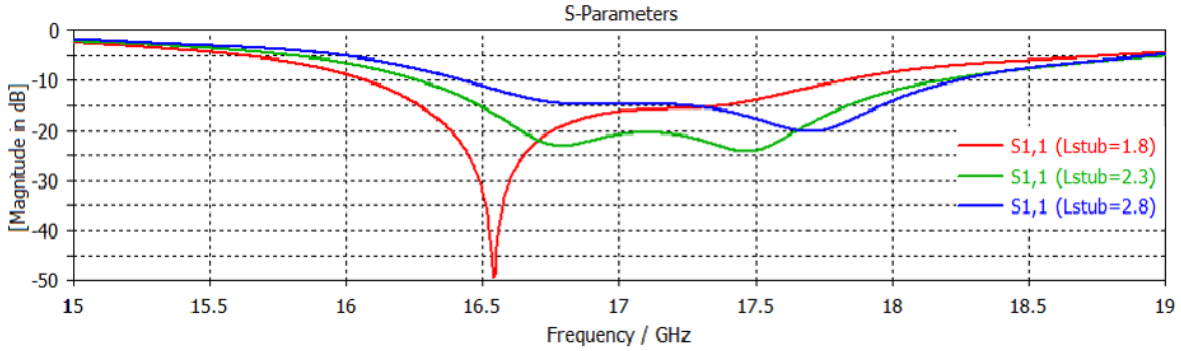

Figure 4.10: Sweep of the Lstub and its influence on the S_{11}

At this point adjustments to the antenna were performed to reach a good impedance matching and an axial ratio below 3 dB. The procedure presented in [38] was followed.

The length of each slot (Lslot1, Lslot2) depends on the ratio Ks, and average of the slots lengths (La), that will define the amount of coupling, and is given by the equations 4.1 to 4.3. The average of the slot length will define the size of each slot, therefore it will define the amount of coupling (*"slot resonance"* [38]). The slot ratio, as already concluded before, *"acts on the conditions required for CP operation"*[38].

Slot ratio:

$$K_s = \frac{Lslot_2}{Lslot_1} \tag{4.1}$$

Length of the shorter slot:

$$Lslot_1 = \frac{2 * L_a}{K_s + 1} \tag{4.2}$$

Length of the longer slot:

$$Lslot_2 = \frac{2 * L_a * K_s}{K_s + 1} \tag{4.3}$$

Therefore, the primary step was to find the La dimension that led to a good amount of coupling. By using the parameter sweep tool of CST MWS the La dimension that presented

a better result in terms of impedance matching was 3.65 mm. Then, using the same method described, the slot ratio that allows to achieve a good polarization level was found to be between 1.1 and 1.2. The dimensions of the designed antenna are presented in table 4.2.

Antenna Parameter	Value
W	4 mm
L	4 mm
La	3.65 mm
Ks	1.15 mm
Z_0	100 Ω
W_{Z_0}	0.55 mm
L_{Z_0}	12.00 mm
Lstub	2.10 mm
Zport	(97.30+0.50)Ω
Antenna size	(48.06 x 48.06) mm

Table 4.2: Calculated dimensions of the microstrip patch with crossed slot

However, the antenna at this point is matched to 100 Ω and for manufacturing it is desired to be matched to 50 Ω. Thus, it was used a quarter wavelength transformer to obtain the desired 50 Ω. It was used a quarter wavelength transformer of 70 Ω that corresponds to a microstrip line with a length of 3.11 mm and 1.25 mm of width, calculated using the TXLINE program.

The SMA connector was considered on the antenna structure designed in CST MWS, as it can be seen in figure 4.11, it presented an impedance of 52.31 Ω. The SMA connector deteriorated the imaginary part of the impedance seen at the port. So, to solve this problem without changing the antenna structure it was adjusted the length of the impedance transformer (2.2 mm).

4.1.2 Simulation results

The antenna designed in CST MWS is shown in the following figure.

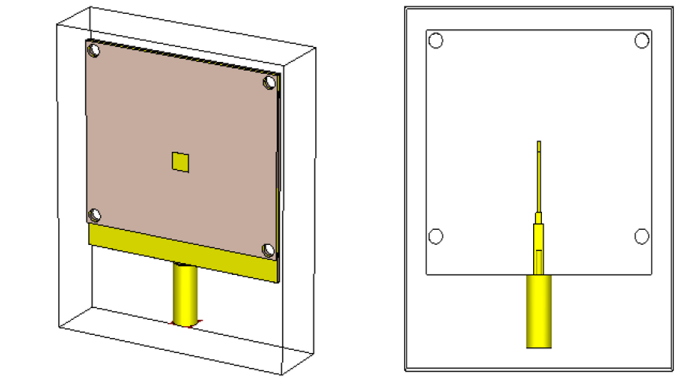

Figure 4.11: Aperture coupling microstrip patch antenna with crossed slot implemented in CST MWS (front and back view)

With the cross-slot configuration it was possible to obtain a good impedance matching, the antenna presents a return loss of -25.9 dB at 17 GHz and an impedance bandwidth of 2.3 GHz (from 15.9 GHz to 18.2 GHz), as it can be verified in figure 4.12 .

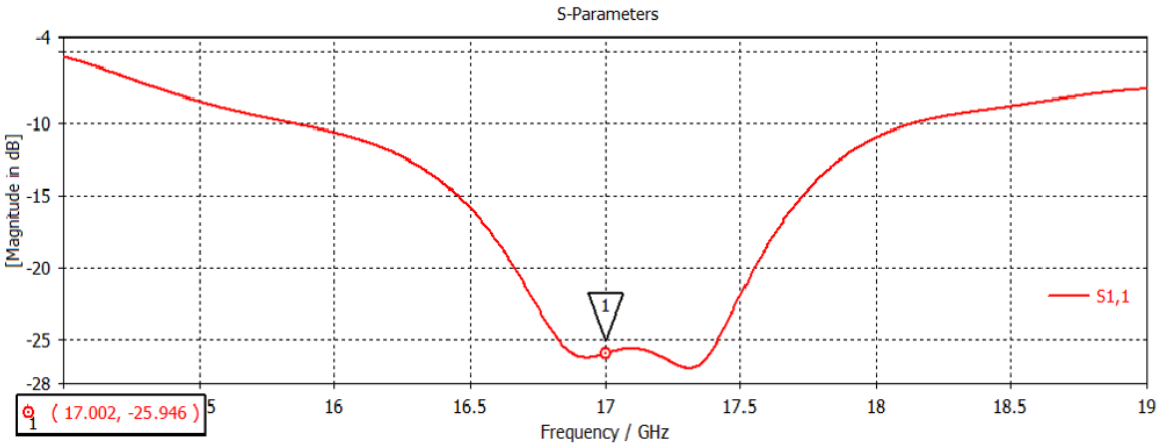

Figure 4.12: S_{11}(dB) of the microstrip patch antenna

It was also possible to achieve an axial ratio of 0.56 dB at 17 GHz as it can be seen in figure 4.13. The axial ratio measures the quality/purity of the circular polarization.

The axial ratio bandwidth is about 500 MHz (16.8 GHz to 17.3 GHz). Therefore, the antenna has the desired characteristics between 16.8 GHz and 17.3 GHz, where it presents a good impedance matching and circular polarization.

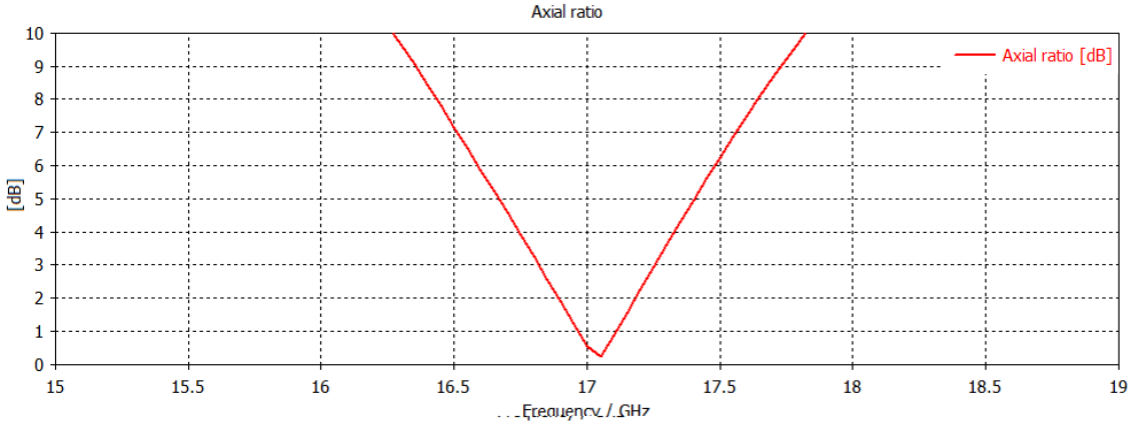

Figure 4.13: Axial ratio[dB] of the patch antenna

In what concerns the circular polarization, by analysing the radiation pattern of the figure 4.14 it is possible to verify that the antenna presents RHCP with a left-hand component rejection of 29.9 dB with respect to θ=0°.

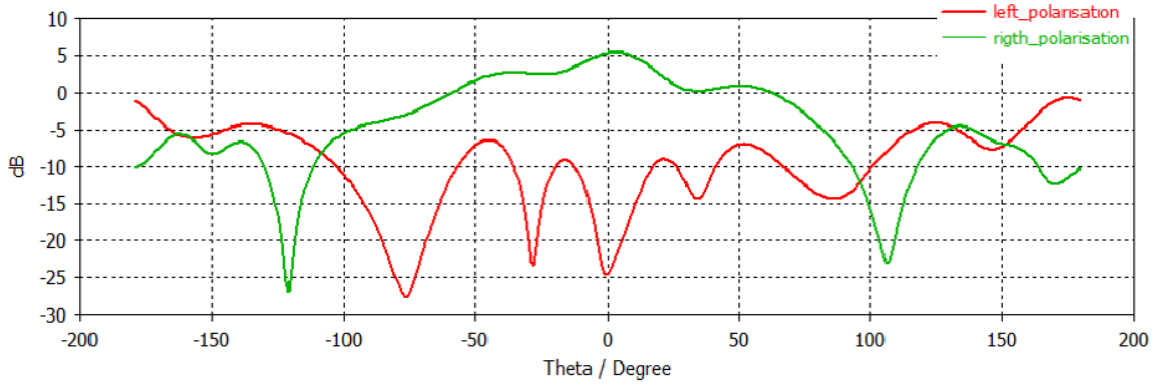

Figure 4.14: Right-hand and left-hand components of the microstrip patch antenna

The antenna has a gain of 5.3 dBi, a directivity of 5.8 dBi in the boresight direction and a radiation efficiency of 89% at the operating frequency (17 GHz). A HPBW of 64°, considering the cut plane of ϕ=0° and 53.8° considering the cut plane of $\phi = 90°$.

It is possible to see the degradation of the radiation pattern created by the SMA connector, the reduction of the patch layer size and the four holes created on the antenna structure in figures 4.15 and 4.16, since the maximum gain is obtained to the direction of θ=4.02°.

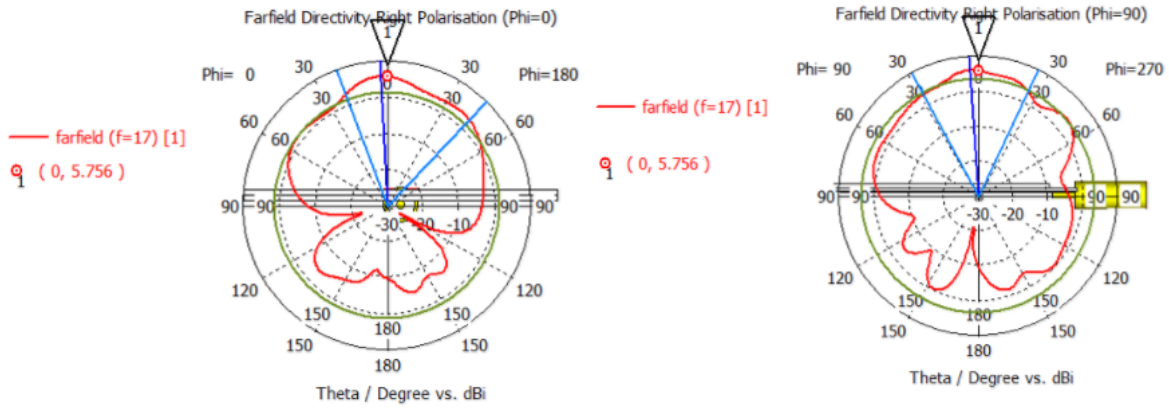

Figure 4.15: Vertical radiation pattern of the patch antenna at 17 GHz for $\phi = 0°$ and $\phi = 90°$

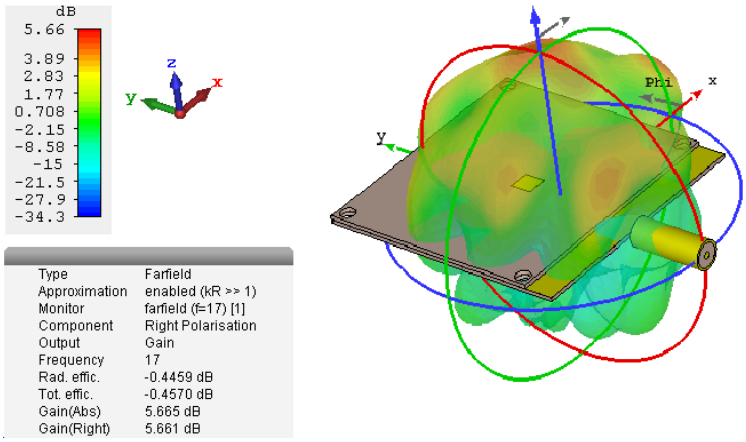

Figure 4.16: 3D radiation pattern of the antenna at 17 GHz

4.1.3 Practical results

The antenna simulated above was manufactured and it is presented on figure 4.17.

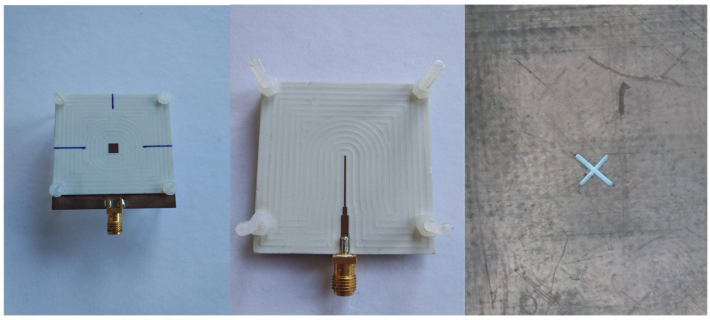

Figure 4.17: Developed microstrip patch antenna with a crossed slot (front, back and ground view)

It was only possible to measure the return loss of the antenna using a VNA. For the rest of the parameters (gain, radiation pattern and polarization) it was not possible to execute any measurement. Therefore, nothing can be concluded about the antenna performance besides the impedance matching.

Once again, it is possible to conclude that the practical return loss has a similar behaviour to the simulated results with deviation of 1 GHz, as it can be observed in figure 4.18.

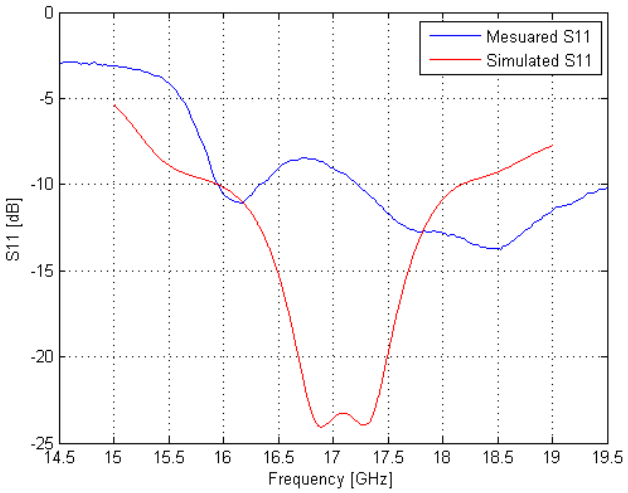

Figure 4.18: Measured S_{11} vs simulated S_{11}

As it can be noticed considering the SMA connector in the simulations did not have a big impact on the practical results. Therefore, this reason was discarded.

Thus, the poor practical results may be due to:

- Antenna fabrication with low precision: the CNC uses a conical tool that decreases the precision of fabrication, modifying the dimensions of the antenna. This can be noticed, for example, on the cross-slot fabricated since they do not present a rectangular shape.

- The substrate can have different characteristics than those used in the simulation.

Study of the manufacturing error

In order to investigate the impact of the fabrication precision on the antenna performance, the antenna dimensions were measured at the microscope using a caliper with a precision of 10 μm. It was verified a difference between the simulated and the real dimensions, as observed in table 4.3.

Parameters	Simulated dimensions	Measured dimensions
W	4.00 mm	3.96 mm
L	4.00 mm	3.96 mm
$W_{100\Omega}$	0.55 mm	0.42 mm
$W_{50\Omega}$	2.10 mm	1.96 mm
$W_{\lambda/4}$	1.25 mm	1.13 mm
L_{slot1}	3.40 mm	3.50 mm
L_{slot2}	3.90 mm	3.93 mm
W_{slot1}	0.34 mm	0.35 mm
W_{slot2}	0.39 mm	0.40 mm

Table 4.3: Simulated vs measured antenna dimensions

At this point, a simulation of the antenna was performed using the measured dimensions. As it can be observed in figure 4.19, the S_{11} of the antenna with the measured dimensions approached the practical S_{11} measured.

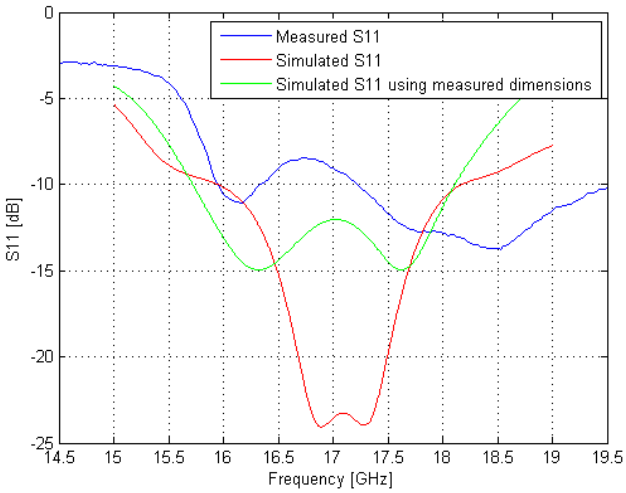

Figure 4.19: Measured S_{11} vs Simulated S_{11} vs Simulated S_{11} using the measured dimensions

It can be noticed that the manufacturing error is different depending on the antenna layer. Starting by the patch layer, it is verified that the measured dimensions are 40 μm smaller than the pretended ones, which justifies the frequency deviation.

On the feeding layer, it is observed a reduction around 130 μm in the microstrip line width of the feed network. This phenomenon will affect mainly the impedance matching that corresponds to a degradation of the S_{11} parameters.

Finally, on the ground layer where the crossed slots are placed it is detected bigger slot dimensions than the pretended ones. This is observed since in the previous cases the conical tool was following an outline wearing more copper than the necessary. On the other hand, in the slot creation the conical tool is generating a "hole" in the ground plane, increasing its dimensions.

Besides the error in the dimensions, it was also noticed an error in the slot elliptical shape considering it was intended to have rectangular slots, yet the fabrication process leaded to elliptical slots. This was recreated on the simulation, as presented in figure 4.20. The error in the slots will have a major impact on the impedance matching and operating frequency of the antenna, since the coupling level and the impedance seen by the feedline will change.

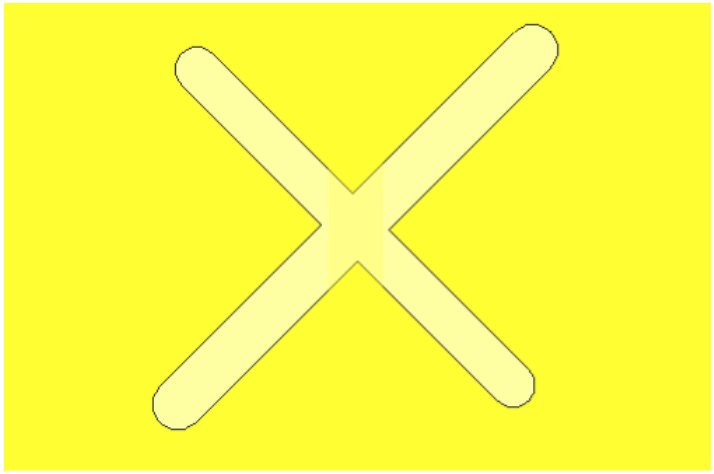

Figure 4.20: View of the crossed slots with a elliptical shape

In summary, it was verified that the manufacturing process had an impact on the antenna performance. However, it was not the only cause for the poor performance of the antenna in terms of impedance matching. The practical S_{11} presented a bigger deviation and degradation than the one obtained in the simulation with the measured dimensions, probably because of some variation of the simulator to the reality.

Note that the manufacturing error may vary since it depends on the configuration of the machine and the wear of the tool. A possibility to circumvent this problem is to design the antenna with elliptical slot shape and manufacture several antennas with different dimensions (in general bigger than the one obtained in simulation) at the same time, in order to find one with the intended performance. This procedure was not performed since it was not possible to analyze the impact of this error in the other antenna parameters (i.e. axial ratio, gain).

4.1.4 Conclusions

The microstrip antenna with the cross-slot developed in this work is an antenna with low profile that can be applied, for example, on a wall. It presents a gain of 5.3 dBi and a omnidirectional coverage in the boresight direction (figure 4.16).

It is also desired that antennas with polarization diversity present a high rejection level between the polarization components [8]. The developed antenna has an isolation between the right and left component of 29.9 dB. Thus, the antenna reveals a high rejection level between orthogonal polarization components and good RHCP proprieties.

It is possible to say that the antenna developed at this point is well suited for indoor Wi-Fi applications.

4.2 Aperture coupling microstrip patch antenna with off-centered feed using a 90° quadrature Hybrid

This configuration is more difficult to design and to achieve polarization purity due to the asymmetry created by this configuration on the patch antenna. However, it will be studied in this work since it allows to choose the orientation of the circular polarization of the antenna

(RHCP or LHCP) without making any change in the antenna structure. This configuration can be advantageous to reuse the spectrum and for MIMO applications.

The off-centered feed method is formed by a square patch above a ground plane where the two non-overlapping off-centered slots are placed and a feed network is placed on the bottom layer, as its shown in figure 4.21. The feed network is composed by a power divider that creates a 90° shift between the ports that feed the slots, which will excite two orthogonal propagation modes creating circular polarization. In this work, it will be used the quadrature (90°) hybrid, also known as branch-line hybrid.

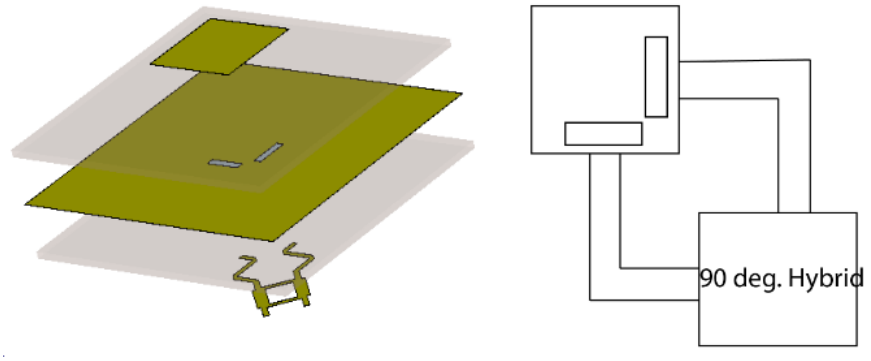

Figure 4.21: Structure and schematic of the Aperture coupling microstrip patch antenna with off-centered slots

4.2.1 The quadrature (90°) hybrid

Quadrature hybrids are four-port devices that present a high degree of symmetry and any port can be used as input [14], [39]. The output ports will be the ones placed in the opposite side of the device from the input port [39]. The quadrature hybrids are classified as a 3 dB directional coupler with 90° phase difference between the output ports.

Considering that the signal is applied at the port 1 and the port 4 is terminated with a match load, the signal is equally divided in amplitude between the ports 2 and 3 but they present a phase difference of 90° [14]. If an eventual mismatch at patch occurs, the reflected wave coming from the patch tends to be absorbed at the load of port 4. Therefore the axial ratio is not degraded [14].

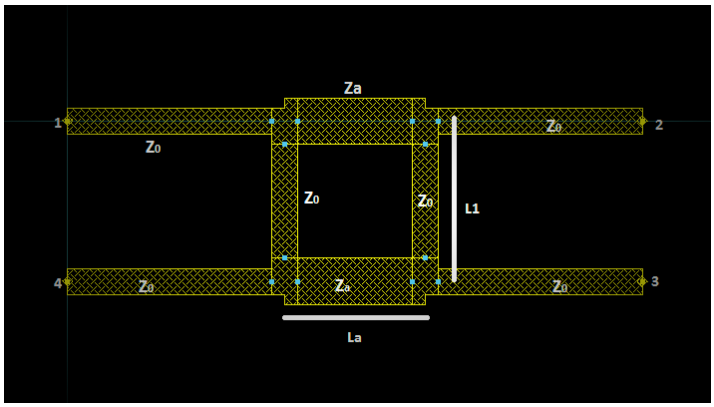

Figure 4.22: Schematic of a quadrature hybrid

Design steps

At this point the quadrature (90°) hybrid was designed standalone to validate this operation. Later it was included in the feed network (section 4.2.2).

To calculate the dimension/impedances it was followed the procedure presented in [39]. The first step is to choose the characteristic impedance (Z_0) of the branch-line hybrid. The length of the lines L1 and La is set to be $\lambda/4$ at the operating frequency (17 GHz for this work) and the branch-line impedances are calculated by the following formula [39].

$$Z_a = \frac{Z_0}{\sqrt{2}} \tag{4.4}$$

In a first approach, the characteristic impedance was set to be 50Ω but it led to an impractical solution since the distance between the microstrip line was too short, as it can be verified in figure 4.23. This enables the occurrence of coupling between them, degrading the operation of the branch-line hybrid coupler. Therefore, the characteristic impedance was set to be 100Ω. This led to an impedance of 70.71Ω (Z_a) for the branch-lines.

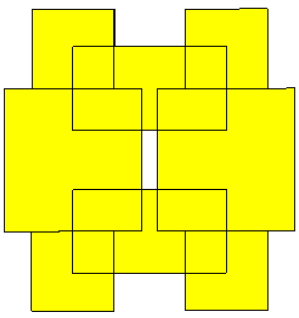

Figure 4.23: Designed quadrature hybrid structure in CST MWS using $Z_0 = 50\Omega$

Initially this structure was simulated on ADS using ideal microstrip lines. The parameters used are listed in the table 4.4.

Z_0	Za	W_{Z_0}	Wa	L1	La	L_{Z_0}
100Ω	70.71Ω	0.63 mm	1.13 mm	2.79 mm	2.79 mm	2 mm

Table 4.4: Design parameters of the hybrid obtained on ADS

Observing the following figures 4.24 and 4.25 it is possible to conclude that a good performance was obtained. It presents a 3 dB power division in ports 2 and 3 and a good isolation and return loss in ports 4 and 1. The phase difference between the ports 2 and 3 is 90°.

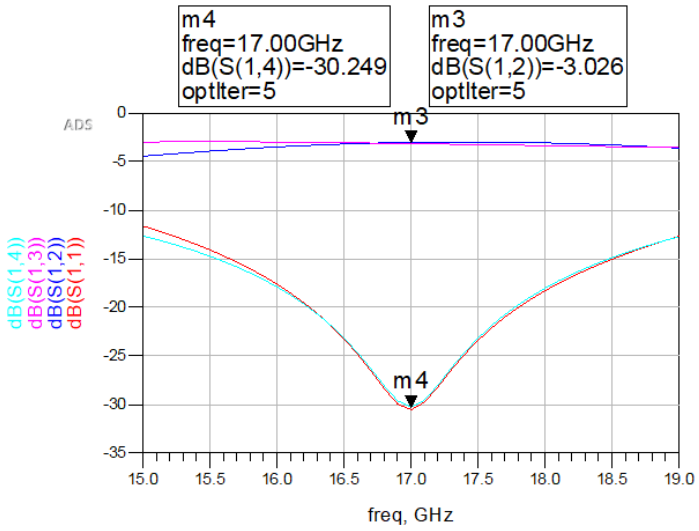

Figure 4.24: Simulation of the losses in quadrature hybrid

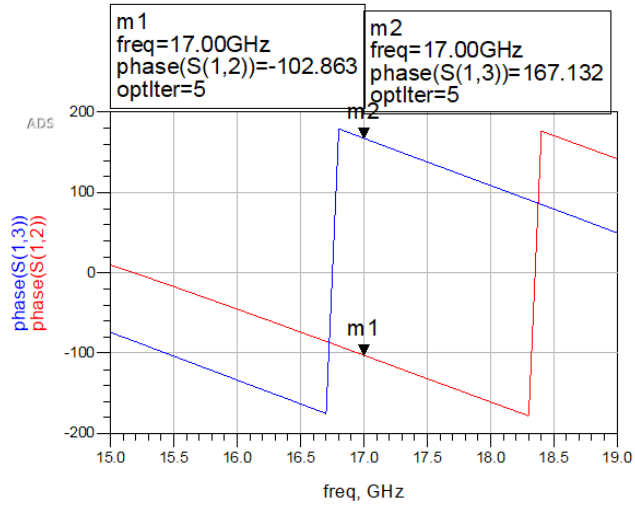

Figure 4.25: Phase at the port 2 and 3 of the quadrature hybrid

However, when the structure was translated to CST MWS, the same good operation was not accomplished. Therefore, it was performed an optimization that led to the following parameters and results.

Z_0	Za	W_{Z_0}	Wa	L1	La	L_{Z_0}
100	70.71	0.55 mm	0.9 mm	3.9 mm	3.6 mm	2 mm

Table 4.5: Design parameters of the hybrid obtained in CST MWS

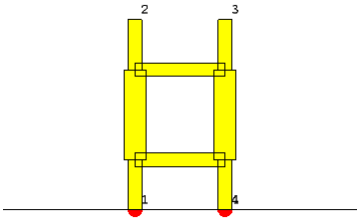

Figure 4.26: Designed quadrature hybrid structure in CST MWS

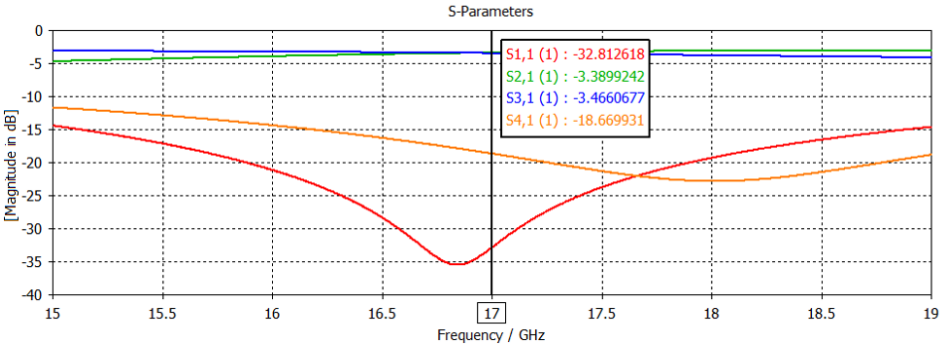

Figure 4.27: Simulation of the losses in quadrature hybrid

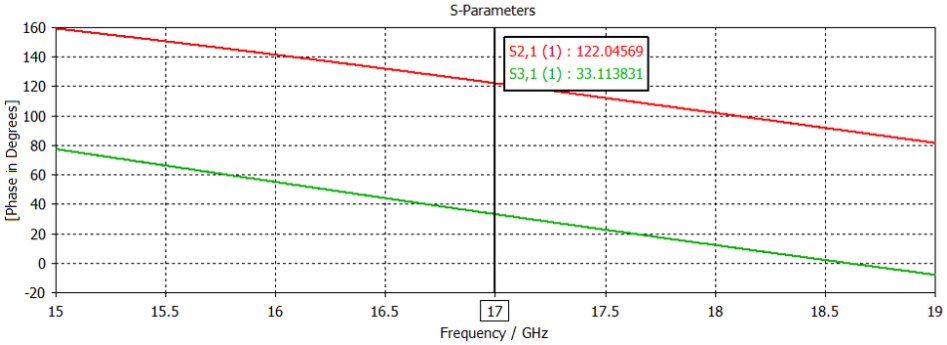

Figure 4.28: Phase at the port 2 and 3 of the quadrature hybrid

As it can be observed in figures 4.27 and 4.28 it was achieved a good power division at the ports 2 (-3.4 dB) and 3 (-3.5 dB) having a phase difference of 89° between them that was considered acceptable. The port 4 presents an isolation of -18.7 dB and the port 1 has a return loss of -32.8 dB. Therefore, the quadrature hybrid coupler has a satisfactory performance.

4.2.2 Microstrip patch antenna with off-centered slots design

It was considered the square patch designed in section 4.1 as a starting point, which dimensions are listed in table 4.1. Then, modifications in this square patch were produced structure to achieve the configuration of the off-centered slots presented in figure 4.21. The structure adjustments were done following the steps presented in [40]. Note that at this point the feed network is formed only by two feedlines (one for each slot) and the phase difference is created by a CST MWS tool and not by the quadrature (90°) hybrid.

It was noticed that the rectangular slots were overlapped, which is not desired as mentioned by [23]. It was not possible to ensure circular polarization and impedance matching, since the overlapping slots presented an unpredictable behaviour. There were made several attempts to avoid the slots interception from changing the dimensions of the slots, shifting the slots to changing the patch dimensions. However, all of them led to unsatisfactory results.

Therefore, the shape of the slot was changed from a rectangular slot to an H-shaped slot. The H-shape slot was first designed by using a single feed line placed at the center of the patch, as it is illustrated in figure 4.29. The antenna dimensions obtained are listed in the table 4.6.

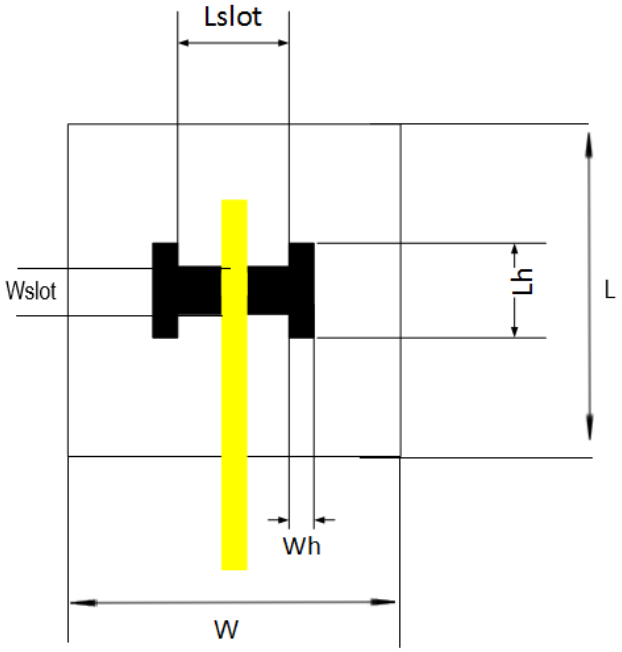

Figure 4.29: Schematic of the H-shaped slot

Antenna Parameter	Value
W	4.24 mm
L	4.24 mm
Lslot	1.60 mm
Wslot	0.48 mm
L_H	0.99 mm
W_H	0.55 mm
Z_0	100 Ω
W_{Z0}	0.55 mm
L_{Z0}	12.00 mm
Lstub	2.46 mm

Table 4.6: Dimensions of the aperture coupling patch antenna with a H-shaped slot

The off-centered slot configuration, shown in figure 4.21 was designed but at this time it was used the H-shaped slots instead of the rectangular slots. Once again it was verified that the slots were overlapped.

The last possibility to avoid the interception of the slots was to change the slot configuration. Therefore, the configuration presented in figure 4.30, proposed by [41], showed to be possible to obtain circular polarization, impedance matching and to avoid the interception of the slots.

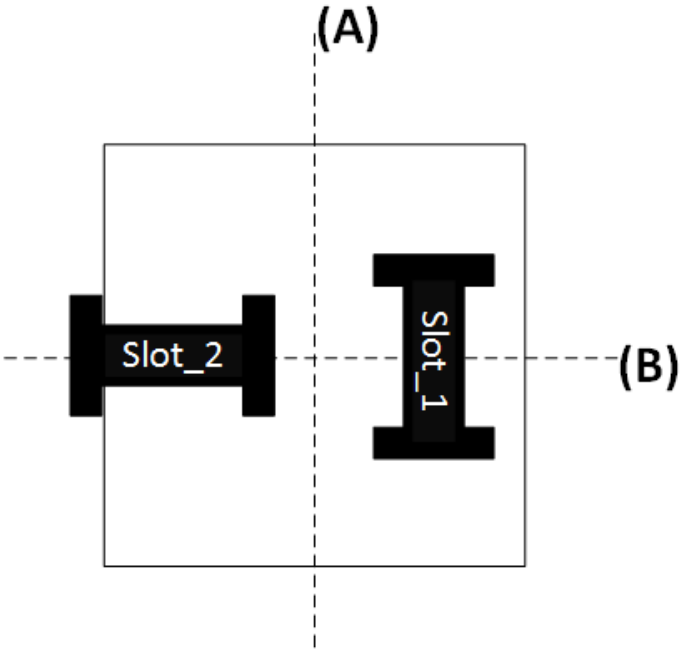

Figure 4.30: Schematic of the used slot configuration

As it can be observed in figure 4.30, there were traced two symmetry axes of the square patch ((A), (B)). The axis (A) divides the patch in two symmetric parts and in each one it was placed one slot centered in the symmetry axis (B), with orthogonal positions (horizontal, vertical), also referred as T configuration [41].

It was expected that the circular polarization would be obtained with the slots in symmetric positions in relation to the shaft(A), in order to guarantee a higher level of symmetry of the antenna structure. This was verified since it was possible to obtain circular polarization, having a distance of 1 mm from the center of each slot to the center of the patch. This was the shortest distance that avoided the interception of the slot and guarantee that the slots were immediately under the patch, as can be verified in figure 4.33 .

Regarding the impedance matching, in the T configuration each of the slots presents a different position relatively to the patch antenna, leading to a different impedance seen by each slot. Therefore, the $slot_1$ and $slot_2$ (figure 4.30) show different dimensions, that presented in table 4.7.

As mentioned before, until this point the feed network was formed by only two straight microstrip lines and the phase difference between the ports was created using a CST MWS capability. Therefore, at this point the final feed network was designed, which incorporated the quadrature (90°) hybrid previously projected.

The steps performed to obtain the feed network presented in figure 4.32 were the following:

- The first step was to design the microstrip lines that were responsible for the "connection" between the slots and the ports 2 and 3 (figure 4.26) of the quadrature (90°) hybrid. It was ensured that the offset between the ports 1-3 and 2-4 (figure 4.31) were the same or the opposite in order to guarantee that the phase difference of the signal at each slot was created exclusively by the quadrature (90°) hybrid. A couple of adjustments in the patch dimensions, slots dimensions and position were made to guarantee the circular polarization and impedance matching.

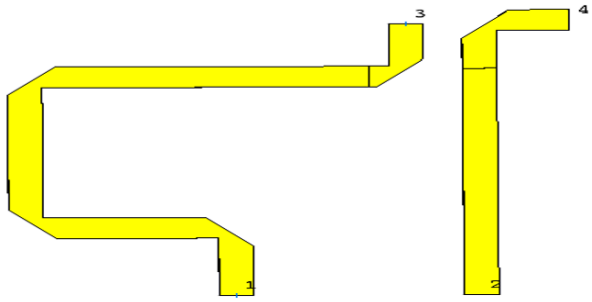

Figure 4.31: Microstrip line responsible for the connection between the slots and the quadrature hybrid

- Then, the quadrature hybrid was inserted in the antenna structure and the performance of this structure was tested. It was possible to obtain a good circular polarization, impedance matching and good isolation level between the input ports.

- The last step was to change from an impedance of 100Ω to the desired 50Ω through quarter wavelength impedance transformers. The impedance value observed in ports 1((115.16+24i) Ω) and 2((89.37-17.37i) Ω) was different, which led to a different quarter wavelength impedance transformers. Both impedances seen at these ports were not purely real. Therefore, the impedance transformers adjusted to compensate this phenomenon. The theoretical values of the quarter wavelength impedance transformers were used as starting points, obtained by the TXline software.

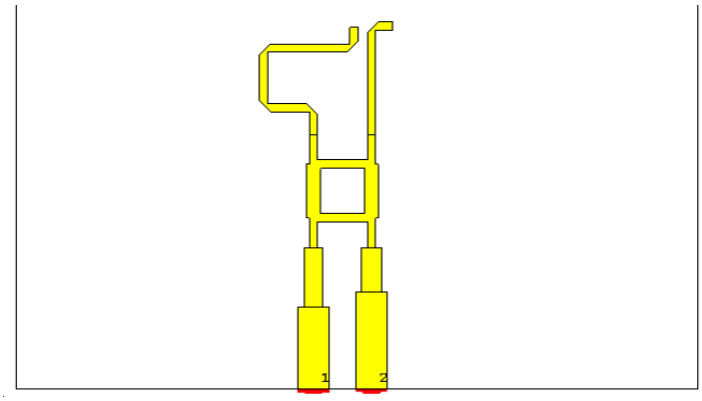

Figure 4.32: Designed feed network for the off-centered configuration

All the antenna dimensions are listed in the table 4.7.

Antenna Parameter	Value
W	4.1 mm
L	4.1 mm
L_{slot1}	1.88 mm
W_{slot1}	0.48 mm
L_{slot2}	1.34 mm
W_{slot2}	0.43 mm
LH_{slot1}	1.30 mm
WH_{slot1}	0.39 mm
LH_{slot2}	1.64 mm
WH_{slot2}	0.45 mm
Position of the horizontal slot	1 mm form the center of the patch
Position of the vertical slot	1 mm from the center of the patch
$Lstub_{slot1}$	1.99 mm
$Lstub_{slot2}$	2.71 mm
$W_{\lambda/4(port1)}$	1.20 mm
$L_{\lambda/4(port1)}$	3.98 mm
$W_{\lambda/4(port2)}$	1.39 mm
$L_{\lambda/4(port2)}$	3.00 mm
Antenna structure size	(45.77 x 45.77) mm

Table 4.7: Dimensions of the designed antenna

4.2.3 Simulation results

After all the design steps performed the antenna structure and feed network were designed and simulated in CST MWS. The produced antenna in the simulation environment can be observed in figure 4.33.

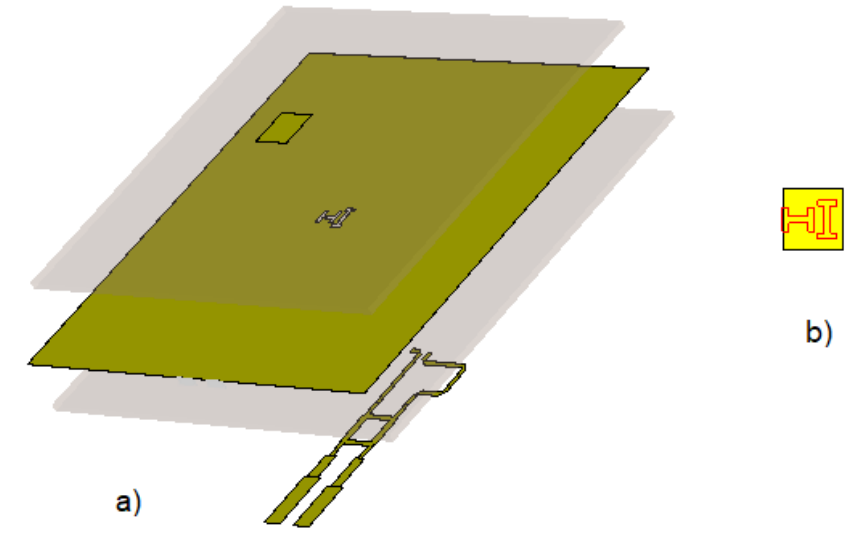

Figure 4.33: a) Designed antenna structure in CST MWS; b) Slot position relatively to the patch

Through the simulations results it is possible to take the first conclusions about the antenna performance.

In what concerns the impedance matching, by observing figure 4.34 it is possible to conclude that a good return loss was obtained, either when the signal was injected in the port 1 (-21.9 dB@17GHz) and when the signal was applied to port 2 (-29.87@17GHz). It was also achieved a good isolation between port 1 and port 2 (-22.3 dB@17GHz) as it can be observed by the parameters S12 and S21 (that are the same) presented in figure 4.34. The antenna presents a different impedance bandwidth depending on which port the signal was applied. Considering that the signal was applied in port 1, the antenna presented an impedance bandwidth of 3.33 GHz [15 GHz,18.33 GHz]. Now considering that the signal was applied in port 2 the antenna presented an impedance bandwidth of 2.86 GHz [16.14GHz,19GHz].

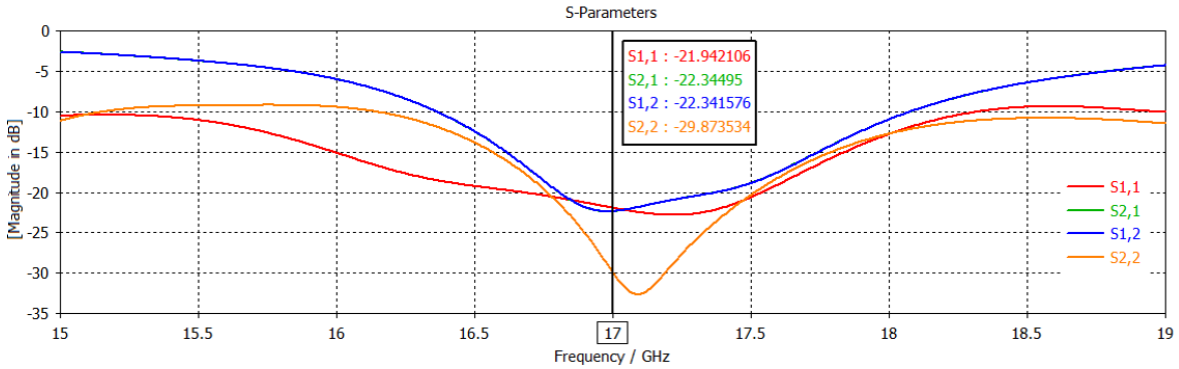

Figure 4.34: S-parameters of the microstrip patch antenna with off-centered feed using a 90° quadrature Hybrid

In terms of the antenna polarization, it is possible to observe the axial ration of the

antenna in figure 4.35, which for the intended operating frequency presents a value of 1.37 dB. The axial ratio bandwidth is 1.32 GHz (8%) between 16.39 GHz and 17.71 GHz, which corresponds to the antenna bandwidth either for the LHCP and RHCP cases.

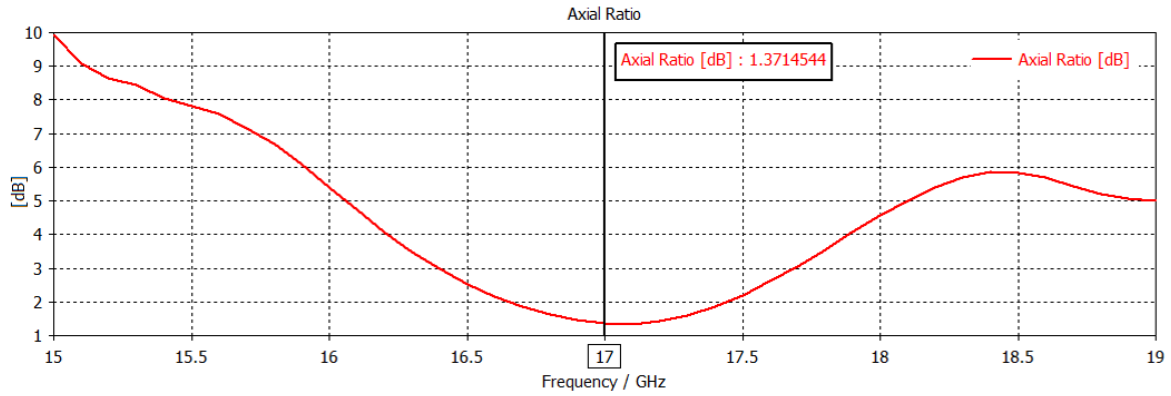

Figure 4.35: Axial ratio of the patch antenna

As mentioned before the configuration used in this antenna allowed to choose the orientation of the circular polarization.

Regarding the LHCP, it was obtained when the signal was applied in port 2 and the port 1 was terminated by a matched load. The antenna presented a right-hand component rejection of 23.7 dB in respect to θ=0° (figure 4.36).

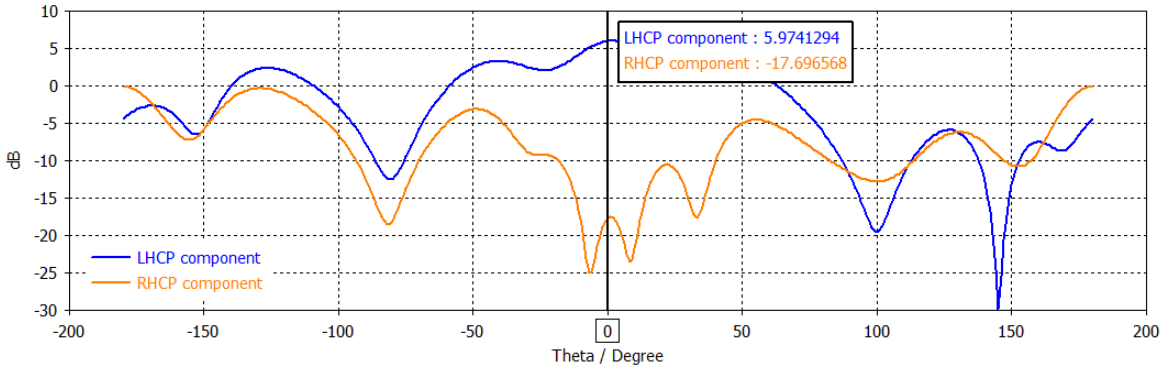

Figure 4.36: Right-hand and left-hand components of the microstrip patch antenna when the signal is applied to port 2

When the signal is injected in the port 1 and the port 2 is terminated by a matched load it is accomplished RHCP. In this case the antenna showed a left-hand component rejection of 22.1 dB in respect to θ=0°, as can be verified in figure 4.37.

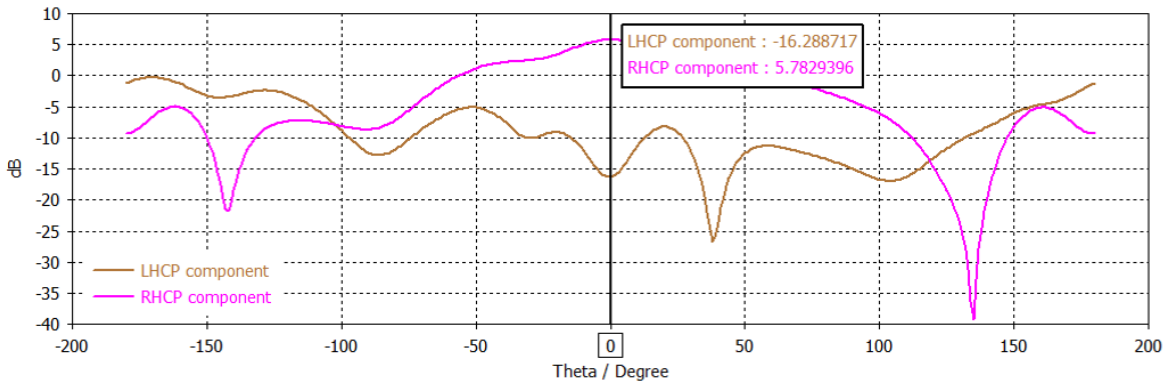

Figure 4.37: Right-hand and left-hand components of the microstrip patch antenna when the signal is applied to port 1

In what concerns the radiation pattern of the antenna for the RHCP, it presented a gain, in respect to θ=0°, of 5.8 dBi and an HPBW of 54.7° and 74.8° considering the cut plane of ϕ=0° and ϕ= 90°, respectively.

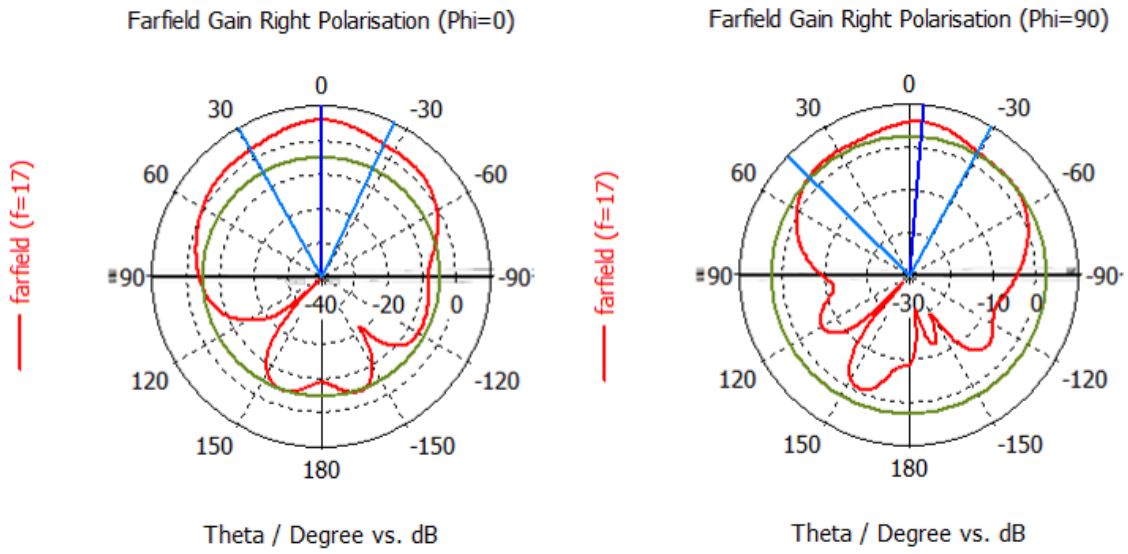

Figure 4.38: Vertical radiation pattern of the antenna at 17 GHz for $\phi = 0°$ and $\phi = 90°$, respectively, with the signal applied to port 1

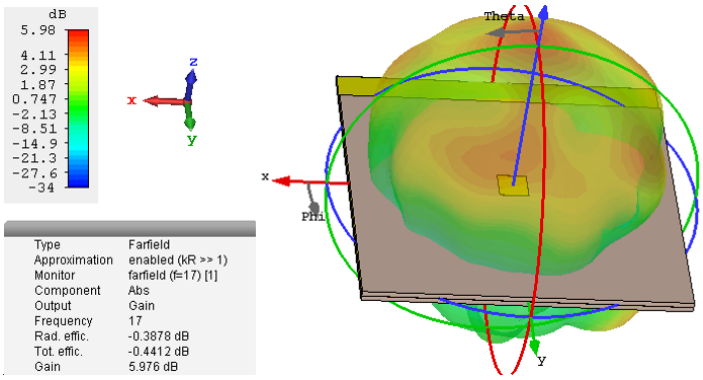

Figure 4.39: 3D radiation pattern of the antenna at 17 GHz with the signal applied to port 1

In the case of the LHCP the antenna has a gain of 5.8 dBi to the desired direction ($\theta = 0°$).

The simulated antenna presents a HPBW of 35.3° considering the cut plane of ϕ=90° and 64.0° considering the cut plane of ϕ= 0°.

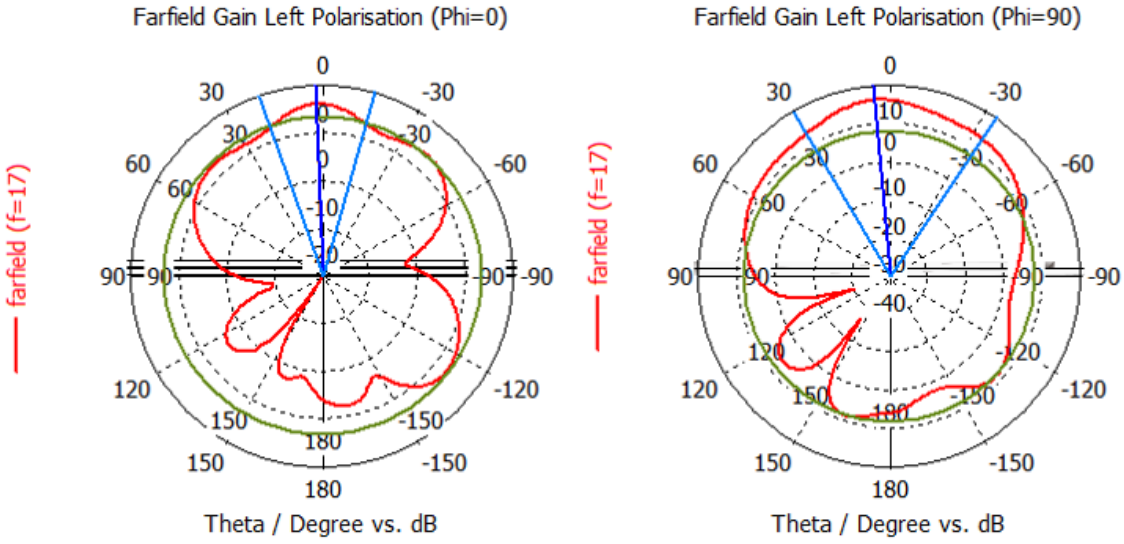

Figure 4.40: Vertical radiation pattern of the antenna at 17 GHz for $\phi = 0°$ and $\phi = 90°$, respectively, with the signal applied to port 2

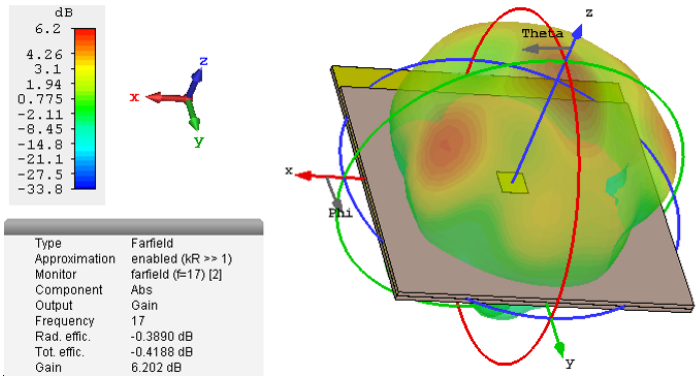

Figure 4.41: 3D radiation pattern of the antenna at 17 GHz with the signal applied to port 2

At the intended operating frequency, the antenna presents a radiation efficiency of 93.77%.

4.2.4 Conclusions

In summary, the antenna performance parameters obtained from the simulations were the following:

Gain: around 5.8 dBi to the desired direction of θ=0°

Size: (45.77x47.77x1.56)mm

Isolation between orthogonal components: between 20 dB and 25 dB

Axial ratio: 1.37 dB

Bandwidth: around 1.3 GHz

As it can be observed in terms of size and gain, the developed antenna meets the demands for the Wi-Fi indoor applications (small and low profile antenna with a gain between 0 and 6 dBi).

In what concerns the polarization, it was not accomplished neither a high isolation between the components or a high purity polarization level, due to a more complex structure of this antenna. According to [8], it is desired to have a component rejection between 30 dB and 40 dB and for a high purity polarization level the axial ratio should be the close to 0 dB.

The antenna does not meet all the specifications for the indoor Wi-Fi applications, consistent with [8]. However, it can be said that the performance of this antenna is satisfactory for this type of application. In addition, the designed antenna accomplished a wide bandwidth showing that it is possible to increase a higher bit rate by a Wi-Fi system that operates at 17 GHz.

4.3 Comparison between the developed microstrip patch antennas for indoor applications

Comparing both the antennas developed, as it is possible to observe in table 4.8, in terms of gain and size they are similar and obey the requirements for Wi-Fi indoor applications. Concerning the polarization, these antenna present different performances. The antenna with crossed slots showed a better polarization purity level and a higher rejection level of the orthogonal component than the antenna with off-centered slots. These results were obtained since the antenna with crossed slots has a simpler structure than the antenna with off-centered slots, which has an impact on the antenna symmetry and consequently on the antenna polarization.

The antenna with off-centered slots was more difficult to design as a result of a higher complexity of its structure. However, it allows to obtain either RHCP and LHCP without performing any change in the antenna structure contrarily to the antenna with crossed slots. In addition, the antenna with off-centered slots achieved a wider bandwidth.

The antenna with crossed slots meets all the demands of an antenna for Wi-Fi applications. On the other hand, the antenna with off-centered slots does not but it can be said that both antennas have satisfactory characteristics for this type of application.

Performance parameters	Antennas for Wi-Fi indoor applications characteristics	Antenna with crossed slots	Antenna with off-centered slots
Gain [dBi]	0 to 6	Around 5	Around 5.8
Polarization orientation	-	RHCP	RHCP and LHCP
Isolation level between the orthogonal component [dB]	30 to 40	Arround 30	20 dB to 25 dB
Axial ratio [dB]	-	0.56	1.37
Bandwidth	-	500 MHZ	around 1.3 GHz
Size	Small and low profile	(40x40x1.56) mm	(45.77x47.77x1.56) mm
Impedance matching	-	Good	Good
Radiation Efficiency (%)	-	92.00	93.77

Table 4.8: Performance parameters of the antennas developed for indoor Wi-Fi applications

Chapter 5

Antenna for outdoor Wi-Fi applications

For Wi-Fi applications that involve big communication distances (Outdoor applications) it is necessary to use an antenna with high gain. As it was possible to observe in the previous chapter, a single antenna is not capable to reach gains higher than 5-7 dBi.

Outdoor antennas for Wi-Fi applications have the following specifications [8]:

- For a directional point-to-point link the antenna should provide a gain up to 29 dBi.
- For point-to-multipoint coverage the antenna should provide gain from 3 to 16 dBi.
- For sectoral coverage, the antenna should provide a gain between 15 and 20 dBi and a HPWB of 60°,90° or 120°.
- Antennas with polarization diversity should present a high isolation, around 30-40 dB between the orthogonal polarizations.

To obtain a higher gain it was developed a microstrip array antenna using the single element with crossed slots.

5.1 Design steps of the array antenna

The primary step was to design an array with two elements, that can be seen in figure 5.1, to understand the influence of the distance between the elements of the array in the gain and the radiation pattern of the antenna.

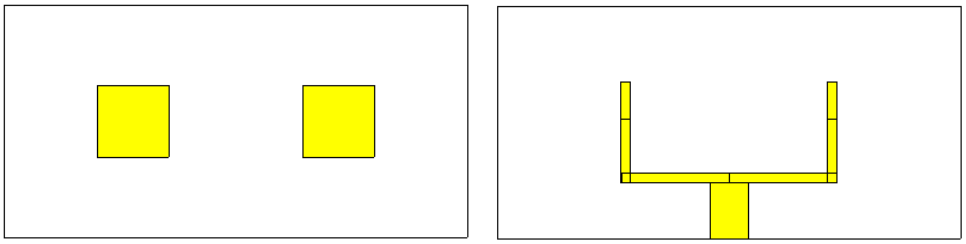

Figure 5.1: 2x1 array designed on CST MWS (front and back view)

It was performed a sweep of the inter element spacing on CST MWS, whereof the maximum gain was obtained with the spacing element of $0.7\lambda_0$, as it is possible to conclude observing the table 5.1.

Spacing element (mm)	Gain (dBi)
0.5 λ_0	7.39
0.6 λ_0	7.92
0.7 λ_0	8.03
0.8 λ_0	7.89
0.9 λ_0	7.81
λ_0	7.79

Table 5.1: Variation of the gain with distance between the elements of the array

In what concerns the radiation pattern of the 1x2 array, it can be verified in the figure 5.2 that for the ϕ=0° cut it is almost the same comparing to the single element. However, when analysing the cut plan of ϕ=90° it is seen that the main lobe is more directive and two secondary lobes appear as the distance between the elements increase.

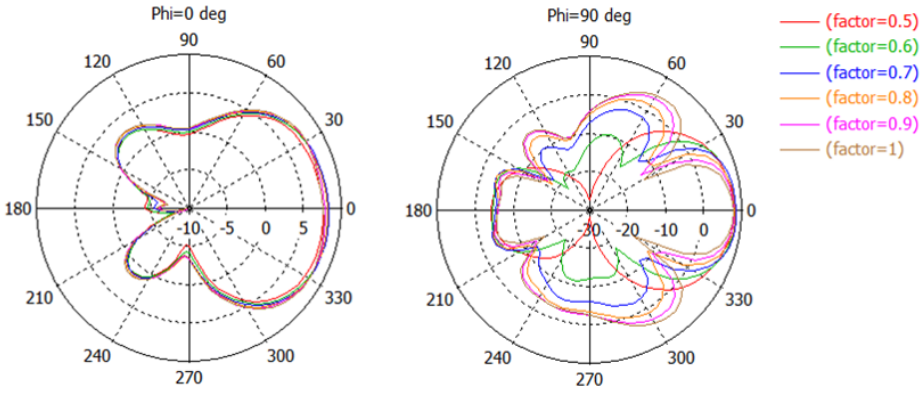

Figure 5.2: Variation of the radiation pattern of the 1x2 array antenna with the distance between the antenna elements

Thus, the distance between elements was chosen to accomplish the higher gain possible with the lowest secondary lobe level. It was set to be $0.65\lambda_0$ that presented a gain of 8 dBi and a side lobe magnitude of -5.3 dB.

Theoretically, when the number of elements doubles, the gain of the antenna also doubles. This is observed in this study. The gain of a single element was around 5 dBi and the gain of the array antenna with two elements was around 8 dBi.

To increase even more the gain and still have a compact antenna it was developed a planar array with four elements (2x2 array). The expected gain of this antenna is four times the gain of the single elements (6 dB bigger), so it is expected to have a gain around 11 dBi.

5.1.1 Design steps of the 2x2 array antenna

In a first instance the element was placed in the 2x2 array configuration without any feed network to connect the elements. They were fed using a CST MWS tool that allowed to feed the four elements simultaneously. Thus, it was possible to notice the impact of the mutual coupling and the feedline corner in the impedance matching and the axial ratio. To compensate this phenomenon the elements were adjusted, the obtained parameters are presented in the table 5.2 (these dimensions are referred to the single element designed in chapter 4.1 that composed the array).

Antenna Parameter	Value
W	3.93 mm
L	3.93 mm
L_a	3.71 mm
K_s	1.12 mm
Lstub	2.10 mm

Table 5.2: Dimension of a single element placed in the array configuration

In the next step, the feed network that connects all the four elements of the array antenna was designed, as it is shown is figure 5.3. It started with a line of 100 Ω from the patch (it was the impedance used to feed the single patch). The feed network is formed by microstrip lines of 50 Ω, 100 Ω and $\lambda/4$ impedance transformers to transform the impedance observed at a certain point to the desired impedance.

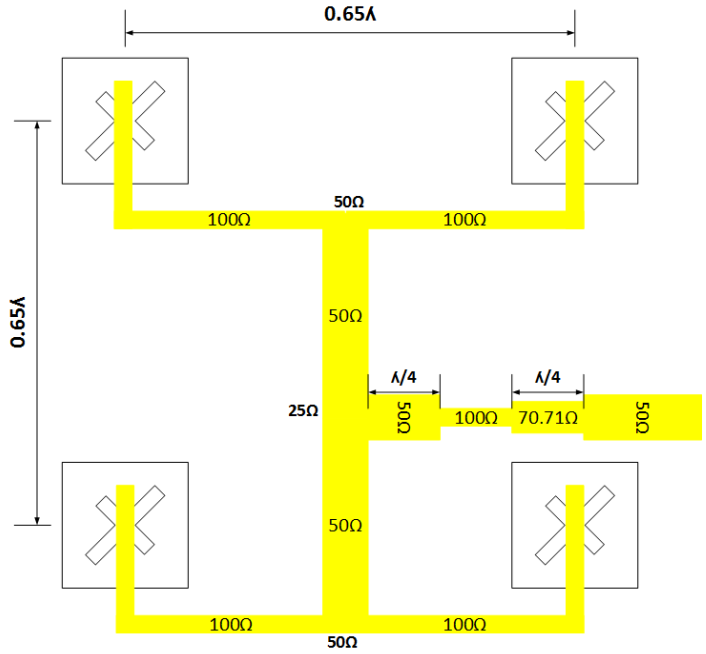

Figure 5.3: Schematic of the antenna array feed network

5.2 Simulation results

Having an idea of the antenna structure and feed network, it was then designed and simulated in CST MWS. The antenna composition is presented in figure 5.4. The result from the simulation allows to take the first conclusion about the antenna parameters as impedance matching, polarization and radiation pattern, which are exhibited in this section.

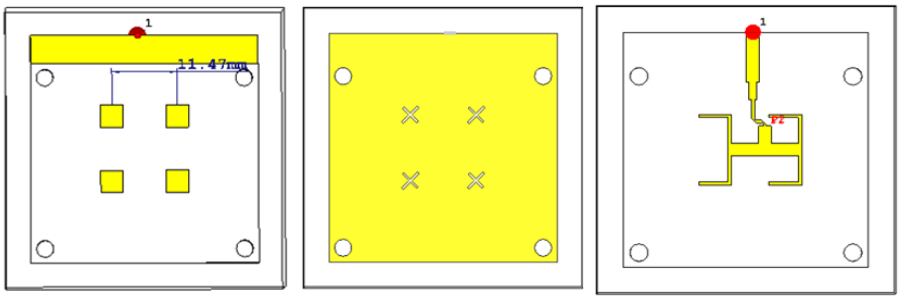

Figure 5.4: Array antenna implemented in CST MWS (front,ground and back view)

In terms of the impedance matching, it is possible to observe the S_{11} (return loss) of the antenna in figure 5.5, which for the operating frequency presents a value of -32.9 dB . In other words, the impedance seen at the port is near to the desired 50 Ω (50.69-2.18i Ω) so it presents an insignificant reflected wave (most of the power was accepted by the antenna). The array antenna has an impedance bandwidth (S_{11} ⩽-10) of 1.27 GHz between 16.33 and 17.60 GHz.

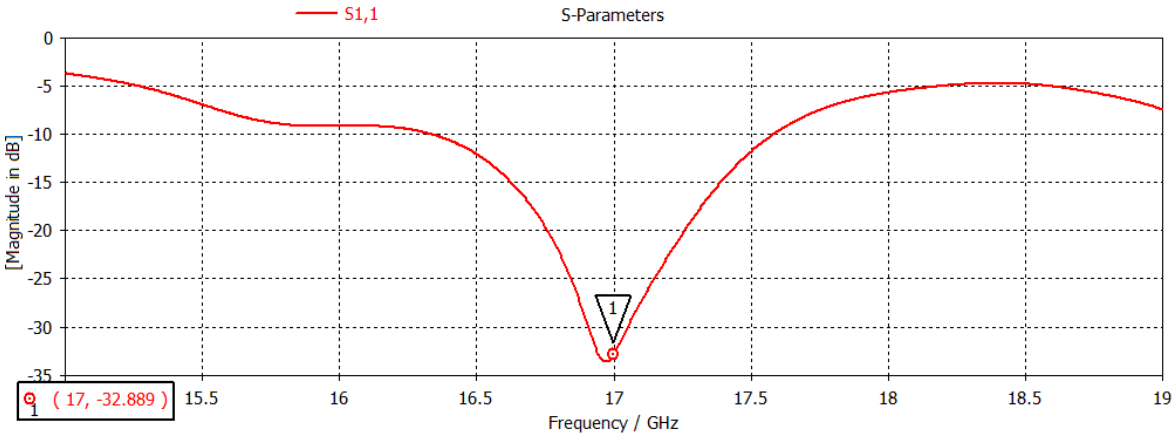

Figure 5.5: S_{11} of the array antenna in dB

Regarding the RHCP, since the single element has this polarization type, it is expected that the array has the same polarization orientation. The antenna shows a left-hand component rejection of 30.3 dB at the maximum direction, as it can be seen in figure 5.6, for the vertical plane of ϕ=0°. The purity of the circular polarization is also corroborated by the axial ratio value, that for the operating frequency is of 0.53 dB, as it is possible to observe in figure 5.7. The array antenna presents a good polarization (axial ratio ⩽ 3 dB) and impedance

matching between 17.19 GHz and 16.85 GHz, so the antenna has a bandwidth of 340 MHz.

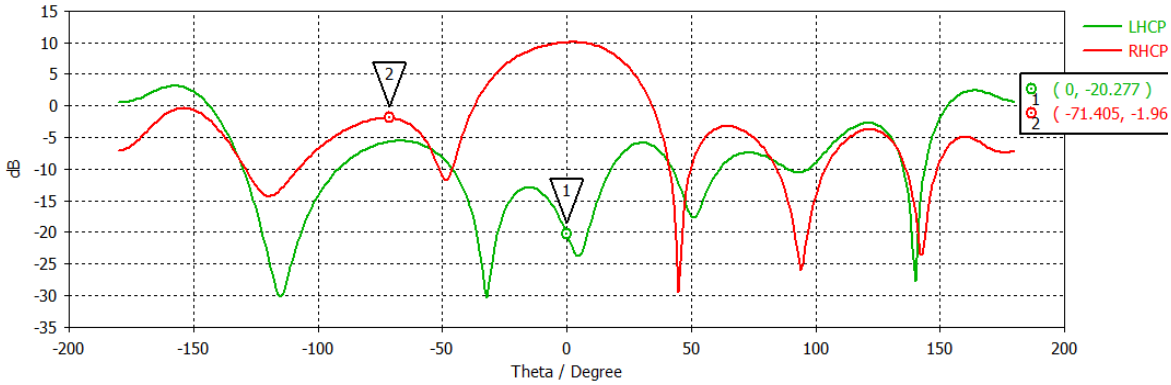

Figure 5.6: Right-hand and left-hand components of the microstrip array antenna

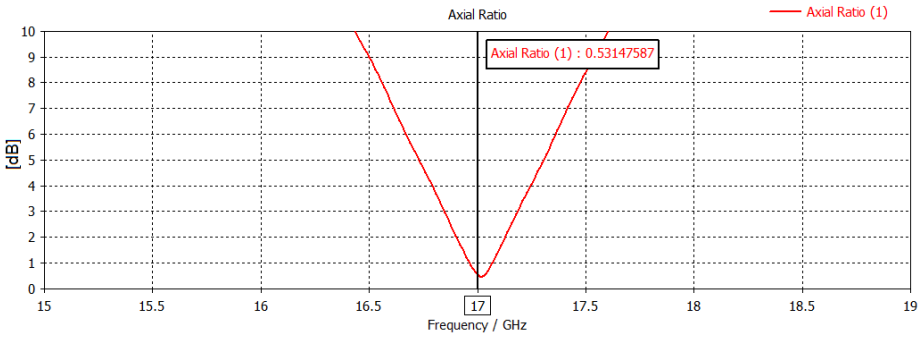

Figure 5.7: Axial ratio of the array antenna in dB referring to frequency

Now looking at the radiation pattern of the array antenna shown in the figures 5.8 and **??** it is possible to conclude that the configuration used (planar array) as an impact in both the components of the radiation pattern (ϕ=0 °,90°). The main lobe of the array antenna is more directive (narrow) in both planes.

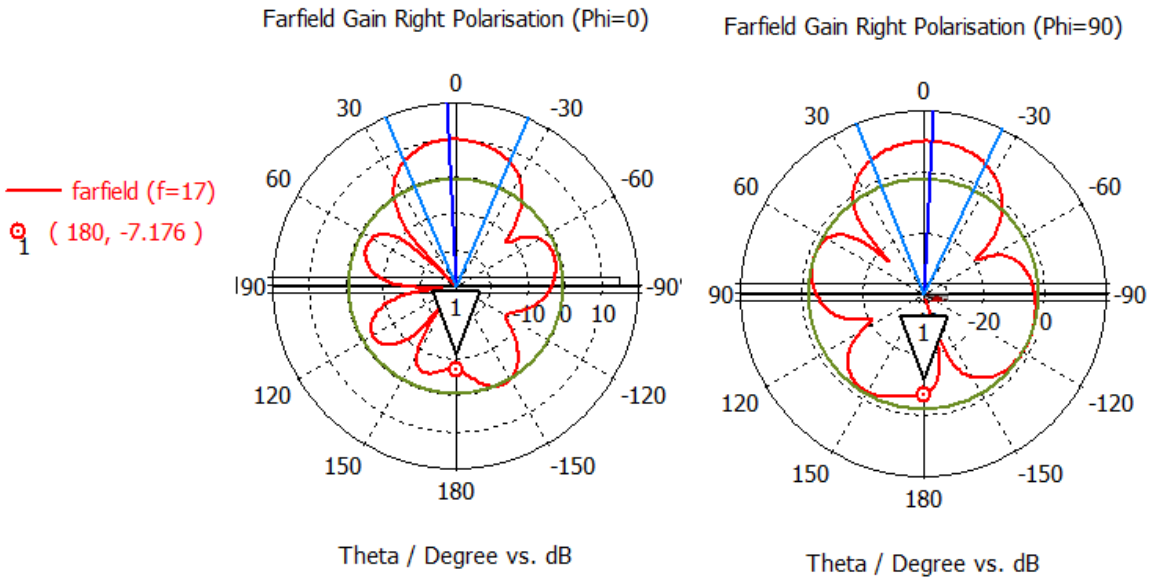

Figure 5.8: Vertical radiation pattern of the array antenna at 17 GHz for $\phi = 0°$ and $\phi = 90°$

The antenna presented a gain of 10.1 dBi, a back radiation of -7.2 dB (in respect to θ=0°) and a side lobe level of -12.2 dB.

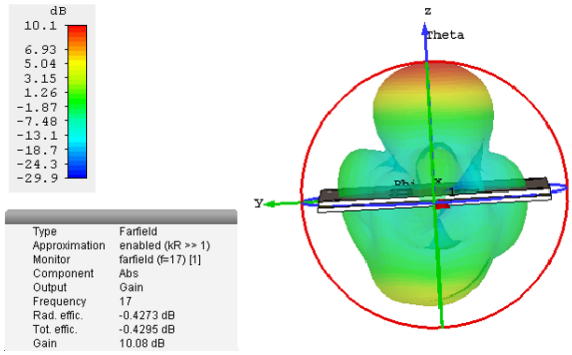

Figure 5.9: 3D radiation pattern of the array antenna at 17 GHz

The antenna has an HPBW of 45.40° in respect to the cut plan of ϕ=0° and 47.20° in respect to the cut plan of ϕ=90°.

The antenna developed uses corners in the feed network, however it is not recommended since the corners can introduce discontinuities that can lead to an unexpected performance. Thus, it was designed a second array now with the corners chamfered. All the previous steps were performed once again, and then led to the following antenna dimension (once again, these dimensions are referred to the single element designed in chapter 4.1 that composed the array).

Antenna Parameter	Value
W	3.99 mm
L	3.99 mm
La	3.69 mm
Ks	1.14 mm
Lstub	2.53 mm

Table 5.3: Adjusted dimensions on each single elemente of the array antenna with chamfered corners

The feed network structure is the same as the previous one. Therefore, the antenna was designed and simulated. The designed antenna array in presented in figure 5.10 and the simulation results are exhibited in this section.

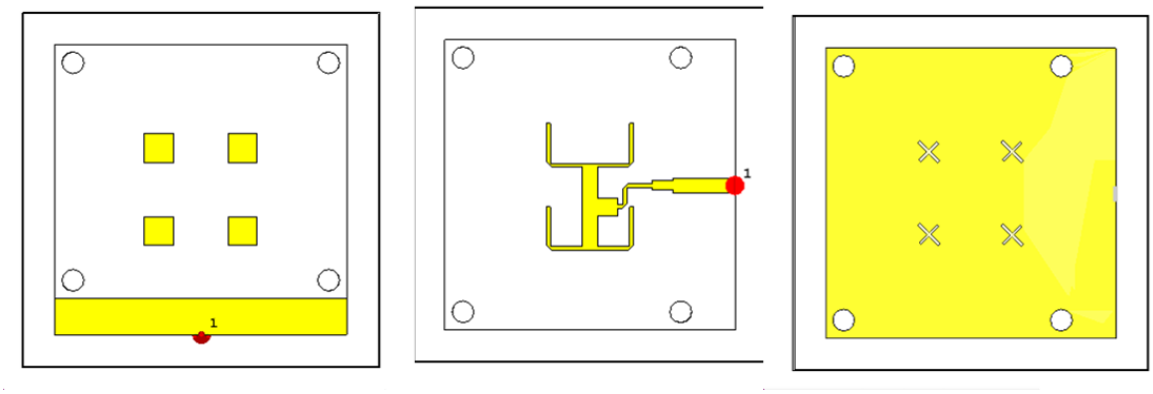

Figure 5.10: Array antenna with chamfered corners (front, back and ground view)

Once again, a good impedance matching was obtained as it can be concluded observing figure 5.11, the antenna presents a S_{11} of -26 dB@17GHz and an impedance matching bandwidth of 2.87 GHz [16.13 GHz;19 GHz].

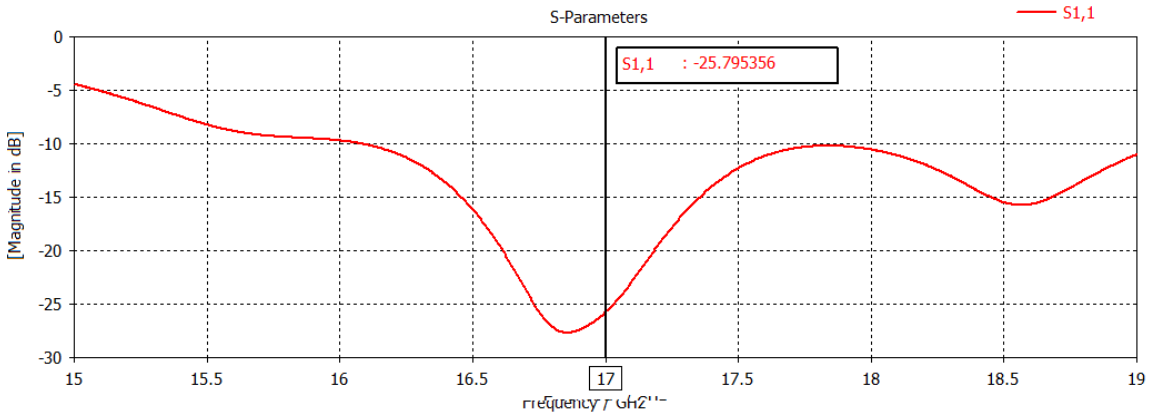

Figure 5.11: S_{11} of the array antenna with chamfered corners in dB

As for the circular polarization, the results show that a good RHCP was accomplished

having a left-hand component rejection of 24.7 dB supported with an axial ratio of 0.9 dB at the pretended operating frequency, as it can be seen in figures 5.12 and 5.13. The range of frequencies where the antenna presents the intended performance was between 16.82 GHz and 17.16 GHz, so it presented a bandwidth of 340 MHz.

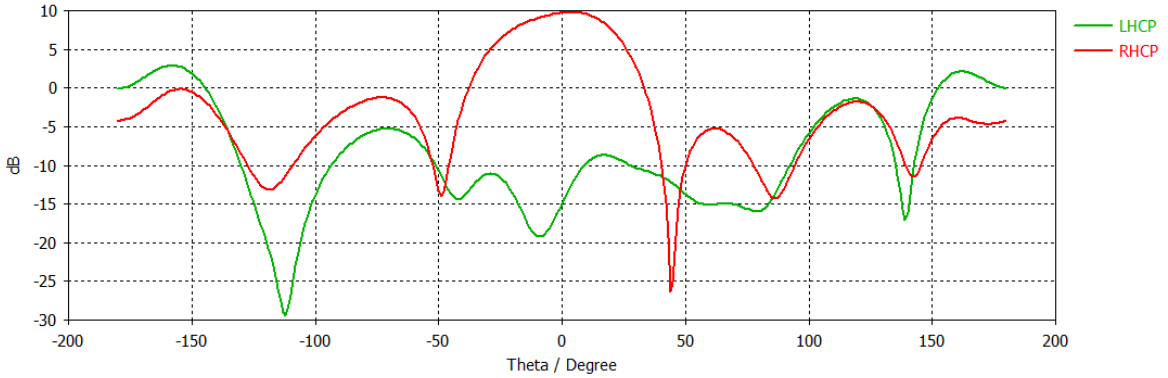

Figure 5.12: Right-hand and left-hand components of the microstrip array antenna with chamfered corners

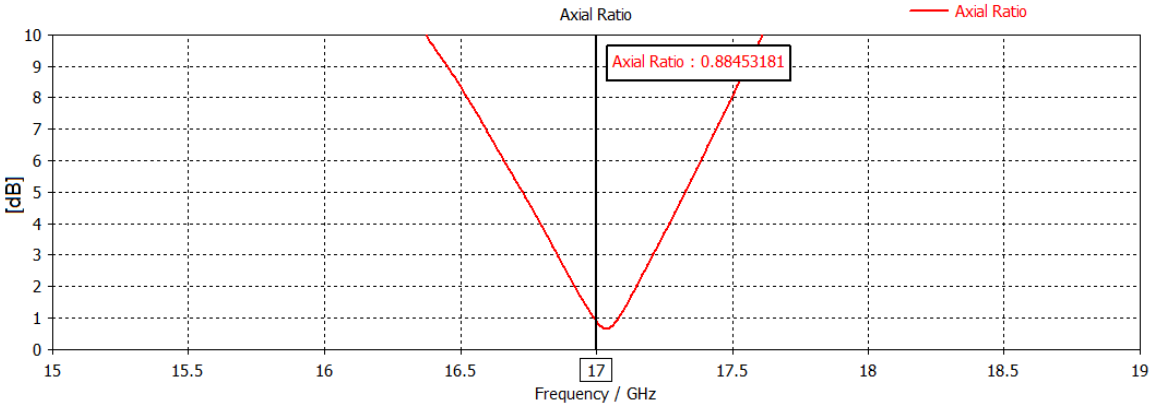

Figure 5.13: Axial ratio of the array antenna with chamfered corners in dB

In what concerns the radiation pattern of the antenna it was obtained a gain of 9.9 dBi and a directivity of 10 dBi with a radiation efficiency of 97.7%. Once again, the gain presented by the array antenna was around 1 dB lower than the expected.

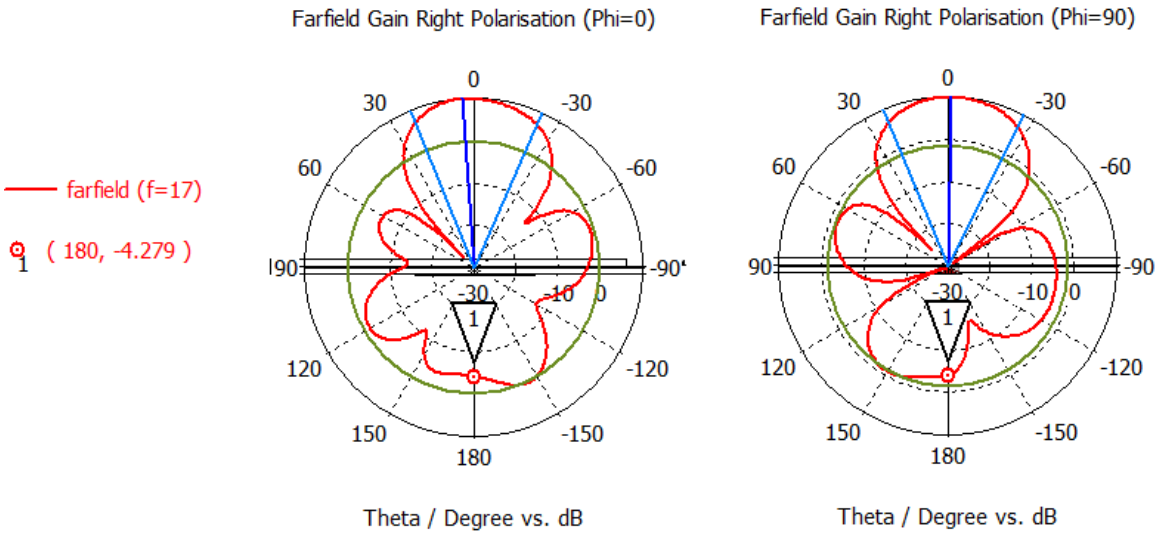

Figure 5.14: Vertical radiation pattern of the array antenna with chamfered corners at 17 GHz for $\phi = 0°$ and $\phi = 90°$

The antenna has an HPBW of 45.70° in respect to the cut plan of ϕ=0° and 48.50° in respect to the cut plan of ϕ=90°. It also presents a back radiation of -4.3 dB(in respect to $\theta = 0°$) and a side lobe level of -11.2 dB.

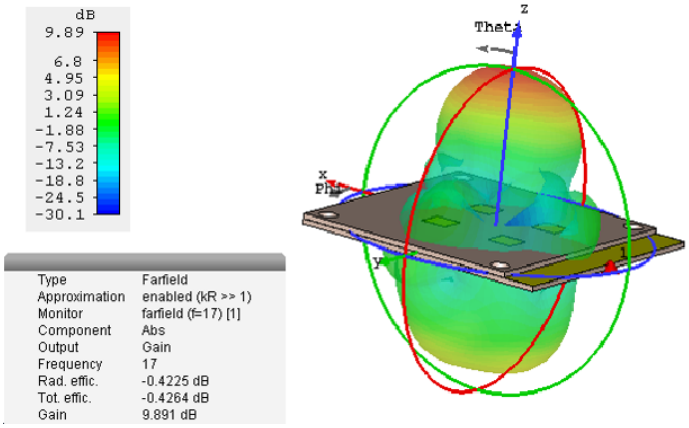

Figure 5.15: 3D radiation pattern of the array antenna with chamfered corners at 17 GHz

5.3 Practical results

Once achieved the results previously exposed, it was decided to manufacture both the antennas simulated. The developed array antenna with corners at its feed network is presented in the figure 5.16.

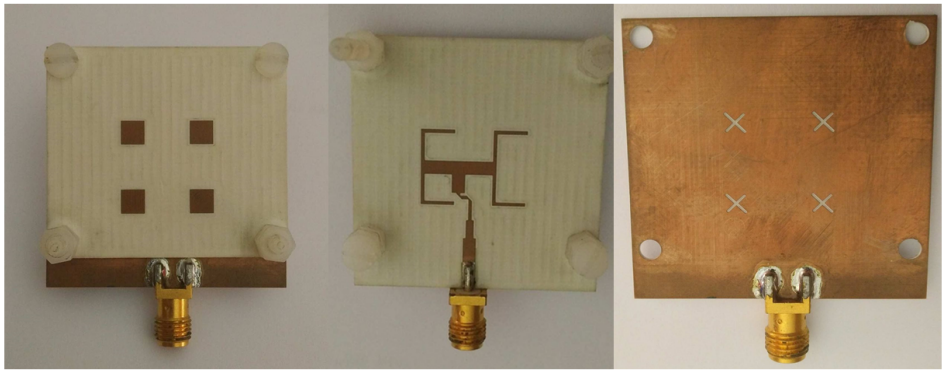

Figure 5.16: Developed microstrip array antenna with corners at the feed network (front, back and ground view)

Once again, it was only possible to measure the S_{11} of the antenna due to the lack of material to perform the rest of the measures. Therefore, not much can be concluded about the operation of the antenna.

Observing the figure 5.17 it is possible to verify that the behaviour of the simulated and measured return loss is different, probably because of the low precision at the construction process and the different characteristics of the substrate of the developed antenna and the one used in the simulation. However, at the operating frequency the antenna had a return loss of -14.3 dB, so a reasonable impedance matching was accomplished.

The array antenna presented an impedance bandwidth of 2.28 GHz [16.26 GHz;18.54GHz].

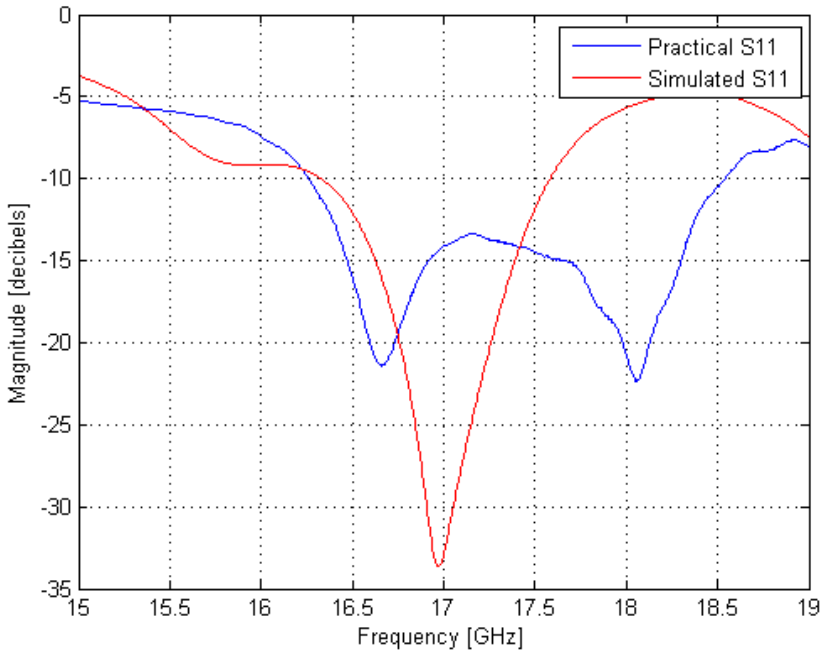

Figure 5.17: Measured S_{11} vs simulated S_{11} of the array antenna with corners at the feed network

The structure of the developed antenna with chamfered corners at its feed network is shown in figure 5.18.

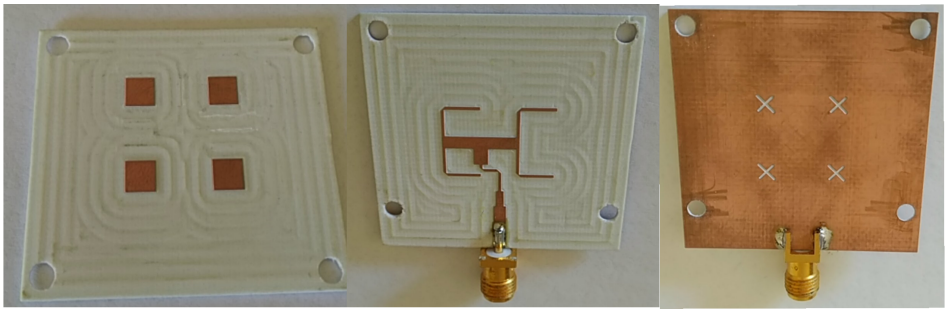

Figure 5.18: Developed microstrip array antenna with chamfered corners at the feed network (front, back and ground view)

Once again it was only possible to measure the return loss of the antenna that is presented in the following figure.

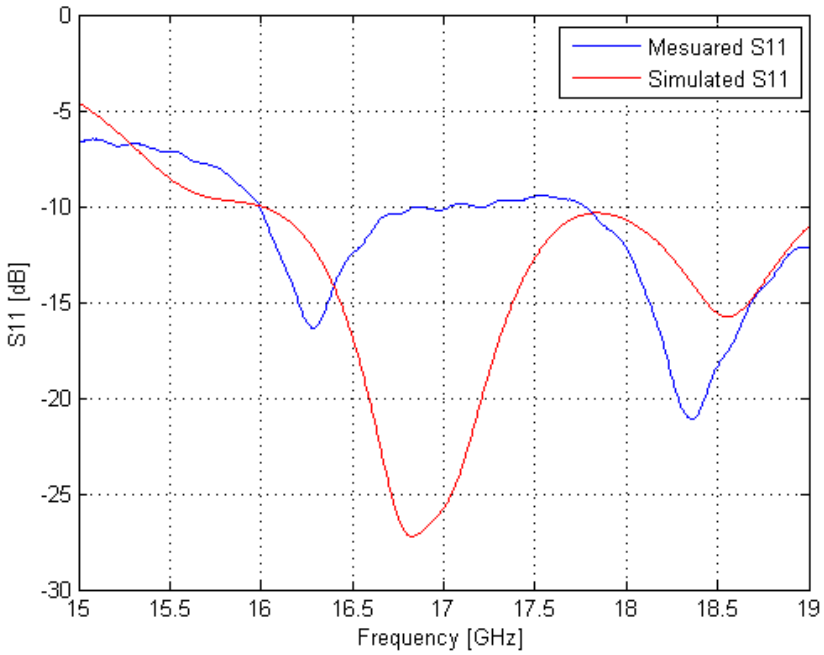

Figure 5.19: Measured S_{11} of the array antenna with chamfered corners at the feed network

Analysing the figure 5.19 it is possible to notice, once again, that the return loss of the simulated antenna and the return loss of the developed antenna are different. The reasons of this difference are the same that were presented for the previous array antenna. The array antenna with the corners chamfered had a return loss of -10.5 dB and presented a bandwidth of 2.30 GHz [(16 GHz to 17.3 GHz and 18 GHz to 19 GHz)].

Theoretically, the feed network with chamfered edges should provide better results in terms of impedance matching, since it decreases the discontinuity effect. However, these two

arrays cannot be directly compared due to the different dimensions of the patch antenna and the crossed-slots. In addition, they were not manufactured at the same time, therefore the error that is presented in the construction is different. In summary, they are two different antennas that use the same feeding method.

Since they are two different antennas it is possible to compare their performance. Both array antennas presented an acceptable return loss. However, by comparing both, it can be observed that the array antennas with corners in the feed network is the one that presents the best impedance matching. It has a lower return loss around 5 dB.

5.4 Conclusions

Considering the simulation results of both the antennas developed, they presented a gain around 10 dBi that is acceptable for a directional point-to-point link (gains up to 29 dBi) and a point-to-multipoint coverage (gain from 3 to 16 dBi) applications. If it is desired to increase even more the antenna gain, the number of elements of the array should increase. This was concluded before considering that when the number of elements doubles, the gain increases in 3 dB, as it was verified in this work.

It is also desired that antennas with polarization present high isolation between both the components and that those are compact antennas (the dimension of the developed antenna is 4 x 4 cm), which was accomplished by the developed antennas. The array antenna with corners at the feed network presents an isolation between the components of 30.3 dB. The array antenna with the cut corners has an isolation between the orthogonal components of 24.7 dB. This meets the demands that are mentioned in [8].

The antenna developed does not match the specifications presented in [8] for sectoral coverage applications, since it presents a gain bellow 15 dB and a beam width different to the desired 60° ,90° and 120°. It is possible to obtain these characteristics by adding more elements to the array, increasing the gain. Regarding the beam width, it can be adjusted by changing the array configuration or by tuning the space between the elements of the planar arrays (one of the possibilities is to adjust the beam width to make the distance between the elements of the array in the vertical orientation different to the distance of the elements placed in the horizontal orientation).

However, the antenna array developed has a beam width around 45° that enables the use of it in sectoral coverage. With this beam width, it is possible to obtain a coverage of 360° using eight antennas in an octagonal configuration. In addition, these arrays presented the 45° beam width in the vertical and horizontal plans, simplifying its installation process, since it is not necessary to pay attention to the orientation of the antennas. As mentioned before, the increase of the operating frequency will lead to a reduction of the coverage that can be obtained, resulting in the increase of antennas necessary to guarantee the same coverage. This is verified in this work.

After all, it is possible to say that the developed antenna is suitable for outdoor Wi-Fi applications.

Chapter 6

Conclusions

This thesis proposed the use of the 17 GHz band as an operating frequency of the Wi-Fi systems. This work had, a focus, the antennas, namely the design and manufacture of antennas for indoor and outdoor Wi-Fi applications.

The work began with the study of microstrip antennas, in particular with the development of simple patch and a study regarding a few of the existing feeding methods. Also, it was acquired some knowledge about the electromagnetic simulator used in this study, the CST MWS.

The analysed feeding methods were the microstrip line feed using a quarter-wavelength transformer, the inset-feed and the aperture coupling feed. It was verified that the aperture coupling had the best performance, presenting an acceptable gain of 5 dB, a bandwidth of 1.38 GHz and prevents the degradation of the radiation pattern by the feedline. Therefore, the aperture coupling feed was the selected feeding method for this work. These antennas were manufactured to take the first practical test. It was only possible to measure the return loss, which presented a frequency deviation around 1 GHz, when compared to the simulation results. This frequency deviation may be due to the precision in the fabrication process, the substrate characteristics of the antenna that can be different from the one on the simulator, not having considered the SMA connector and having used a low mesh in the simulation.

Then, two possible solutions of an antenna for indoor Wi-Fi applications were developed in which it was expected to obtain a gain between 0 dB and 6 dB and circular polarization with an orthogonal component rejection between 30 dB and 40 dB (allowing the receiving and transmitting antenna not to have the same orientation). As a first approach, it was designed an antenna with crossed slot structure using a single feed. This antenna presented a gain of 5.3 dBi and an omnidirectional radiation pattern to the opposite direction of the ground plane. The antenna showed RHCP with an isolation between the polarization components of 29.9 dB, evidencing a high polarization purity that is corroborated by its low axial ratio (0.56 dB). It is possible to conclude that the designed antenna respects all the performance parameters stated to an antenna for indoor Wi-Fi applications. Therefore, the antenna was manufactured. It was only possible to measure the return loss that presented a frequency deviation around 1 GHz. This time the SMA connector was included in the antenna structure and the simulation was performed with a high mesh. However, the practical results did not reveal any improvements. Thus, this reasons were discarded leaving as hypotheses the remaining causes of the error in the practical return loss. It was not possible to take more conclusions about the antenna manufacture since it was not possible to measure the gain, radiation pattern and polarization.

However, this antenna proved to be a good solution for being mounted on a wall due to his structure and radiation pattern (simulation).

Subsequently, it was designed an antenna with off-centered slots configuration with the objective of creating an array formed by independent elements that is useful for MIMO applications. This configuration allows to obtain either RHCP and LHCP by using a quadrature (90°) hybrid coupler. On the other hand, the design of this antenna presented a higher level of difficulty.

The developed antenna presented a gain around 5.8 dBi that is acceptable for this application, but when analysing the circular polarization, it was possible to observe that polarization component rejection (20-25 dB) and polarization purity was not satisfactory (axial ratio of 1.37 dB). The low polarization purity can be justified by the high complexity of the antenna structure, which has an influence on its level of symmetry. The polarization level is positively related with the symmetry on the antenna structure.

The design antenna does not respect all the necessary characteristics for indoor WIFI applications mentioned in [8] but it can be considered that the antenna has a satisfactory result for this purpose. The antenna with off-centered slots has some interesting features such as a wide bandwidth (around 1.37 GHz) and allows to obtain RCHP/LHCP without making any changes in the antenna structure (this is an interesting characteristic to create an array formed by independent elements for MIMO applications).

A antenna for outdoor applications, was also developed, that typically demands a high antenna gain. Thus, a planar array antenna (2x2) was developed using the element with the crossed slot configuration. Initially the antenna was designed for point-to-point links in which it is desired to have a gain up to 29 dBi. However, the results obtained by the designed antenna showed to be possible to use it for point-to-multipoint and sectoral coverage applications. The antenna array presented a gain around 10 dBi, a HPBW of 45° in the vertical and horizontal plans and a RHCP with an isolation between the orthogonal polarization components of 30.3 dBi. Therefore, manufacturing was carried out but once again it was just possible to measure the return loss (-14.3 dB @ 17 GHz) which does not allow to conclude much about the array antenna performance.

Finally, a study regarding the manufacturing error was carried out using the antenna with crossed slots. It was noticed that the dimensions of the fabricated antenna were smaller than the pretended ones, justifying the frequency deviation and the attenuation observed on the S11 parameter. The fabrication error was different depending on the antenna layer. Thus, the manufacturing error is related with the wear of the conical tool. It was also observed that the machine is not capable of creating the intended rectangular slots, creating instead a slot with rounded ends. This influences the coupling level, which affects the impedance matching of the antenna.

6.1 Future Work

Here are some suggestions for future work:

- Perform the measurements of the antennas and make the necessary adjustments on them.

  In order to achieve better results, it is recommended to design the antenna using slots with rounded ends. In the manufacturing process, it is suggested to produce several antennas simultaneously with different dimensions (slightly bigger than the ones obtained in the simulation, since the machine presented an error between 40 μm and 130 μm).

- Manufacture the antenna with off-centered slots configuration, perform the measurements and then design an array formed by independent elements for MIMO applications.

Bibliography

[1] D. K.Dinakaran, M.Vajikabanu, Piriyadharsini, "Design of Microstrip Patch Antenna For Wi-Fi Applications", *Ijarece*, vol. 5, no. 1, pp. 38–41, 2016. [Online]. Available: http://calhoun.nps.edu/public/handle/10945/4036.

[2] T. Engineering, T. Author, S. Garc, E. Garcia, and V. Date, "Characteristics and evaluation of IEEE 802 . 11n standard", 2013.

[3] M. Elsdon, O. Yurduseven, and X. Dai, "Wideband Metamaterial Solar Cell Antenna for 5 GHz Wi-Fi Communication", vol. 71, no. November 2016, pp. 123–131, 2017.

[4] *Did You Know Non-802.11 Devices Can Interfere With Your Wi-Fi?* [Online]. Available: https://boundless.aerohive.com/experts/Did-You-Know-Non-80211-Devices-Can-Interfere-WithYour-Wi-Fi.html (visited on 06/05/2017).

[5] M. Unbehaun, "Scalability of wireless LAN systems in the unlicensed 17 GHz frequency band", in *GLOBECOM'01. IEEE Global Telecommunications Conference (Cat. No.01CH37270)*, vol. 6, IEEE, pp. 3599–3603, ISBN: 0-7803-7206-9. DOI: 10.1109/GLOCOM.2001.966352. [Online]. Available: http://ieeexplore.ieee.org/document/966352/.

[6] "2 EFEITOS E MODELOS DA ATENUAÇÃO POR CHUVAS", Tech. Rep. [Online]. Available: https://www.maxwell.vrac.puc-rio.br/4174/4174{_}3.PDF (visited on 09/25/2017).

[7] C Kienmayer, R Th, M Tiebout, W Simb, and A. L. Scholtz, "An Integrated 17 GHz Front-End for ISM / WLAN Applications in CMOS", *Proceedings of ESSCIRC, Grenoble, France, 2005*, no. 1, pp. 12–15, 2004.

[8] Z. N. Chen, X. Qing, T. S. P. See, and W. K. Toh, "Antennas for WiFi connectivity", *Proceedings of the IEEE*, vol. 100, no. 7, pp. 2322–2329, 2012, ISSN: 00189219. DOI: 10.1109/JPROC.2012.2183830.

[9] N Mohamed, S. Banu, M Ramkumar Prabhu, U. T. Sasikala, P. Student, and A. Prof, "Design A Square Microstrip Patch Antenna for S-Band Application", *IOSR Journal of Electronics and Communication Engineering Ver. IV*, vol. 10, no. 2, pp. 2278–2834, 2015. DOI: 10.9790/2834-10242430. [Online]. Available: www.iosrjournals.org.

[10] C. A. Balanis, *Antenna Theory Analysis and Design*, 3. 2005, p. 1136, ISBN: 9786468600. DOI: 10.1049/ep.1982.0113.

[11] E. R. Committee, E. Conference, and T. Administrations, "THE EUROPEAN TABLE OF FREQUENCY ALLOCATIONS AND UTILISATIONS COVERING THE FREQUENCY RANGE 9 kHz TO 275 GHz Lisboa January 2002-Dublin 2003-Turkey 2004-Copenhagen 2004", Tech. Rep. January 2002, 2004.

[12] E. communication Committee, "The European table of frequency allocations and application in the frequency range 9 kHz to 3000 GHz", Tech. Rep. June, 2011, p. 275. [Online]. Available: http://www.erodocdb.dk/Docs/doc98/official/pdf/ERCREP025.PDF.

[13] W. L. Stutzman and G. A. Thiele, *Antenna Theory and Design*. 2013, p. 843, ISBN: 9780470576649.

[14] R. Garg, P. Bhartia, I. Bhal, and A. Ittipiboon, *Microstrip Antenna Design Handbook*. 1994.

[15] *Broadband Antennas: Genetic Algorithms or Traditional Methods?* [Online]. Available: http://fab.cba.mit.edu/classes/862.06/students/alki/GA.html (visited on 04/25/2017).

[16] T. M. V. Varum, "ANTENA PARA COMUNICACOES DSRC", Master's thesis, Universidade de Aveiro, 2010, p. 66.

[17] *Antenna-Theory.com - Rectangular Microstrip (Patch) Antenna - Feeding Methods*. [Online]. Available: http://www.antenna-theory.com/antennas/patches/patch3.php (visited on 04/10/2017).

[18] Y. Hu, E. Lundgren, D. R. Jackson, J. T. Williams, and S. A. Long, "A Study of the Input Impedance of the Inset-Fed Rectangular Microstrip Antenna as a Function of Notch Depth and Width", Department of Electrical and Computer Engineering University of Houston, Houston, TX 77204-4005, 2005, pp. 330–333, ISBN: 0780388836.

[19] M. Abdul and M. Universiti, "A design rule for inset-fed rectangular microstrip patch antenna A Design Rule for Inset-fed Rectangular Microstrip Patch Antenna", *WSEAS TRANSACTIONS on COMMUNICATIONS*, no. May, 2016, ISSN: 11092742.

[20] "Design and fabrication of microstrip antennas integrated in three dimensional orthogonal woven composites", *Composites Science and Technology*, vol. 69, no. 7-8, pp. 1004–1008, 2009, ISSN: 0266-3538. DOI: 10.1016/J.COMPSCITECH.2009.01.013. [Online]. Available: http://www.sciencedirect.com/science/article/pii/S0266353809000165.

[21] A. Verma, O. P. Singh, and G. R. Mishra, "Analysis of Feeding Mechanism in Microstrip Patch Antenna", *International Journal of Research in Engineering and Technology*, vol. 03, no. 04, pp. 786–792, 2014.

[22] T. Kour, R. Amanpreet, and K. Rajesh, "Design of Aperture Coupled Micro-Strip patch Antenna for Wireless Communication applications at 5 . 8Ghz", *IOSR Journal of Engineering (IOSRJEN)*, vol. 2, no. 7, pp. 96–99, 2012.

[23] D. M. Pozar, "A review of aperture coupled microstrip antennas: History, operation, development, and applications", *University of Massachusetts at Amherst*, no. May, pp. 1–9, 1996.

[24] M. Johansen, "Ku-band patch antenna design", Master's thesis, Satellite Engineering Faculty of Engineering Science and Technology Department of Electrical Engineering UiT The Arctic University of Norway, 2016.

[25] Girish Kumar; K.P. Ray, *Broadband Microstrip Antenna*. 2003, p. 424, ISBN: 1580532446. [Online]. Available: `https://books.google.com.my/books/about/Broadband{\_}Microstrip{\_}Antennas.html?id=wfl84429CsEC{\&}redir{\_}esc=y`.

[26] *electromagnetism - How is the combination of electric and magnetic waves (electromagnetic wave) illustrated as a single wave? - Physics Stack Exchange*. [Online]. Available: `https://physics.stackexchange.com/questions/291571/how-is-the-combination-of-electric-magnetic-waves-electromagnetic-wave-illus` (visited on 07/04/2017).

[27] J. Maria, L. Coll, A. Skrivervik, J. Manuel, R. Casals, and S. M. Veljovic, "X-BAND ANTENNA FOR CUBESAT SATELLITE", Master's thesis, 2017.

[28] *Polarization — Electronics World*. [Online]. Available: `http://elektroarsenal.net/polarization-2.html` (visited on 07/04/2017).

[29] A. Majumder, "Rectangular microstrip patch antenna using coaxial probe feeding technique to operate in S-band", *International Journal of Engineering Trends and Technology (IJETT)*, vol. 4, no. April, pp. 1206–1210, 2013. [Online]. Available: `http://www.ijettjournal.org/volume-4/issue-4/IJETT-V4I4P340.pdf`.

[30] W. Bengal, "Effect of Dielectric Permittivity and Height on a Microstrip-Fed Rectangular Patch Antenna", *IJECT VOL. 5, ISSUE SPL-2, JAN - MARCH 2014*, vol. 7109, no. 2, pp. 129–130, 2014, ISSN: 2230-9543.

[31] A Kuchar, "Aperture-coupled microstrip patch antenna array", Master's thesis, Technischen Universit at Wien, 1996.

[32] R. C. Paryani, "Design of a Wideband Dual-Polarized Cavity Backed Slot Antenna", Master's thesis, School of Electrical Engineering, Computer Science in the College of Engineering, and Computer Science at the University of Central Florida Orlando, Florida, 2010.

[33] M. Dias, B. Franciscatto, E. Nogueira, and T. Vuong, "On the design of a dual feed aperture coupled circularly polarized microstrip patch antenna", *SBMO/IEEE MTT-S International Microwave and Optoelectronics Conference Proceedings*, pp. 1–5, 2013. DOI: `10.1109/IMOC.2013.6646527`.

[34] D Pavithra and K. R. Dharani, "A Design of H-Shape Microstrip Patch Antenna for WLAN Applications", *International Conference on Signal Processing, Embedded System and Communication Technologies and their applications for Sustainable and Renewable Energy (ICSECSRE)*, vol. 2, no. 6, pp. 71–74, 2013.

[35] Intelsat, "Circular Polarization vs . Linear Polarization". [Online]. Available: www.intelsat.com/network.

[36] A Adrian and D. H. Schaubert, "Dual aperture-coupled microstrip antenna for dual or circular polarisation", *Electronics Letters*, vol. 23, no. 23, pp. 1226–1228, 1987, ISSN: 00135194. DOI: 10.1049/el:19870854. [Online]. Available: http://ieeexplore.ieee.org/stamp/stamp.jsp?tp={\&}arnumber=4259094.

[37] M. Albooyeh, N. Kamjani, and M. Shobeyri, "A Novel Cross-Slot Geometry To Improve Impedance Bandwidth of Microstrip Antennas", *Progress In Electromagnetics Research Letters*, vol. 4, pp. 63–72, 2008. DOI: 10.2528/PIERL08050203.

[38] G. S. Kirov and D. P. Mihaylova, "Circularly polarized aperture coupled microstrip antenna with resonant slots and a screen", *Radioengineering*, vol. 19, no. 1, pp. 111–116, 2010, ISSN: 12102512.

[39] David M.Pozar, *Microwave Engineering*, Fourth Edi. JohnWiley &Sons, Inc., p. 725, ISBN: 9780470631553.

[40] H. Ayad, A. Khalil, M. Fadlallah, and J. Jomaah, "Practical design for circularly polarized dual off-center aperture-coupled microstrip antenna for GPS application", *Proceedings of the 2014 International Conference on High Performance Computing and Simulation, HPCS 2014*, pp. 816–819, 2014. DOI: 10.1109/HPCSim.2014.6903772.

[41] S. C. Gao and L. W. Li, "Wideband dual-polarised microstrip patch antenna", *Electronics Letters*, vol. 37, no. 20, pp. 1213–1214, 2001, ISSN: 00135194. DOI: 10.1049/el:20010828.